SAIMM
THE SOUTHERN AFRICAN INSTITUTE OF MINING AND METALLURGY
VOLUME 121 NO. 9 SEPTEMBER 2021

Presidential Address
Thoughts on the value of history
by I.J. Geldenhuys

Introduction to our new President
Isabel Geldenhuys

Isabel Geldenhuys was born in 1970 in Pretoria and spent most of her childhood in Clayville, a suburb of Olifantsfontein. Her formative schooling years started at Olifantsfontein Primary School, and she completed her high school career in Centurion in 1988. Isabel holds a BEng degree in chemical engineering from the University of Pretoria and has completed an MEng degree in metallurgical engineering (cum laude) from the University of Stellenbosch. She is a registered professional engineer and a fellow of the SAIMM.

During her final school year, Isabel was selected from many applicants to spend a gap year at the South African Women's Army College as part of the 1989 intake. She joined 220 young women in George for a year of military training, mainly focused on leadership development. The year in George, away from family and school friends, laid the foundation for her lifelong passion for leadership development. After completing the gap year, she was fortunate enough to qualify for the chemical engineering programme at the University of Pretoria, where she was active in charity and community-based projects throughout her studies.

As a fresh graduate, her career almost took a direction into polymer research, but fortunately, the CSIR opted to release her from her bursary obligations, which led to her appointment in March 1996 in Mintek's Pyrometallurgy Division. At Mintek, as an engineer-in-training, Isabel discovered her passion for pyrometallurgy. Entranced by the subtle science and exact art of pyrometallurgy, she was privileged to work with many leading experts. Mintek's pyrometallurgy group supported her technical development and an in-depth understanding of the engineering and business principles of the metallurgical industry. At Mintek she developed expertise across various commodities, specializing in open-bath smelting processes for ferrochromium, titaniferous magnetite, ilmenite, precious metals, ferronickel, and various waste materials, among many others. In 2021 she started a new career as an independent consultant but continues her association with Mintek as a consulting pyrometallurgist.

Isabel represented Mintek at numerous conferences as a seasoned presenter with a passion for telling a story. She is the author and co-author of 19 conference and journal papers, over 80 technical reports, the inventor of processes, and frequently presents at technical conferences and events. Her involvement in the SAIMM stems from her passion for her community. She believes that the SAIMM offers professionals a unique opportunity to give back to the community and the country.

In her early 40s she tackled and completed three Comrades Marathons and ran the Great Wall of China marathon – she believes in regularly challenging herself, both personally and professionally. In the last few years, Isabel has combined her love of running and the environment with plastic litter activism *via* 'plogging' (picking up litter while jogging). She never leaves for a run or a walk without a bag (and sanitizer) to pick up litter. She shares her life with her soulmate, Carl Bergmann, also a metallurgist. Together they adore their brood of rescue cats and long-coated German Shepherds, and love spending time in their garden or hiking in their local nature reserve.

OFFICE BEARERS AND COUNCIL FOR THE 2021/2022 SESSION

Honorary President

Nolitha Fakude
President, Minerals Council South Africa

Honorary Vice Presidents

Gwede Mantashe
Minister of Mineral Resources, South Africa

Ebrahim Patel
Minister of Trade, Industry and Competition, South Africa

Blade Nzimande
Minister of Higher Education, Science and Technology, South Africa

President

I.J. Geldenhuys

President Elect

Z. Botha

Senior Vice President

W.C. Joughin

Junior Vice President

E Matinde

Incoming Junior Vice President

G.R. Lane

Immediate Past President

V.G. Duke

Honorary Treasurer

W.C. Joughin

Ordinary Members on Council

Z. Fakhraei
B. Genc
K.M. Letsoalo
S.B. Madolo
F.T. Manyanga
T.M. Mmola
G. Njowa
S.J. Ntsoelengoe
S.M. Rupprecht
A.J.S. Spearing
M.H. Solomon
S.J. Tose
A.T. van Zyl
E.J. Walls

Co-opted Members

M. Aziz
M.I. van der Bank

Past Presidents Serving on Council

N.A. Barcza
R.D. Beck
J.R. Dixon
R.T. Jones
A.S. Macfarlane
M.I. Mthenjane
C. Musingwini
S. Ndlovu
J.L. Porter
S.J. Ramokgopa
M.H. Rogers
D.A.J. Ross-Watt
G.L. Smith
W.H. van Niekerk

G.R. Lane–TPC Mining Chairperson
Z. Botha–TPC Metallurgy Chairperson

A.T. Chinhava–YPC Chairperson
M.A. Mello–YPC Vice Chairperson

Branch Chairpersons

Johannesburg D.F. Jensen
Namibia N.M. Namate
Northern Cape Jaco Mans
Pretoria J. Mans
Western Cape A.B. Nesbitt
Zambia D. Muma
Zimbabwe C.P. Sadomba
Zululand C.W. Mienie

PAST PRESIDENTS

*Deceased

* W. Bettel (1894–1895)
* A.F. Crosse (1895–1896)
* W.R. Feldtmann (1896–1897)
* C. Butters (1897–1898)
* J. Loevy (1898–1899)
* J.R. Williams (1899–1903)
* S.H. Pearce (1903–1904)
* W.A. Caldecott (1904–1905)
* W. Cullen (1905–1906)
* E.H. Johnson (1906–1907)
* J. Yates (1907–1908)
* R.G. Bevington (1908–1909)
* A. McA. Johnston (1909–1910)
* J. Moir (1910–1911)
* C.B. Saner (1911–1912)
* W.R. Dowling (1912–1913)
* A. Richardson (1913–1914)
* G.H. Stanley (1914–1915)
* J.E. Thomas (1915–1916)
* J.A. Wilkinson (1916–1917)
* G. Hildick-Smith (1917–1918)
* H.S. Meyer (1918–1919)
* J. Gray (1919–1920)
* J. Chilton (1920–1921)
* F. Wartenweiler (1921–1922)
* G.A. Watermeyer (1922–1923)
* F.W. Watson (1923–1924)
* C.J. Gray (1924–1925)
* H.A. White (1925–1926)
* H.R. Adam (1926–1927)
* Sir Robert Kotze (1927–1928)
* J.A. Woodburn (1928–1929)
* H. Pirow (1929–1930)
* J. Henderson (1930–1931)
* A. King (1931–1932)
* V. Nimmo-Dewar (1932–1933)
* P.N. Lategan (1933–1934)
* E.C. Ranson (1934–1935)
* R.A. Flugge-De-Smidt (1935–1936)
* T.K. Prentice (1936–1937)
* R.S.G. Stokes (1937–1938)
* P.E. Hall (1938–1939)
* E.H.A. Joseph (1939–1940)
* J.H. Dobson (1940–1941)
* Theo Meyer (1941–1942)
* John V. Muller (1942–1943)
* C. Biccard Jeppe (1943–1944)
* P.J. Louis Bok (1944–1945)
* J.T. McIntyre (1945–1946)
* M. Falcon (1946–1947)
* A. Clemens (1947–1948)
* F.G. Hill (1948–1949)
* O.A.E. Jackson (1949–1950)
* W.E. Gooday (1950–1951)
* C.J. Irving (1951–1952)
* D.D. Stitt (1952–1953)
* M.C.G. Meyer (1953–1954)
* L.A. Bushell (1954–1955)
* H. Britten (1955–1956)
* Wm. Bleloch (1956–1957)
* H. Simon (1957–1958)
* M. Barcza (1958–1959)
* R.J. Adamson (1959–1960)
* W.S. Findlay (1960–1961)
* D.G. Maxwell (1961–1962)
* J. de V. Lambrechts (1962–1963)
* J.F. Reid (1963–1964)
* D.M. Jamieson (1964–1965)
* H.E. Cross (1965–1966)
* D. Gordon Jones (1966–1967)
* P. Lambooy (1967–1968)
* R.C.J. Goode (1968–1969)
* J.K.E. Douglas (1969–1970)
* V.C. Robinson (1970–1971)
* D.D. Howat (1971–1972)
* J.P. Hugo (1972–1973)
* P.W.J. van Rensburg (1973–1974)
* R.P. Plewman (1974–1975)
* R.E. Robinson (1975–1976)
* M.D.G. Salamon (1976–1977)
* P.A. Von Wielligh (1977–1978)
* M.G. Atmore (1978–1979)
* D.A. Viljoen (1979–1980)
* P.R. Jochens (1980–1981)
* G.Y. Nisbet (1981–1982)

A.N. Brown (1982–1983)

* R.P. King (1983–1984)

J.D. Austin (1984–1985)

* H.E. James (1985–1986)

H. Wagner (1986–1987)

* B.C. Alberts (1987–1988)
* C.E. Fivaz (1988–1989)
* O.K.H. Steffen (1989–1990)
* H.G. Mosenthal (1990–1991)

R.D. Beck (1991–1992)

* J.P. Hoffman (1992–1993)
* H. Scott-Russell (1993–1994)

J.A. Cruise (1994–1995)
D.A.J. Ross-Watt (1995–1996)
N.A. Barcza (1996–1997)

* R.P. Mohring (1997–1998)

J.R. Dixon (1998–1999)
M.H. Rogers (1999–2000)
L.A. Cramer (2000–2001)

* A.A.B. Douglas (2001–2002)

S.J. Ramokgopa (2002-2003)
T.R. Stacey (2003–2004)
F.M.G. Egerton (2004–2005)
W.H. van Niekerk (2005–2006)
R.P.H. Willis (2006–2007)
R.G.B. Pickering (2007–2008)
A.M. Garbers-Craig (2008–2009)
J.C. Ngoma (2009–2010)
G.V.R. Landman (2010–2011)
J.N. van der Merwe (2011–2012)
G.L. Smith (2012–2013)
M. Dworzanowski (2013–2014)
J.L. Porter (2014–2015)
R.T. Jones (2015–2016)
C. Musingwini (2016–2017)
S. Ndlovu (2017–2018)
A.S. Macfarlane (2018–2019)
M.I. Mthenjane (2019–2020)
V.G. Duke (2020–2021)

Honorary Legal Advisers
M H Attorneys

Auditors
Genesis Chartered Accountants

Secretaries
The Southern African Institute of Mining and Metallurgy
Fifth Floor, Minerals Council South Africa
5 Hollard Street, Johannesburg 2001 • P.O. Box 61127, Marshalltown 2107
Telephone (011) 834-1273/7 • Fax (011) 838-5923 or (011) 833-8156
E-mail: journal@saimm.co.za

Typeset and Published by
The Southern African Institute of Mining and Metallurgy
P.O. Box 61127
Marshalltown 2107
Telephone (011) 834-1273/7
Fax (011) 838-5923
E-mail: journal@saimm.co.za

Printed by
Camera Press, Johannesburg

Advertising Representative
Barbara Spence
Avenue Advertising
Telephone (011) 463-7940
E-mail: barbara@avenue.co.za

ISSN 2225-6253 (print)
ISSN 2411-9717 (online)

Directory of Open Access Journals

SAIMM
JOURNAL OF THE SOUTHERN AFRICAN INSTITUTE OF MINING AND METALLURGY
VOLUME 121 NO. 9 SEPTEMBER 2021

Contents

PAPERS OF GENERAL INTEREST

Some incentives for peer reviewers

Welcome to another edition of papers about the SAMCODES and of general interest.

Every article published in the SAIMM *Journal* goes through a rigorous peer reviewing process and is reviewed by at least two independent reviewers who are experts in their fields. Peer reviewing is a widely accepted procedure for evaluating the validity, quality, and originality of academic work, and is done on a voluntary basis in scholarly publishing. It is a time-consuming exercise, and sometimes it is difficult to find researchers to undertake peer reviewing as the SAIMM *Journal* covers a wide range of topics. Although most academics do peer reviewing as part of their scholarly activities, nevertheless it is important to recognize peer reviewers for their contribution to improving the quality and integrity of the *Journal*.

The Editorial Board of the SAIMM *Journal* has been working on new ways to reward peer reviewers. Hence, it was decided to recognize peer reviewers by awarding them the following incentives:

- **Letter of thanks:** After each completed review, the reviewer will receive a 'thank you' letter in the form of an email.
- **Certificate of acknowledgement:** Every reviewer will be issued each year with a signed SAIMM *Journal* certificate showing how many reviews he/she completed in that year.
- **Annual list of peer reviewers:** The names of the reviewers who participated in the peer reviewing process will be published every year. The *Journal* also acknowledges the top peer reviewers annually on the website and at the AGM.
- **Discounts on conference attendance:** A 20% discount will be granted to reviewers for one SAIMM conference of their choosing.

There are some other incentives which are currently being considered, and these will be communicated to our readers as soon as they become a part of our initiative.

Enjoy the September edition of the Journal!

B. Genc

Conditioning monitoring with intelligent drives in Industry 4.0

By Sydney Govender, Danfoss Drives South Africa Senior Country Sales Manager

Johannesburg, 16 September 2021

The fourth industrial revolution, which is also known as Industry 4.0, refers to the combination of physical assets and advanced digital technologies that communicate, analyse, and act upon information, which in turn enables organizations and consumers to be flexible and make more intelligent, responsive, data-driven decisions.

Industry 4.0 has emerged as a result of the intelligent networking of computers, people, and devices, fueled by data and machine learning, using all possibilities of digitalization across the entire value chain.

This significant change in technology has led to a whole new way of working in a digital world. It embraces the internet of things (IoT), artificial intelligence (AI), robots, drones, autonomous vehicles, 3D printing, cloud computing, and nanotechnology, to name a few.

Trends in industry 4.0 automation systems

In automation systems, the impact of Industry 4.0 on motor systems is a migration from the 'automation pyramid' to 'networked systems'. This means that the various elements of the system, such as motors, drives, sensors, and controls, are interconnected and connected to a cloud data centre, where data is stored, processed, and analysed, and decisions are made.

In an automation network, the amount of data is prominent. As data is mainly produced by sensors, the number of sensors in modern automation systems is increasing. Sensors are required to collect data from motors and motor-driven machines such as fans, pumps and conveyors, and are connected to the data network by various means to use the data.

Modern variable-speed drives open new opportunities in the Industry 4.0 automation network. Traditionally, drives have been considered power processors for controlling the motor speed. Today, drives are also part of the information chain, using the advantage of built-in processing power, storage capacity, and communication interface within the drive itself.

What is an intelligent drive?

In the Industry 4.0 network, the drive plays an important role and is characterized by some enabling features:

- **Secure connectivity:** The drive can connect to other elements in a secure manner. Other elements in the network may include drives, PLCs, sensors, and a cloud data centre.
- **The drive acts as a sensor:** The drive uses motor current and voltage signature analysis to sense the motor and application performance.
- **The drive acts as a sensor hub:** The drive acquires data from external sensors related to the process, which is controlled by the drive.
- **The drive acts as a controller:** The drive can replace the PLC wherever application constraints allow.
- **Bring your own device concept:** This uses wireless connectivity to smart devices such as smartphones or tablets.

Information from the drive can be identified as follows:

- **Instantaneous signals:** Signals which are directly measured by the drive using built-in sensors. Data such as motor current, voltage, drive temperature, and their derivative, which is power as a multiplication of current and voltage, or motor torque. Moreover, the drive can be used as a hub for connecting external sensors that provide instantaneous signals.
- **Processed signals:** Signals which are derived from the instantaneous signal, which can include statistical distribution (maximum, minimum, mean, and standard deviation values), frequency domain analysis, or mission profile indicators.
- **Analytics signals:** Signals which provide indications of the condition of the drive, motor, and application. The signals are used to trigger maintenance or lead to system design improvements.

Conditioning monitoring with intelligent drives in Industry 4.0

(continued)

Motor current signature analysis techniques enable the drive to monitor the condition of the motor and application. The technique allows the system to potentially eliminate physical sensors, or extract early fault signatures that might not otherwise have been possible to detect. For example, this technique makes it possible to detect winding faults in advance, or mechanical load eccentricity.

The concept of the drive as a sensor hub involves connecting external sensors to the drive, thus eliminating the need for a gateway to connect the physical sensor to the data network. Vibration sensors, pressure sensors, and temperature sensors are examples of sensors which can be connected to the drive.

The advantages of the concept include the ability to correlate sensor data with different types of data present in the drive.

Why is condition-based maintenance needed?

The condition of a piece of equipment typically degrades over time. The introduction of Industry 4.0 and the availability of sensor data means that condition-based and predictive maintenance is now possible. The idea of condition-based maintenance is to detect a potential failure before an actual failure occurs.

Such maintenance strategies use actual sensor data to determine the condition of the equipment in service (condition-based maintenance) or to predict future failures (predictive maintenance).

Condition-based maintenance uses data from the equipment itself to monitor the health of the equipment in service. For this purpose, key parameters are selected as indicators to identify developing faults.

In this case, planning maintenance actions provides many advantages such as:

- Downtime reduction
- Elimination of unexpected production stops
- Maintenance optimization
- Reduction in spare part stock inventory.

Condition monitoring follows a three-step procedure:

- Establish a baseline
- Define thresholds
- Perform monitoring.

Conclusion

Today, drives are more than simple power processors – they are vital elements in modern automation systems, with the ability to act as sensors and sensor hubs, and to process, store, and analyse data, along with connectivity capabilities.

Drives are often already present in automation installations and therefore present a great opportunity to upgrade to Industry 4.0. This enables new ways of performing maintenance, such as condition-based maintenance. The functions are already available in some drives, and early adopters have already started using the drive as a sensor.

For more information:

Lynne McCarthy, Senior Marketing Communications Specialist, Danfoss Turkey, Middle East & Africa,
Email: mccarthyl@danfoss.com, www.danfoss.co.za, Phone: +27 11 785 7628

Danfoss engineers technologies that enable the world of tomorrow do more with less. We meet the growing need for infrastructure, food supply, energy efficiency and climate-friendly solutions. Our products and services are used in areas such as refrigeration, air conditioning, heating, motor control, and mobile machinery. We are also active in the field of renewable energy, as well as district heating infrastructure for cities and urban communities. Our innovative engineering dates back to 1933, and today Danfoss is a world leader, with 22 500 employees and serving customers in more than 100 countries. We are still privately held by the founding family. Read more about us at www.danfoss.com.

2018 Mining Charter is policy, not law!

By Jonathan Veeran, Bruce Dickinson, & Rita Spalding from Webber Wentzel

The High Court has ruled that the 2018 Mining Charter is policy, not law, and has set aside various aspects of the Charter as unconstitutional. While sound, this judgment is likely to be appealed.

On 21 September 2021, the High Court of South Africa, Gauteng Division, Pretoria handed down judgment in the matter between the Minerals Council South Africa v *the Minister of Mineral Resources and Energy and Others* (case no. 20341/18).

The Minerals Council had brought an application, under the Promotion of Administrative Justice Act 3 of 2000 (PAJA), seeking to review and set aside certain clauses of the Broad-Based Socio-Economic Empowerment Charter for the Mining and Minerals Industry, 2018 (the 2018 Charter). In the alternative, the Minerals Council sought a declarator that the challenged clauses are inconsistent with the principle of legality and should be set aside.

The application was previously heard on 5 May 2020, after which the Court ordered the joinder of the joined respondents and postponed the merits for hearing. The joined respondents comprise host communities affected by mining operations, organizations representing those mining communities, and trade unions. The trade union respondents opposed the relief sought by the Minerals Council. The communities did not oppose the relief sought by the Minerals Council but sought additional relief on the basis that: (i) there was inadequate consultation with them prior to the publication of the 2018 Charter; and (ii) that the 2018 Charter fails to substantially address environmental degradation and gender-based injustice caused by mining, as well as the poverty and inequality of mining-affected communities.

The matter was heard before a full bench comprised of Kathree-Setiloane J, Van der Schyff J, and Ceylon AJ. The Court ruled in favour of the Minerals Council, with Kathree-Setiloane J writing the judgment and Van der Schyff J and Ceylon AJ concurring.

Key Points

The question before the Court was the power of the Minister of Mineral Resources and Energy (the Minister) under section 100(2) of the Mineral and Petroleum Resources Development Act (MPRDA) to make law in the form of subordinate legislation, and whether the 2018 Charter constitutes law or policy.

The Minister argued that section 100(2) of the MPRDA empowered him to make law through the development of the 2018 Charter and that the 2018 Charter thus constitutes a sui generis form of legislation which is binding on the holders of mining rights. The Minerals Council contended that the 2018 Charter is a formal policy document developed by the Minister in terms of the MPRDA and is therefore binding on the Minister when he considers applications for mining rights, in accordance with section 23(1)(h) of the MPRDA. This provision permits the Minister to grant a mining right only if, amongst other things, the grant would be in accordance with the Charter contemplated in section 100(2) of the MPRDA.

Kathree-Setiloane J concluded that a contextual approach must be adopted in interpretating section 4 of the MPRDA.

In interpreting the language of the MPRDA, Kathree-Setiloane J noted that section 100(2)(a) empowers the Minister to '*develop a broad-based socio-economic empowerment Charter that will set the framework for targets and timetable for effecting the entry into and active participation of historically disadvantaged South Africans into the mining industry*…'. While the word 'charter' is recognized in South African law, it is noted that the more commonly used 'law' and 'regulation' are used in the MPRDA. Indeed, the Minister is expressly authorized to make subordinate legislation in section 107.

Kathree-Setiloane J concluded that the word 'charter' was chosen deliberately by the Legislature to indicate something other than a law. Similarly, the word 'develop' is not used by the Legislature to describe law-making, but with reference to formulating policy. Furthermore, the permissive rather than peremptory wording of section 100(2) indicates that the Legislature did not intend the Charter to be subordinate legislation, as the Legislature would have used peremptory wording if the Charter was intended to be anything other than guiding principles. Kathree-Setiloane J concluded the interpretation

2018 Mining Charter is policy, not law!
(continued)

of the MPRDA by noting that if section 100(2) were to be construed as a delegation of the power to make legislation, it would offend the doctrine of the separation of powers and lead to further unbridled law-making.

Having concluded that the language of the MPRDA does not give the Minister the power to make law in the form of subordinate legislation, Kathree-Setiloane J considered the purpose of section 100(2), which is transformational. Contrary to the argument of the Minister, the transformational objectives of the section do not require that the Charter take the form of subordinate legislation. The MPRDA contains an enforcement structure, as no person may mine without a mining right and section 23(1)(h) stipulates that the Minister may only grant such a right if it will further the transformational objects of the Act's section 2(d) and (f), in accordance with the Charter contemplated in section 100(2). The holder of a mining right is also obliged to report on compliance with the objects of the MPRDA and compliance with the Charter, in terms of sections 25(2)(h) and 28(2)(c). Therefore, the purpose of section 100(2) is fulfilled without the 2018 Charter constituting binding law.

The Minister advanced the argument that the transformation of the mining industry has been ineffective. Transformation could be expedited if the 2018 Charter was directly enforceable law. Kathree-Setiloane J noted that a failure to achieve the objects identified in section 100(2) of the MPRDA is a legitimate concern; however, the Minister's argument failed to account for additional factors contributing to transformation, such as security of tenure, conversion of old order rights into new order rights, and the Minister's own failure to make regulations in terms of section 107 regarding the achievement of the objectives set out in sections 2(c), (d), (e), (f), or (i) of the MPRDA.

In light of the above, Kathree-Setiloane J declared, inter alia that:

Section 100(2) does not empower the Minister to make law and that the 2018 Charter is therefore not binding subordinate legislation but is rather an instrument of policy.

Certain clauses of the 2018 Charter are reviewed and set aside in terms of PAJA. Inter alia, the following aspects of the 2018 Charter have been found to be unconstitutional:

i. Provisions which require compliance with the 30% Historically Disadvantaged South African (**'HDSA'**) ownership requirement upon renewals and/or transfers of rights issued under the MPRDA;
ii. Provisions which require the implementation of mandated structures, such as community, employee, and HDSA entrepreneur schemes;
iii. The provisions which render the HDSA ownership requirement applicable to holders of permits under the Diamonds Act, 1986 and the Precious Metals Act, 2005;
iv. Provisions which allow for a beneficiation offset;
v. The provision dealing with preferential procurement; and
vi. The enforcement provisions which allow for suspension and cancellation of rights in the event of non-compliance with the 2018 Charter.

Implications

The judgment is explicit that the 2018 Charter is not binding legislation, It is only binding on the holder of a mining right to the extent that its terms were lawfully incorporated by the Minister into the mining right. The implication of the judgment is therefore that a mining right holder will not be required to 'top up' its empowerment credentials on renewal of the mining right and will have more flexibility in structuring empowerment transactions. The judgment is sound in law but is likely to be appealed.

Nadine Van Tonder

Presidential Address: Thoughts on the value of history

I.J. Geldenhuys[1]

Affiliation:
[1] Mintek, Pyrometallurgy Division, South Africa.
[2] Isabel Geldenhuys Consulting, South Africa.

Correspondence to:
I.J. Geldenhuys

Email:
isabel@pyro.co.za

Dates:
Received: 13 Sep. 2021
Published: September 2021

How to cite:
Geldenhuys, I.J. 2021 Presidential Address: Thoughts on the value of history. Journal of the Southern African Institute of Mining and Metallurgy, vol. 121, no. 9, pp. 457–464

DOI ID:
http://dx.doi.org/10.17159/2411-9717/2021

ORCID:
I.J. Geldenhuys
https://orcid.org/0000-0002-5995-2722

Synopsis

South Africa's mining and metals industries have an illustrious history dating back to the Late Iron Age. We live in a complex and data-intensive world that has already fundamentally changed how we work and live. The outbreak of the global COVID-19 pandemic in 2020 resulted in immeasurable suffering worldwide, but the crisis also accelerated many technological developments and altered the way we think about, and experience, technology and work. Problem-solving requires new and rapidly changing skills to manage the data tsunami. Whether at the rock face or on the processing plant, the fundamentals have not changed, although how we interact with minerals and their properties has changed dramatically. Sustainable processing and design are non-negotiable if we genuinely want to achieve the aim of the cradle-to-cradle principle. As we venture forth, what can scientists, engineers, technologists, and mathematicians learn from history?

History is data presented in a context; sometimes, the context is also important. We exist in an age of data, with most of the world's data created in only the past two years. History can enhance our understanding of the present and enhance our future outcomes. Lessons from history can help provide insights into making ethical and sustainable choices related to technology or engineering in the mining and metallurgical industry.

Shifting the perspective of mining and metallurgy professionals from a narrow focus on complex technical solutions towards a broader context for problem-solving and designs that includes the entire ecosystem is crucial. In other words, using or reflecting on historical process development is, at its core, systems thinking.

Keywords
titaniferous magnetite, open arc smelting, historical perspective, systems thinking, project development.

Introduction

South Africa's mining and metallurgical industry have an illustrious history dating back to the Late Iron Age. The mining and metallurgical professionals of today live in a complex and data-intensive world with challenging technical and ethical demands that increasingly require multi- and transdisciplinary approaches. The outbreak of the global COVID-19 pandemic In 2020 resulted in immeasurable suffering, but the crisis also accelerated the adoption of new ways of working, and changed how we think about, and even how we experience, technology and work. Amid overwhelming trends, events, challenges, and changes, what can we learn from history?

The emergence of Big Data and digitalization

The emergence of data as a megatrend has already fundamentally changed society, as we now easily access information digitally *via* smartphones and other devices. No longer is recorded knowledge found in a single location, such as the Library of Alexandria; today our information is increasingly decentralized, with digital information being created, analysed, and stored at an astonishing rate. Considering that 90% of the world's data has been produced in just the last two years, it is best described as an explosion of information, known as 'Big Data'. This trend is transforming the world around us, with data consisting of a greater variety, increased volume, and created at an increasing rate. As one of the megatrends of modern society, data is constantly changing our understanding of the world. Not only is new data created at an unprecedented rate, similarly changed is our ability to access historical data, as data and information storage is no longer confined to brick-and-mortar libraries.

Presidential Address: Thoughts on the value of history

In the context of the mining and metallurgy ecosystem, history is captured in publications such as journal and conference papers, textbooks, theses, and dissertations, and more recently recorded via webinars and digital and hybrid conferences. Recorded presentations will likely become a tangible and searchable part of our digital libraries and knowledge base. For now, we still have an enormous collection of valuable information to mine.

Relevant knowledge connects information to help us understand things. Connectedness is defined by the Oxford Dictionary as 'a state of being joined or linked'. Through a literature review dating back to the Late Iron Age, the history of processing titaniferous magnetite is presented here to illustrate the value of historical publications. An atypical literature review highlighting various case studies and historical perspectives within the context of the processing of titaniferous magnetite is used to illustrate the value of historical scientific publications.

Brief overview of the nature and occurrence of titaniferous magnetite

Titaniferous magnetite (also known titanomagnetite) deposits are numerous and significant in size. Titanomagnetite is generically defined as magnetite with more than 1% by mass titanium dioxide (TiO_2) and is typically vanadium-bearing. The iron and titanium in titanomagnetite occur as a mixture of magnetite (Fe_3O_4) and ilmenite ($FeTiO_3$) with magnetite intergrown or spatially associated with ilmenite, which prevents clean separation of the magnetite and ilmenite via physical beneficiation (Fischer, 1975; Rohrmann, 1985; Henry *et al.*, 1987; Taylor *et al.*, 2005; Peck and Huminicki, 2016).

Deposits of titanomagnetite are found in significant numbers throughout the world. The most important deposits are in the Panzhihua Complex in Sichuan Province, China (Pang *et al.*, 2010), the Windimurra Complex in Australia (Ivanic *et al.*, 2010), the Kachkanar deposit in Russia (Smirnov, Tret'yakov, and Gladyshev, 2000), and the vanadiferous titanomagnetite of the Bushveld Complex of South Africa. Chen and Chu (2014) report that titaniferous magnetite deposits account for about 90% of China's titanium reserves. However, during pyrometallurgical processing to extract iron and vanadium via blast furnace smelting the majority of the titanium is lost to the discarded slag. The Kachkanar deposit in Russia is also primarily exploited for its iron content using blast furnaces, with vanadium as a co-product (Badmatsyrenova and Orsoev, 2005).

South Africa's Bushveld Complex is uniquely rich in vanadium and titanium, and both pyrometallurgical means (smelting) and direct extraction processes (roast-leach) have been used to extract vanadium (Cawthorn *et al.*, 2005; US Geological Survey, 2021). Detailed reviews of the various extractive practices for titaniferous magnetite, current and historical, are described by (Taylor *et al.* (2005) and Geldenhuys, Akdogan, and Reynolds (2021).

Connecting historical perspectives

The value of historical perspectives is presented as a connected journey through the history, challenges, and fundamental nature of smelting titaniferous magnetite. The review is drawn from a wide variety of scientific publications, illustrating the value of a multidisciplinary perspective. History provides us with a rich collection of case studies and options, and can greatly enhance our understanding of the present.

An introduction to Dr William Bleloch

In 2015, EVRAZ Highveld Steel and Vanadium (Highveld Steel) closed down after about 50 years of processing titaniferous magnetite to recover primarily iron and vanadium (EVRAZ Highveld Steel and Vanadium, 2015). The associated job losses were devastating for the economy of the region, but South Africa also lost a particularly unique smelting capacity. Highveld Steel was one of only two processing plants in the world where vanadium-bearing titaniferous iron ore was processed using electric smelting technology (Rohrmann, 1985; Steinberg, Geyser, and Nell, 2011). As reported by Steinberg, Geyser, and Nell (2011) the Highveld Steel process flow sheet was '*developed in the early 1960s, based on the research done by Dr William Bleloch in 1949. He showed that Bushveld complex magnetite ore could be melted using submerged-arc furnace (SAF) technology in a process that controls the carbon addition to selectively reduce vanadium and iron while leaving titania dissolved in the slag*.' This brief historical perspective presented references the well-known paper by Rohrmann (1985), titled '*Vanadium in South Africa*'. In this exceptional review paper, the history and development of Highveld Steel is described in more detail, referencing Dr Bleloch's 1949 paper '*The electric smelting of iron ores for production of alloy irons and steel and recovery of chromium and vanadium*'. The work that led to the flow sheet being implemented at Highveld Steel in the 1960s spans a period of over 30 years (Bleloch, 1949),culminating in the establishment of Highveld Steel.

Dr Bleloch's role in the establishment of Highveld Steel cannot be overstated, and his work contributed greatly to the establishment of the South African submerged-arc furnace smelting industry. The research and development work on which Highveld Steel's process was based aimed to unlock the potential of the Bushveld Complex. Dr Bleloch's belief was that there is scope '*for the electric smelting process in Southern Africa because of the existence of workable reserves of chromium and vanadium bearing iron ores*' (Bleloch, 1949), and he viewed electric smelting as a unique opportunity for the country to beneficiate its rich mineral wealth. Dr Bleloch was elected as the President of the South African Institute of Mining and Metallurgy (SAIMM) in 1956, and his Presidential Address was widely acclaimed for his visionary presentation of the prospects for electric smelting in South Africa. In his own words, an extract from his Brigadier Stokes Memorial Award citation in 1981: '*It is not really in the research laboratory that these problems are solved. It is in the minds of men that they are solved by the ability of mankind to think*' SAIMM, 1981).

Dr Bleloch's accomplishments and his in-depth understanding of the fundamentals of smelting, techno-economics, and insights into the potential of South Africa's resources beyond mining are inspirational. His 1949 paper, despite being published over 70 years ago, is still a comprehensive and valuable reference point, which describes in detail all aspects of the journey that led to the establishment of Highveld Steel, more than a decade after its publication. The paper features aspects of fundamentals and thermodynamics, technology perspectives, as well as economic considerations, and continues to offer valuable insights into the mechanics of project development, showing that historical scientific publications can offer a wealth of knowledge to a willing reader.

The unusual history of Lowveld ironmaking

Archaeometallurgy is described by Killick and Finn (2012)

as an interdisciplinary and international field of study that examines all aspects of the production, use, and consumption of metals in preindustrial societies. The story of titaniferous magnetite smelting in South Africa is an example of the value of interdisciplinary studies and offers great insights. The history of ironmaking in South Africa is particularly relevant and interesting, and an excellent reminder that the fundamental principles do not change with time.

The northern Lowveld of South Africa has a rich archaeological record of mining and smelting activities, with siteS estimated to date back to 350 CE. Evidence of ironmaking agriculturalists is found in the Tzaneen area. Around Phalaborwa, archaeologists have logged high concentrations of mining and smelting sites dating back to about 1000 CE, likely due to the nearly inexhaustible quantities of accessible magnetite outcrops found in this region. It is likely that these early settlers were not attracted to the region for the abundant iron deposits, but they needed iron and through experimentation adapted their bloomery smelting practices to use the unusual iron ore of the region to produce the metal they required (Miller, Killick, and van der Merwe, 2001; Killick and Miller, 2014).

Figure 1 shows a photograph of a typical bloomery furnace from the Lowveld region (around Phalaborwa) (Killick and Miller, 2014). In bloomery furnaces, the ironworkers converted iron ore directly into a bloom' of low-carbon iron, with the raw materials and fuel loaded into the furnace and a blast of air provided by some form of bellows. When the bowl was filled with slag, the process was halted and both the bloom of iron and slag were broken out (Brothers, 2001). The modern blast furnace still uses principally the same concept of blasting air through tuyeres to activate the fuel, typically coke. The scale and efficiency of modern blast furnaces are many orders of magnitude removed from the bloomery furnaces found in the Lowveld, but the principal metallurgical concepts are still valid.

Records of African bloomery smelters show that most smelting sites favoured lateritic iron ores, which are dominated by iron hydroxide minerals. Laterite ores are not found in the Lowveld, but the abundance of magnetite and titaniferous magnetite created a unique scenario for the ironworkers. Even in the global archaeological context, magnetite ores were rarely used in bloomery furnaces as the reduction of lumps of magnetite proceeds much slower than that of similarly sized lumps of hydroxide ores. For effective reduction of a magnetite ore in the short stack of the bloomery furnaces (typically only about 1 m high), smaller particle sizes were required. The Lowveld ironworkers adapted to their circumstances by grinding and crushing the massive magnetite ore found in the region. Evidence of crushing of the magnetite is scattered around Phalaborwa, where grinding hollows can be found from which magnetite grains can reportedly still be extracted with a magnet.

Figure 1—A photograph of an early iron smelting furnace from the Mashishimali Hills (Killick & Miller, 2014, Figure 6)

A unique characteristic of the magnetite from the northern Lowveld region is the high titania content, which would have also challenged the metallurgical talents of the bloomery ironworkers. Slags tested by archaeometallurgists contained from 12 to 25% TiO_2 by mass, which is highly unusual for the time. The Lowveld ironworkers added fluxes to their furnaces to enable them to overcome the high titania contents of the slags, which would have been highly viscous. The bloomery ironworkers thus adapted their smelting technique to accommodate the strange iron ore of the region, demonstrating impressive metallurgical skills.

Everywhere else in the world where magnetite was processed in bloomery furnaces the magnetite was typically recovered from beaches and rivers. These 'black sands' result from natural erosion as the magnetite grains are liberated, and typically consist of granular particles smaller than 2 mm. This type of magnetite sand, also called 'ironsand', is still being processed to produce iron. A modern example of such a deposit is found in New Zealand. Magnetite sand is found on the black sand beaches of the west coast of the North Island in New Zealand. New Zealand Steel was established in 1965 by the New Zealand government to produce steel billet from the abundant titaniferous magnetite in the region. The iron concentrate processed by New Zealand Steel is mined from the Waikato North Head site, south of Auckland, as well as from the Tahãroa deposit on the west coast of the North Island. The sands from the beaches are lower in titania and vanadium than the magnetite from the Bushveld Complex processed by Highveld Steel. With the closure of Highveld Steel in 2015, New Zealand Steel is currently the only facility in the world that employs electric smelting to recover iron and vanadium from titaniferous magnetite (Hukkanen and Walden, 1985; Kelly, 1993; New Zealand Steel, 2017, 2018).

The evolution of electric smelting of titaniferous magnetite

Highveld Steel and New Zealand Steel were both commissioned during the mid- to late 1960s. While both process flow sheets are embodiments of the rotary kiln-electric furnace (RKEF) process, they differ in concept and there are several interesting connections and historical perspectives.

Highveld Steel and Vanadium started smelting ore from the Mapochs Mine in 1968, following an implementation programme initiated in 1960 as described earlier (Bleloch, 1949; Rohrmann, 1985). The original RKEF process flow sheet for Highveld Steel comprised co-current rotary kilns for prereduction of the generally lumpy titaniferous magnetite concentrate. Steinberg, Geyser, and Nell (2011) report that there is no clear evidence for, or record of, the reasons for selected the co-current kiln designs.

The prereduced concentrate from the kilns was fed into submerged-arc furnaces together with fluxes and reductant, producing vanadium-bearing pig iron and waste slag. The use of conventional blast furnace technology had been regarded as being too high a risk due to the unusually high concentration of titanium in the Bushveld Complex ores.

Dr Bleloch pioneered the recovery of iron from the Bushveld magnetite ore, proposing the use of South Africa's 'atypical iron ore' *via* 'electrometallurgy' – the use of electric arc furnaces to recover metals. His work was interrupted by the outbreak of World War II, but in the post-war years he turned his attention back to metallurgy and in particular electric smelting projects. in 1948 he oversaw the smelting of 100 tons of Bushveld magnetite in Norway and successfully demonstrated the production of pig iron and recovery of vanadium (Bleloch, 1949). Much like the adaptations of the Lowveld ironmaking of the Late Iron Age, the process required fluxing, and although the energy source would be supplied by electrical energy the same metallurgical principles were applied in the modern embodiment of processing the unusual iron ore from the Bushveld Complex.

The Highveld Steel flow sheet remained unchanged until the late 1990s, when a series of studies was conducted to identify opportunities to address operational problems and inefficiencies that had been part of the process since inception. As a result of successful testing on-site, Highveld Steel converted four furnaces from submerged arc to open arc mode over a period of about 6 years (starting in 2004), eliminating the dependence of the power input on the burden and slag composition. The conversion yielded several operational improvements as the open-arc smelting mode greatly improved metallurgical control and operational outcomes. The change to open-arc smelting improved vanadium recovery, lowered coal , electrode, and energy consumption, and could use less-reactive coal and process more fine ore directly in the smelting process. The benefits observed are typical and comparable to the principles of processing high-titania ores in an open-arc furnace (Jones and Geldenhuys, 2011; Geldenhuys, 2017). The overall metallurgical and operational performance at Highveld Steel improved substantially after the conversion, as reported by Steinberg, Geyser, and Nell (2011).

It is noteworthy that the only other RKEF operation processing vanadium-bearing titaniferous magnetite to produce iron and recover vanadium, namely New Zealand Steel, operated with a shielded open arc, similar to that used by ilmenite smelters such as Rio Tinto's Quebec Fer et Titane (formerly known as QIT) and Richards Bay Minerals (RBM) in South Africa (Hukkanen and Walden, 1985; Matyas *et al.*, 1993).

According to Matyas *et al.* (1993), shielded-arc electric smelting furnace technology was developed by Falconbridge in the 1960s for the smelting of prereduced nickel laterite ores. However, in the 1950s, large electric furnaces were commissioned at Sorel (known today as Rio Tinto Fer et Titane) in Canada with the purpose of smelting the atypical ilmenite ($FeTiO_3$) deposits in Quebec. These furnaces were designed to operate with open arcs, partially shielded by feed and without the use of slag modifiers, producing high-titania slags containing about 80% titania (Sorel slag) from hard-rock ilmenite with a starting grade of about 34% TiO_2 (Habashi, 2010).

Matyas *et al.* (1993) illustrate the princlples of submerged arc (Figure 2a), shielded open arc (Figure 2b), and open arc smelting (Figure 2c). The representations are very useful for visualizing the differences between these three modes of electric smelting and are applicable to circular and rectangular furnaces as well as DC or AC power sources. The total number of electrodes may be configured depending on the power source with either 1, 2, 3, or 6 electrodes, depending on the electrical and mechanical configuration of the furnace. For a DC furnace, it is usual for the anode to be embedded in the hearth (not indicated in the graphics), but is it possible to configure a DC furnace as a dual-electrode furnace, with one electrode acting as the cathode and the second as the anode.

Figure 2a illustrate the original Highveld Steel smelting mode, and Figure 2c shows the evolution as implemented, and described by Steinberg , Geyser, and Nell (2011). The smelting furnaces at New Zealand Steel are shielded arc operations, as represented by Figure 2b. To operate with a shielded arc, feed ports are strategically located to manage the feed in such a way that the arc is always shielded by feed. There is clearly a continuum of modes of operation between shielded arc and open arc smelting, and it may be more accurate to describe shielded arc smelting and open bath smelting as sub-types of open arc smelting as the mechanism of heat transfer is fundamentally the same. There are clear benefits in covering at least part of the bath with feed, as the majority of heat radiation is from the molten slag bath surface, a common challenge for open arc open bath smelting operations.

These reports of shielded open arcs are a reminder of the fact that most scientific discoveries and inventions are made independently and more or less simultaneously, by multiple inventors (Kelly, 2011). The various historical references highlight that even in the relatively small industry of electric smelting, process developments across various commodities often occur in parallel or nearly simultaneously, within different commodity types. It is a reminder that great value is created through cross-pollination and is possibly one of the most valuable contextual lessons one can learn from historical publications.

Magnetite reduction perspectives

The prereduction technology at New Zealand Steel comprised coal-based direct reduction using rotary kilns to produce metallized iron, which was smelted in the electric furnaces. This technology, which is known as the SL/RN (Stelco-Lurgi/Republic Steel-National Lead) process, is widely used and is known for being able to process a wide range of iron-bearing materials, including lumpy ore, pellets, and finely sized iron-bearing feedstocks such as ilmenite. Carbon (in solid form) is fed together with the iron ore into a rotary kiln, where the coal is gasified and the iron ore is reduced. Notably, coal consumption is considerably

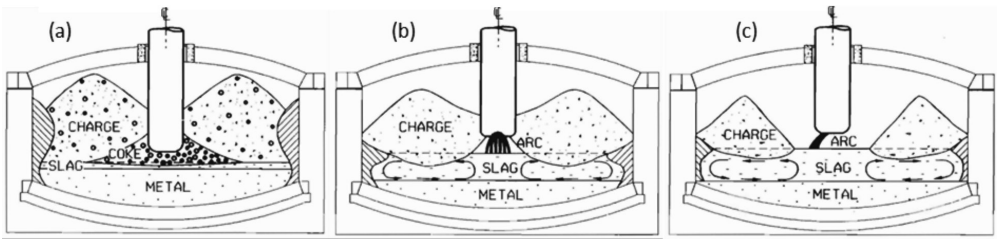

Figure 2—Illustration of three typical modes of smelting as described by Matyas *et al.* (1993). (a) Submerged arc, (b) shielded arc, and (c) open arc smelting

higher than for a blast furnace, and the energy efficiency of individual plants depends on how efficiently the residual gas is utilized in the plant (Kelly, 1993; Lepinski, 2000).

New Zealand Steel initially fed green (unfired) titanomagnetite pellets directly to the rotary kiln while coal was injected into the kiln. Kelly (1993) describes the various process improvements that were required. It was found that the green pellets deteriorated significantly in the kiln, resulting in excessive fines generation. The waste gas handling system could not cope with the excess dust, which limited the throughput of the reduction step. Coal injection was found to be unsuccessful, with poor temperature control resulting in accretion problems in the kilns. In 1972, the plant abandoned pellet production and coal injection, and resorted to feeding iron concentrate directly together with the coal. Although the operation immediately improved, the plant was still operating below design capacity. The bottleneck remained the high volumes of waste gas from the coal. To address this issue, the plant implemented a coal charring step before feeding the reductant to the kiln. This led to the development of the multi-hearth furnaces currently in use at New Zealand Steel (Richards and Davies, 1980; Kelly, 1993).

Steinberg, Geyser, and Nell (2011) concluded that the Highveld Steel plant needed to improve the efficiency of prereduction, and that multi-hearth furnaces were being evaluated as an option. Perhaps if the process changes had been introduced earlier, Highveld Steel might still be in operation today. According to Kelly (1993), the energy released as part of the charring step is used to preheat the concentrate, and the overall productivity of the kilns improved about 35% as a result.

Prereduction of the iron prior to smelting in electric furnaces was a key process innovation for both New Zealand Steel and Highveld Steel. The benefits of prereduction in electric smelting are well-established. Highveld Steel's kiln operations were notoriously variable and ineffective, but unlike New Zealand Steel, no significant changes were ever implemented. During the submerged arc smelting era, fines were not well tolerated by the smelters, thus lumpy ore was favoured, which further compounded the problem at Highveld. As described earlier, bloomery furnaces generally processed magnetite only from black sands, where the magnetite was liberated through natural erosion. In the Lowveld slag samples from the many smelting sites around Phalaborwa have been recovered and studied by archaeologists and archaeometallurgists. An example of a slag from the region

Figure 3 (reproduced from Killick and Miller, 2014) shows a micrograph of a slag sample. The magnetite has been reduced to metallic iron (white) around its exterior, but the ulvöspinel laths were not reduced, and laths of Fe_2TiO_4 can be seen within the iron rim at the upper left of the frame. Manamela and Pistorius (2005) concluded that '*Ore size does affect direct reduction of titaniferous magnetite*' and that there is a limit to direct reduction for titania-rich ores. The ironworkers of the Late Iron Age already established that ore size for magnetite ores was crucial, and magnetite was generally processed only if naturally occurring as black sands or, as found in the Lowveld, innovatively crushed into smaller sizes. The overall conclusions of the ironworkers from the Lowveld and modern researchers are aligned, and the unusual minerals processing activities in the Lowveld demonstrates that the ironworkers also realized that particle size matters.

The exsolved ülvospinel (Fe_2TiO_4) in the metallic rim (Figure 3) clearly shows that during direct reduction of titanomagnetite in a bloomery furnace, Fe associated with the exsolved ülvospinel phase is essentially unavailable for direct reduction. In both papers (Manamela and Pistorius, 2005; Killick and Miller, 2014) the direct reduction mechanism of titaniferous magnetite is investigated, although from different perspectives and different disciplines: Killick and Miller (2014) via a postmortem study of the slag from bloomery furnace ironmaking in the Lowveld (archaeometallurgy perspective) and Manamela and Pistorius (2005) *via* a study of direct reduction of titaniferous magnetite in the context of reduction in the rotary kilns at Highveld Steel (metallurgical engineering perspective).

Manamela and Pistorius (2005) concluded that the particle size of ore matters, but they also quantified the degree of direct reduction that can be achieved. The Lowveld ironworkers relied on direct reduction in the short shafts of their bloomery furnaces, and the slag samples from the region show that only partial reduction was achieved. Manamela and Pistorius (2005) concluded that the direct reduction of titaniferous magnetite proceeds via a two-step process and that due to the nature of titaniferous magnetite, the theoretic maximum metallization for titaniferous ore depends on the Fe-to-Ti ratio.

In the first step, titaniferous magnetite is converted to a mixture of wüstite (FeO) and ülvospinel. This reaction appears to occur uniformly throughout the ore particles and is not significantly affected by particle size. In the second reduction step the wüstite formed during the first step is reduced to metallic iron, but for larger ore particles, metallization is confined to the outer regions of the particles, with an unreduced core consisting of a mixture of wüstite and ülvospinel. This would suggest that gaseous diffusion through the product layer limits the rate of reduction (Manamela and Pistorius, 2005). Figure 4 shows a partially reduced ore sample, and the similarities with Figure 3 are clear. Once fully reduced, the titaniferous magnetite ore would consist of a mixture of metallic Fe and ülvospinel, and as is clear from Figure 3, the product of direct reduction will contain metallic Fe together with Fe trapped in as ülvospinel as no further reduction of the ülvospinel occurs.

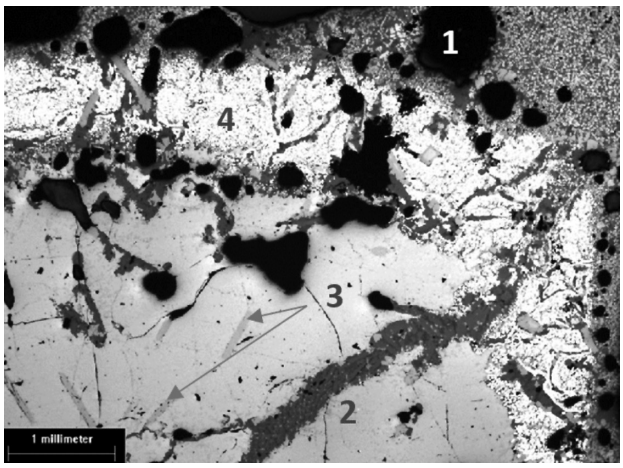

Figure 3—Micrograph of a slag sample from a Phalaborwa archaeological site (Killick and Miller, 2014, Figure 10). The slag shows typical features of a slag obtained through the reduction of magnetite by CO. Large, trapped bubbles of CO_2 appear as black cavities (1). A matrix of low-titanium magnetite (light grey areas (2) with small laths of exsolved ulvöspinel (darker grey areas (3) is seen in the lower half of the frame. Metallic iron (white areas, 4) on the outer regions or rims shows the zone where the magnetite was fully reduced to metal, while the ulvöspinel within the rim was not reduced

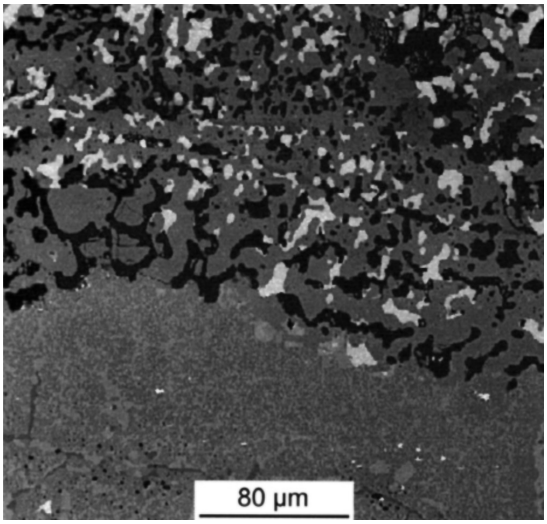

Figure 4—Scanning electron micrograph (backscattered electron image) of the reaction front of partially reduced titaniferous magnetite ore, showing the partially reduced core consisting of wüstite (FeO) and ülvospinel (Fe_2TiO_4) in the lower part of the frame and the product layer consisting of metallic iron and ülvospinel in the upper part (reproduced from Manamela and Pistorius, 2005, FIgure. 6)

Manamela and Pistorius (2005) explain that for a titaniferous magnetite ore with an Fe-to-Ti ratio of 6 (*i.e.*, for every six moles of Fe there is one mole of Ti), out of every six moles of iron in the original ore, approximately two moles would be trapped in the ülvospinel phase (from the chemical formula Fe_2TiO_4) and a maximum of four moles of iron could be reduced to the metal. For ore with an Fe-to-Ti ratio of 6, the theoretical maximum reduction would be about 66%.

Project development lessons from history

The journey from ore to metal is often fraught with challenges. New projects are typically beset by commissioning delays, ramp-up challenges, and financial constraints, but usually the operation achieves the desired outputs. In general, mining and metallurgical projects have a poor track record of delivering on time or budget. The McNulty curves (McNulty, 1998; McNulty, 2004)are a series of graphs which predict the level of pain that companies will endure when ramping up a project, based on historical case studies. An excellent example of how history can add value to current and future projects in a systematic and scientific sense. The work by McNulty clearly demonstrates the challenges associated with developing and implementing a complex mining and mineral process. Pyrometallurgical processes are extremely prone to difficulties in ramping up, despite significant development efforts and careful planning. McNulty published an update of the earlier works in 2014 in a paper titled '*Plant ramp-up profiles an update with emphasis on process development*'. In the paper he indicates that '*some very carefully developed and executed projects can ramp-up quickly and that owners of new projects should avoid being too pessimistic … if they are certain that they have done their homework*' (McNulty, 2014).

The case of the Albemarle Iron Works

According to available records, the Albemarle Iron Works, consisting of a cold blast furnace, was completed in early 1772, but closed in September of 1772 with no useable iron ever produced. Cold blast furnaces in ironmaking are differentiated from modern blast furnaces as cold air was blown into the furnace – an evolution of the bloomery iron furnace.

In an affidavit by one of the investors about the management problems experienced during the short life of the project the following statement stands out, namely that the Albemarle Iron Works 'were carried on at a very great expense and never produced any profit …' (Brothers, 2001).

From the very beginning, Albemarle was in trouble because of perceived management problems and during a short period in 1771-1772, three of the five partners in the company tried to run the iron works. At that time, the cause of the failure was poorly understood, but certainly, management challenges contributed. Following the closure in 1772, many subsequent attempts were made to produce iron at Albemarle, but without success (Brothers, 2001).

The historical perspectives and the postmortem investigation into the failure of the Albemarle Iron Works are documented by Brothers (2001). The author presents some valuable insights into the true cause of the failure and the investigations highlight the complexities encountered when starting up a project. In the 18th century, iron blast furnaces were among the most expensive and complex businesses of their time and from just the smelting perspective, not much has changed in the 21st century (as demonstrated by the McNulty curves).

The following quote from Brothers (2001) summarizes the challenges faced by the investors well: '*The 18th century iron blast furnaces of the British North American Colonies … required an enormous capital investment both for construction and acquisition of land, required large crews of skilled and unskilled labor, and operated continuously for months at a time. They consumed tons of raw materials, which had to be delivered to a relatively tight schedule, and produced tons of cast iron a day*.'

At the time, blast furnaces were owned by groups of investors, not craftsmen, an thus relied heavily on a diverse group with specialist skills to manage and operate them. Despite the abject failure of the Albemarle project, the investors appeared to have done their homework before setting up their business venture. For example, the site selection for Albemarle Iron Works took two of the partners over seven years to finalize, and on the surface they appeared to have done an excellent job. The selected site was near a river for the water wheels, situated in a well-wooded area for the charcoal, with abundant beds of iron ore in the area. Despite the apparent attention to detail, the company failed during its first year of operation and never produced any usable iron.

In 1882. analysis of ore from the Betsy Martin Mine that supplied the site of iron ore to the ill-fated iron works revealed a high titanium content, the first indications of the possible reasons for the failure of the venture. In 1977 it was established that the ore also contained ilmenite, apatite, and even rare earth oxides. In 1999, slag samples (Figure 5) were recovered from the Albemarle site and evaluated, revealing that the primary cause for Albemarle's failure was indeed the titania content of the iron, which showed there had been a true mismatch between process and due diligence done by the partners and investors (Brothers, 2001; Brothers, Grime, and Swann, 2002). The high levels of titania would have resulted in highly viscous slags with up to 40% titania and relatively high levels of phosphorus. Sadly, even if the plant had adapted their operation like our bloomery ironworkers from the Lowveld, by adding fluxes, the cast iron would have been too brittle due to the high phosphorous content of the ore.

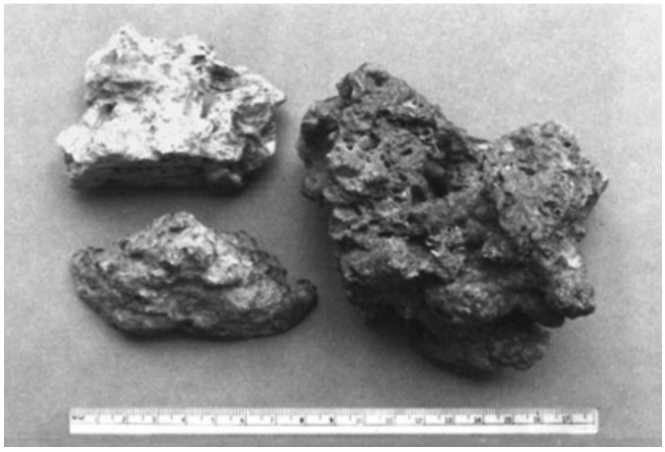

Figure 5—A photograph of three Albemarle slag samples collected from the historical site in 1999. The texture and shading are indicative of poor slag quality (bottom scale 18 cm). The slag is described as containing mottled gray areas, glassy regions, and with a large iron prill visible to the naked eye (reproduced from Brothers, Grime, and Swann, 2002)

The outcomes of the Albemarle Iron Works project, and the subsequent historical and archaeological assessment, comprise an excellent case study of the pitfalls of project development.

Data is not knowledge, and knowledge is not wisdom

Data sciences can be described as a way of knowing. All data does not necessarily lead to knowledge; for data to become useful it needs to be organized or categorized in an appropriate or relevant manner to transform the data into useful information. Information in turn, enables knowledge, of which learning is the primary protagonist.

Relevant knowledge creates connectivity leading to true understanding and insight, which enables the application of data towards achieving a goal or the desired impact. The DIKW framework or pyramid is widely used to represents the relationship between data (D), information (I), knowledge (K), and wisdom (W), and while there are many alternative models or frameworks, the DIKW framework offers a useful way to represent the relationships, and as a result is still widely used. In the DIKW model, each stage is a step towards a higher level, starting with data, and ending with wisdom. Each step answers different questions about the data, increasing the value along the way. The more we enrich data with meaning and context, the more knowledge, and insights we get out of it. Figure 6 shows an expanded version of the DIKW framework and the relationship between data and impact, illustrating the various stages and the relationships well, as visualized by Gapingvoid®.

Historical perspectives or narratives, in the context of publications found in technical journals, conference proceedings, theses, and dissertations, form part of the value chain described in the DIKW model. Technical publications can provide us with a rich collection of case studies, and through the experiences and results described by authors, the good, the bad, and even the ugly, we can enhance our understanding of the nature of current challenges or trends. The words of author Anais Nin: 'We don't see things as they are, we see things as we are', highlight the importance of perspective and context. Both aspects are crucial ingredients of wisdom and insight.

While knowledge ages quickly, wisdom is more unyielding and steadfast, and for now, wisdom is still a uniquely human skill. The pace of innovation has accelerated dramatically over the past 100 years, and the challenges faced by the mining and metals industry require a multidisciplinary and transdisciplinary systems approach. At the rock face or on the processing plant, the fundamentals have not changed. The minerals and the physical properties of the materials we process are the same, but our technologies and our understanding of some of the interactions have advanced considerably.

We sometimes confuse the ability to generate data with generating information and knowledge. If we design our model according to physical properties that are not accurately known or well understood, our models can generate masses of data with little or no value. There are many representations, possible solutions, frameworks, definitions, approaches, and techniques available. Historical insights are one avenue that can help us connect and interpret the appropriate dots, help identify gaps in knowledge, and importantly, help eliminate options from the tsunami of alternatives.

This paper draws not only on publications from the expected fields or disciplines associated with mining, minerals processing, and extractive metallurgy. Publications across various multi- and transdisciplinary fields added significant perspectives to the case studies. This diversity is well aligned with the ever-increasing awareness that problem solving and innovation in industry requires a systems thinking approach. because silo thinking limits potential.

History can offer inspiration via 'an inventory of alternatives' and a future-focused perspective by demonstrating which elements of our present are transient and which are more enduring (Gaynor and Crebbin, 2013).

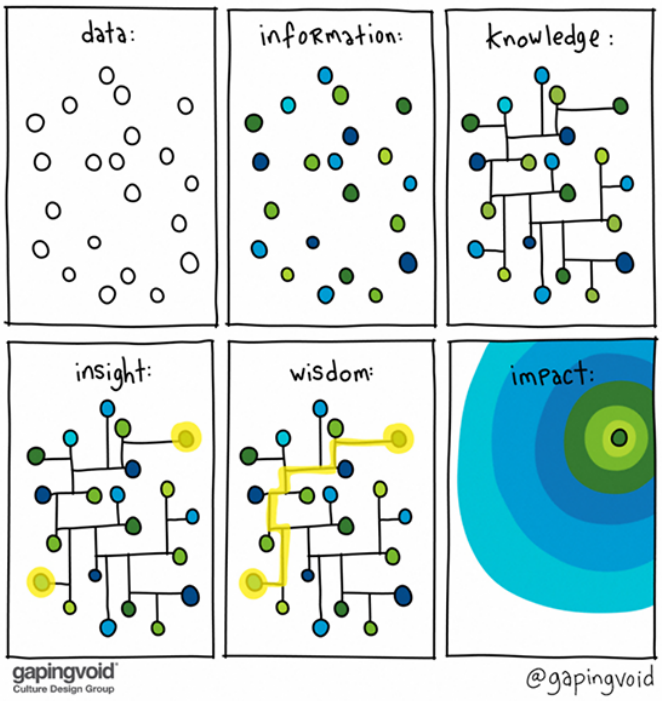

Figure 6—An interpreted representation of the DIKW framework, illustrating the relationships and value addition across the data, information, knowledge, and wisdom value chain (Gapingvoid, 2019)

Conclusions

History can play an important role in how we categorize or organize data at various stages in the value-adding processes when converting data into knowledge and, ultimately, wisdom. History can benefit our understanding of the present and thus enhance future outcomes.

Technical publications can illuminate our thoughts, change our perspectives, or even help us to discover new or alternative ways of thinking which can be used to transform data, information, and knowledge into insight and wisdom.

The growing awareness around ethical and socially responsible processing in the mining and metallurgical industry can be greatly enhanced through the lenses of historical case studies. From successes and failures of the past, it is possible to identify which of the options or choices are the more ethical and socially responsible. Lessons from history can help provide insights into making ethical and sustainable choices in the mining and metallurgical industry.

References

Badmatsyrenova, R. and Orsoev, D. 2005. Origin of titanomagnetite-ilmenite mineralization, Arsentyev gabbro-syenite massif, Transbaikalia, Russia. *Mineral Deposit Research: Meeting the Global Challenge*. Springer, Berlin, Heidelberg. pp. 725–727. doi: 10.1007/3-540-27946-6_184

Bleloch, W. 1949. The electric smelting of iron ores for production of alloy irons and steels and recovery of chromium and vanadium. *Journal of the Chemical, Metallurgical and Mining Society of South Africa*. March. pp. 363–402.

Brothers, J.H. 2001. 'Carried on at a very great expense and never produced any profit': The Albemarle Iron Works (1770-72). doi: 10.21220/s2-psqr-4m85

Brothers, J.H., Grime, G.W., and Swann, C.P. 2002. Albemarle Iron Works (1771-1772): Why did this operation fail? *Nuclear Instruments and Methods in Physics Research, Section B: Beam Interactions with Materials and Atoms*, vol. 189, no. 1–4. pp. 340–343. doi: 10.1016/S0168-583X(01)01083-7

Cawthorn, R.G., Barnes, S., Ballhaus, C., and Malitch, K.N. 2005. Platinum group element, chromium and vanadium deposits in mafic and ultramafic rocks. *Economic Geology 100th Anniversary Volume*. V. 100th Anniversary of the Society of Economic Geologists. pp. 215–249.

Chen, S. and Chu, M. 2014. A new process for the recovery of iron, vanadium, and titanium from vanadium titanomagnetite. *Journal of the Southern African Institute of Mining and Metallurgy*, vol. 114, no. 6. pp. 481–487.

EVRAZ Highveld Steel and Vanadium. 2015. Business tescue. http://www.evrazhighveld.co.za/businessrescue.asp [accessed 18 February 2017].

Fischer, R.P. 1975. Vanadium resources in titaniferous magnetite deposits. *US Geological Survey Professional Paper*. 926-B:1–9.

Gapingvoid. 2019. Data-Information-Knowledge-Insight-Wisdom. https://www.gapingvoid.com/content/uploads/2019/03/data-information-knowledge-insight-wisdom-impact.jpg [accessed 9 September 2021].

Gaynor, A. and Crebbin, G. 2013. What can engineers learn from the past? A potential role for history in engineering education. *International Journal of Engineering, Social Justice, and Peace*, vol. 2, no. 2. pp. 43–54. doi: 10.24908/ijesjp.v2i2.3512

Geldenhuys, I.J. 2017. The exact art and subtle science of DC smelting: Practical perspectives on the hot zone. *JOM*. vol. 69, no. 2. pp. 343–350. doi: 10.1007/s11837-016-2171-z

Geldenhuys, I.J., Akdogan, G., and Reynolds, Q.G. 2021. Towards sustainable processing of vanadium-bearing titaniferous magnetite deposits - an overview of barriers and opportunities. *Proceedings of IMPC2020*. pp. 18–22. http://www.mintek.co.za/Pyromet/Files/2021Geldenhuys.pdf

Habashi, F. 2010. A short history of electric furnaces in iron and steel making. Part 2 Induction and smelting. *Steel Times International*. vol. 34, no. 7. p. 48.

Henry, J., Stephens, W., Blue, D.. and Maysilles, J. 1987. Bureau of Mines development of titanium production technology. http://trove.nla.gov.au/work/152481664

Hukkanen, E. and Walden, H. 1985. The production of vanadium and steel from titanomagnetites. *International Journal of Mineral Processing*, vol. 15, no. 1–2. pp. 89–102. doi: 10.1016/0301-7516(85)90026-2

Ivanic, T.J., Wingate, M.T.D., Kirkland, C.L., van Kranendonk, M.J., and Wyche, S. 2010. Age and significance of voluminous mafic–ultramafic magmatic events in the Murchison Domain, Yilgarn Craton. *Australian Journal of Earth Sciences*. vol. 57, no. 5. pp. 597–614. doi: 10.1080/08120099.2010.494765

Jones, R.T. and Geldenhuys, I.J. 2011. The pros and cons of reductive matte smelting for PGMs. *Minerals Engineering*, vol. 24, no. 6. pp. 495–498. doi: 10.1016/j.mineng.2011.03.007

Kelly, B.F. 1993. Kelly Ironmaking at BHP New Zealand Steel Limited, Glenbrook. New Zealand. *Australasian Mining and Metallurgy: The Sir Maurice Mawby Memorial Volume (2nd edn). Monograph Series* no. 19. Australasian Institute of Mining and Metallurgy, Melbourne.pp. 348–353.

Kelly, K. 2011. What Technology Wants. Penguin Books.

Killick, D. and Fenn, T. 2012. Archaeometallurgy: The study of preindustrial mining and metallurgy. *Annual Review of Anthropology*, vol. 41, no. 1. pp. 559–575. doi: 10.1146/annurev-anthro-092611-145719

Killick, D. and Miller, D. 2014. Smelting of magnetite and magnetite-ilmenite iron ores in the northern Lowveld, South Africa, ca. 1000 CE to ca. 1880 CE. *Journal of Archaeological Science*, vol. 43, no. 1. pp. 239–255. doi: 10.1016/j.jas.2013.12.016

Lepinski, J.A. 2000. Iron by direct reduction. *Kirk-Othmer Encyclopedia of Chemical Technology*. Wiley, Hoboken, NJ. pp. 1–15. doi: 10.1002/0471238961.0918151412051609.a02

Manamela, M.M. and Pistorius, P.C. 2005. Ore size does affect direct reduction of titaniferous magnetite. *Journal of the South African Institute of Mining and Metallurgy*, vol. 105, no. 3. pp. 183–185.

Matyas, A.G., Francki, R.C., Donaldson, K.M., and Wasmund, B. 1993. Application of new technology in the design of high-power electric smelting furnaces. *CIM Bulletin*, vol. 86, no. 972.. pp. 92–99.

Mcnulty, T. 1998. Developing innovative technology. *Mining Engineering*, vol. 50. pp. 50–55.

Mcnulty, T. 2014. Plant ramp-up profiles an update with emphasis on process development. *COM 2014 - Proceedings of the Conference of Metallurgists*. CIM, Montreal.

McNulty, T.P. 2004. Minimization of delays in plant startups. *Improving and Optimizing Operations: Things That Actually Work - Proceedings of the Plant Operators' Forum* 2004. Dowling, E.C. and Marsden, J.J. (eds). Society for Mining, Metallurgy, and Exploration, Inc., Littleton, CO. pp.113–120.

Miller, D., Killick, D., and van der Merwe, N.J. 2001. Metal working in the northern lowveld, South Africa a.d. 1000–1890. *International Journal of Phytoremediation*, vol. 21, no. 1. pp. 01–417. doi: 10.1179/jfa.2001.28.3-4.401

New Zealand Steel. 2017. Ironmaking. http://www.nzsteel.co.nz/new-zealand-steel/the-story-of-steel/the-steel-making-process/iron-making/ [accessed 31 January 2017].

New Zealand Steel. 2018. The History of Ironsand. Available: https://www.nzsteel.co.nz/new-zealand-steel/the-story-of-steel/the-history-of-ironsand/ [2018, December 02].

Pang, K.N., Zhou, M.F., Qi, L., Shellnutt, G., Wang, C.Y., and Zhao, D. 2010. Flood basalt-related Fe-Ti oxide deposits in the Emeishan large igneous province, SW China. *Lithos*, vol. 119, no. 1–2. pp. 123–136. doi: 10.1016/j.lithos.2010.06.003

Peck, D.C. and Huminicki, M.A.E. 2016. Value of mineral deposits associated with mafic and ultramafic magmatism: Implications for exploration strategies. *Ore Geology Reviews*, vol. 72. pp. 269–298. doi: 10.1016/j.oregeorev.2015.06.004

Richards, S.R. and Davies, C.E. 1980. Smelting alternatives for New Zealand titaniferous minerals. *Proceedings of the Annual Conference*, New Zealand. Australian Institute of Mining and Metallurgy, Melbourne.pp. 237–253.

Rohrmann, B. 1985. Vanadium in South Africa. *Journal of the South African Institute of Mining and Metallurgy*,.vol. 85, no. 5. pp. 141–150.

SAIMM. 1981. Minutes of the Annual General Meeting of the South African Institute of Mining and Metallurgy. http://www.saimm.co.za/Journal/v081n09p257.pdf%0A

Smirnov, L.A., Tret'yakov, M.A., and Gladyshev, V.I. 2000. Processing vanadium-bearing and titanomagnetite iron ores. *Metallurgist*, vol. 44. pp. 230–232. doi: 10.1007/BF02466943

Steinberg, W., Geyser, W., and Nell, J. 2011. The history and development of the pyrometallurgical processes at Evraz Highveld Steel & Vanadium. *Journal of the Southern African Institute of Mining and Metallurgy*, vol. 111, no. 10. pp. 705–710.

Taylor, P.R., Shuey, S.A., Vidal, E.E., Wang, W., and Gomez, J.C. 2005. Extractive metallurgy of vanadium containing titaniferous magnetite ores: A review. *Proceedings of the 2005 SME Annual Meeting*. (May). Society for Mining, Metallurgy & Exploration, Englewood, CO. pp. 1–9.

US Geological Survey. 2021. Mineral Commodity Summaries 2021. Reston, VA. ◆

Who is a Competent Person?

T.R. Marshall[1]

Affiliation:
[1]Explorations Unlimited, South Africa.

Correspondence to:
T.R. Marshall

Email:
marshall.tania@gmail.com

Dates:
Received: 12 Nov. 2020
Revised: 1 Jun. 2021
Accepted: 1 Jul. 2021
Published: September 2021

How to cite:
Marshall, T.R. 2021
Who is a Competent Person?
Journal of the Southern African Institute of Mining and Metallurgy, vol. 121, no. 9, pp. 465–468

DOI ID:
http://dx.doi.org/10.17159/2411-9717/1422/2021

This paper was first presented at the *SAMCODES 2020 Conference*, 17 November 2020 Misty Hills Conference Centre, Muldersdrift, Johannesburg, South Africa.

Synopsis

SAMREC (The South African Code for the Reporting of Exploration Results, Mineral Resources and Mineral Reserves) Clause 7 notes that 'Documentation detailing Exploration Results, Mineral Resources and Mineral Reserves from which a Public Report is prepared must be prepared by, or under the direction of, and signed by a Competent Person.' Similar statements with respect to Competent Valuators (CVs) and Qualified Reserves Evaluators (QREs) are contained in the SAMVAL (South African Code for the Reporting of Mineral Asset Valuations) and SAMOG (South African Code for the Reporting of Oil & Gas Resources) codes respectively.
What does it mean to be a Competent Person (CP) in the context of compiling/signing-off on SAMCODE (South African Mineral Code) compliant documents? What do the registration and experience requirements mean? Who is ultimately responsible for the report and what does such responsibility prescribe?

Keywords
Reporting Codes, SAMREC, Competent Person.

Introduction

SAMREC (The South African Code for the Reporting of Exploration Results, Mineral Resources and Mineral Reserves) Clause 7 notes that 'Documentation detailing Exploration Results, Mineral Resources and Mineral Reserves from which a Public Report is prepared must be prepared by, or under the direction of, and signed by a Competent Person (CP).' Similar statements with respect to Competent Valuators (CVs) and Qualified Reserves Evaluators (QREs) are contained in the SAMVAL (South African Code for the Reporting of Mineral Asset Valuations) and SAMOG (South African Code for the Reporting of Oil & Gas Resources) codes respectively.

The definition of a CP is one of the fundamental definitions embodied in the CRIRSCO (Committee for Mineral Reserves International Reporting Standards) template (www.crirsco.com/template.asp), and this paper emphasises that this (CRIRSCO definition) is the only criterion that qualifies an author to sign off on Public Documents under the SAMCODES and/or the jurisdiction of the Johannesburg Stock Exchange (JSE). Various international/regional bodies have different definitions for CPs (for example, the United Nations Framework Classification (UNFC) (UNECE, 2020), the African Mineral and Energy Resources Classification and Management System(UNFC-AMREC-PARC, 2019), and associated Pan-African Reserves and Resources Reporting Code (PARC) definitions) or for persons who are simply deemed competent as per common dictionary definitions. These definitions are not relevant for SAMCODE compliance. Persons who define themselves as CPs in terms of any definition not aligned to the CRIRSCO Template may not necessarily be acceptable to the SAMCODE or the JSE (or, in fact, to any CRIRSCO-aligned Code or reporting jurisdiction). It is incumbent on the individual to be aware of the specific definitions and any additional requirements of the jurisdiction in which they are reporting.

A CP is defined by the SAMCODE in terms of both registration and relevant experience. Both registration and experience criteria are required; one without the other is not acceptable.

While the term Competent Person (*sensu stricto*) is defined in terms of CRIRSCO-type documentation, in this paper mention is made of Competent Valuators (defined in terms of the SAMVAL Code) and Qualified Reserves Evaluators (defined in terms of the SAMOG Code) for completeness, since all of these codes form part of the South African mineral reporting regime (SAMCODE).

Who is a Competent Person?

Registration

For SAMREC/SAMVAL, registration of CPs and CVs is typically defined in terms of statutory bodies (SACNASP, ECSA, SAGC), professional membership (GSSA, SAIMM, IMSSA), SAICA (for SAMVAL), and applicable Recognised Professional Organisations (RPOs). SAMOG registration requires a professional to be in good standing with SACNASP, ECSA, the SPEE, the AAPG (Certified Petroleum Geologist category), and/or a member of any other relevant RPO.

The acronyms used in this section are listed below:

- SACNASP—South African Council for Natural Scientific Professions
- ECSA—Engineering Council of South Africa
- SAGC—South African Geomatics Council
- GSSA—Geological Society of South Africa
- SAIMM—Southern African Institute of Mining & Metallurgy
- IMSSA—Institute of Mine Surveyors of South Africa
- SAICA—South African Institute of Chartered Accountants
- SPEE—Society of Petroleum Evaluation Engineers
- AAPG—American Association of Petroleum Geologists

Statutory Registration

There are currently three South African statutory bodies that are applicable for SAMCODE registration – SACNASP, ECSA, and SAGC.

South African Council for Natural Scientific Professions (SACNASP)

SACNASP has several different registration categories:

- Professional (Pr.Sci.Nat.), which requires a recognized 4-year degree/diploma or equivalent, plus three years' experience (or some 10 years of recognized prior learning (RPL)
- Certificated (Cert.Sci.Nat.), which recognises
  - A 2- or 3-year degree/diploma or equivalent, with less than three years' experience.
  - Some 10 years of RPL.
- Can didate (Cand.Sci.Nat.), which recognizes a 4-year degree or 2- or 3-year diploma or equivalent, with no work experience – effectively a newly graduated geoscientist in training.

The Pr.Sci.Nat. category is the only acceptable category for CP, CV, or QRE sign-off. Certificated Natural Scientists with a 2- or 3-year degree or diploma (or equivalent) may qualify as long as they fulfil the +10-year RPL/work experience criteria.

Engineering Council of South Africa (ECSA)

Likewise, ECSA recognizes two different categories:

- Professional, which comprises the Professional Engineer (Pr.Eng.), the Professional Engineering Technologist, the Professional Certificated Engineer, and the Professional Engineering Technician.
- Candidate (persons who meet the academic requirements for registration in the Professional categories referred to above and who are undergoing professional development). 'Engineers in Training' are the equivalent of 'Candidate Engineers'.

Only the Professional Engineer (Pr.Eng.) category fulfils the registration requirement for CP (and, by extension, CV and/or QRE) status.

South African Geomatics Council (SAGC)

Similarly, surveyors need to be registered in the Professional registration category; technologist, technician or candidate categories are not sufficient.

Professional Membership

Applicable professional/chartered bodies include the GSSA, SAIMM, IMSSA, and SAICA.

No Member/Fellow of the GSSA, SAIMM, or IMSSA may sign off on a publicly released Competent Person Report (CPR) or Competent Valuators Report (CVR) without undergoing the peer review process. This is not applicable for members also registered with a statutory body (e.g. SACNASP, ECSA, or SAGC. This peer review requirement was put in place by the Councils/MANCOs of the professional bodies (GSSA by-law 1.18.4 / SAIMM by-law G). The purpose of the process is to confirm that a person wishing to sign off as a CP/CV satisfies all the requirements of a CP/CV and that their professional status (in terms of appropriate education and relevant experience) has been validated by their professional association – it does not imply competence or proficiency.

In South Africa, all practising geoscientists are required by law to be registered with SACNASP, so this requirement is generally applicable to non-South-African geoscientists wishing to use their GSSA membership to sign off on CPRs. Under specific circumstances, some South African resident geoscientists may not be registered with SACNASP (some academic, research or government geoscientists, for example), but still wish to sign off on Public Reports – they would also be subject to the peer review requirement. South African engineers, in contrast, are not currently legislated to be registered with ECSA. Therefore, many mining engineers signing off as CPs/CVs/QREs may wish to use their SAIMM membership for this purpose.

Members of the GSSA, SAIMM, or IMSSA who wish to sign off on a specific Public Report lodged with any Stock Exchange must submit to this peer review process. This process is to be followed for each public, newly released CPR, or Valuation Report attached to a CPR. Those members wishing to apply for such review should download the relevant application form from the SAMCODES website..

Recognised Professional Organisations

Typical requirements of an RPO are that it should:

- Be a self-regulatory organization covering professionals in the mining and/or exploration industries
- Admit members primarily based on their academic qualifications and experience (*i.e. not purely a learned/ scientific society*)
- Require compliance with the professional standards of competence and ethics established by the organization (*inclusive of a Continuing Professional Development (CPD) programme*)
- Be able to discipline members and have the power to suspend or expel a member (*Code of Ethics/Conduct; Complaints & Disciplinary procedures*).

Notwithstanding the above, the JSE reserves the right, in conjunction with the SAMCODES Standards Committee (SSC), to include additional criteria (for example, to require specific categories of membership or fields of practice) or even waive certain criteria for specific organizations or individual members. Such rights of waiver are applicable to all international reporting

jurisdictions where the relevant stock exchange may impose such additional criteria. It is incumbent upon authors wishing to sign off documents for any other jurisdiction to check the current requirements and specifications on the relevant code/exchange website.

A list of RPOs is posted on the SAMCODES website for reference. Any organization that believes it fulfils the requirements of an RPO may apply in writing to the SSC to be included in this list.

Experience

All of the Codes require relevant experience in addition to registration.

- SAMREC requires that a CP must have a minimum of five years *relevant* experience in the style of mineralization or type of deposit under consideration, and in the activity which that person is undertaking (for example, exploration, Resource estimation or Reserve estimation).
- SAMOG requires that a QRE have a minimum of ten years' practical experience in petroleum engineering, geology, or geophysics, with at least three recent years of such experience in the evaluation of Reserves and Resources.
- SAMVAL, in contrast, simply states that the CV needs *sufficient* relevant experience in valuing mineral assets; listing instead a set of specific competencies and occupational tasks that the CV needs to be able to master (Appendix B of the 2016 SAMVAL Code).

Responsibilities of the CP

1. Persons called upon to sign as a CP must be clearly satisfied in their own minds that they are able to face their peers and demonstrate competence in the commodity, type of deposit, and situation under consideration. It is fundamental to understand that the SSC (or any of the SAMREC, SAMVAL, or SAMOG Code Committees) does not confer competence on anyone. Just completing a SAMCODE workshop/course does not mean that an individual is competent – this simply means that they should have the tools to understand what is required for SAMCODE compliance. There are no 'competency exams'; such competence is claimed by the author subject to the provision that the author may be called on by their peers to demonstrate their competence. There is also no list of approved CPs or CVs held by the SSC, the professional/statutory bodies, or the JSE.
2. If a lead CP is appointed, it is important that they accept overall responsibility for a Mineral Resource or Mineral Reserve report that has been prepared in whole or in part by others and are satisfied that the work of the other contributors, who may be CPs in their own right, is acceptable and that the constituent parts of the Report have been signed off by such contributors. It is not necessary that the lead CP be classified as a CP in each of the aspects contained in the report. It is, however, necessary for him/her to have sufficient background in all of the aspects covered in the report to be able to take overall responsibility for the document.
3. Facing one's peers does not mean always being in agreement. It is understood that authors will always have different backgrounds, abilities, and experience and that personal preferences will also come into play in the estimation and/or valuation of Mineral Resources/Reserves. However, the concept of 'reasonableness' should hold sway in cases of disagreement between CPs. In this context, reasonableness means that other appropriately qualified and experienced professionals with access to the same information, as of the same effective date, should arrive at a broadly comparable result. A 'reasonableness test' serves to identify estimations or valuations that may be out of step with industry standards or norms.
4. SAMREC Sections 7-11 (under the heading 'Competence and Responsibility') detail the requirements for the author of a Public Report or CP. Nowhere in these sections is allowance made for the CP to devolve his/her responsibility to the commissioning entity (if they are not the same). A company (the commissioning entity) may have an agreement with the CP (whether as a consultant or an employee) to provide administrative and technical assistance, reviews, and as well as legal support for any public document authored under their name, but that does not abrogate the professional responsibility of the CP.

All professional/statutory bodies also note that any complaints in respect of a Public Report are made against a member of that body (not against a company), indicating that the responsibility for the Public Report lies with the author/CP. They retain that responsibility even if they should leave the company and join another (or even retire). There is no prescription for responsibility for a Public Report.

The South African Companies Act (Act 71 of 2008) notes that the final responsibility for any statement signed, consented to, or authorized by the Board of Directors is the responsibility of the Board or the specific signatory.

References

ECSA. 2020. Registration Categories. Engineering Council of South Africa. https://www.ecsa.co.za/register/SitePages/Registration%20Categories.aspx

GSSA. 2018. Constitution & ByLaws. Geological Society of South Africa, Johannesburg.

South African Government. 2020. SA Companies Act 71 of 2008. https://www.gov.za/documents/companies-act

SACNASP. 2020. Requirements for Registration. South African Council for Natural Scientific Professions. https://www.sacnasp.org.za/requirements-for-registration

SAGC. 2020. Registration.: https://sagc.org.za/4regnotesprof.php

SAIMM. 2018. Constitution & By-Laws 2013, as ammended. Southern African Inetitute of Mining and Metallurgy, Johannesburg.

SAMCODES. 2020. Recognised Professional Organisations. https://www.samcode.co.za/samcodes-standards-committee-ssc/rpos

SAMOG. 2016. South African Mineral Code for the Reporting and Valuation of Oil & Gas Deposits. SAMCODES Standards Committee, Johannesburg.

SAMREC. 2016. The South African Code for the Reporting of Exploration Results, Mineral Resources and Mineral Reserves. SAMCODES Standards Committee, Johannesburg.

SAMVAL. 2016. The South African Code for the Reporting of Mineral Asset Valuations. SAMCODES Standards Committee, Johannesburg.

UNECE. 2020. United Nations Framework Classification for Resources (Update 2019). Geneva. https://www.unece.org/fileadmin/DAM/energy/se/pdfs/UNFC/UNFC-Guidance-Notes/Guidance_Note_on_Competent_Person_Requirements_and_Options_for_Resource_Reporting

UNFC-AMREC-PARC. 2019. African Mineral and Energy Resource Classificaton and Management System (UNFC-AMREC); Draft Version 8.0 (31 August 2019). African Union, Addis Ababa. ◆

Obituary: Henry Edward James

Henry Edward James was born in Parys on 19 April 1939, and was educated at Grey College in Bloemfontein. He completed high school there in 1956. He spent a year with Gold Fields working at Libanon and Venterspost gold mines before going to the University of the Witwatersrand on a Chamber of Mines bursary to study chemical engineering. After graduating in 1961 with a BSc degree, he was awarded a postgraduate bursary by the Atomic Energy Board (AEB), which led to an MSc degree in chemical engineering from the same university. The subject of his thesis was 'The dynamic response of a packed tower to step changes in the concentration of the inlet gas for a single-phase gas and countercurrent gas-liquid flow'. In 1964, Henry began his professional career as a research officer with the Extraction Metallurgy Division of the AEB.

It was around this time that Henry met the love of his life, a secretary who was employed at the National Institute for Metallurgy (NIM), Joan Barnes. Joan had undertaken the typing of Henry's MSc dissertation outside working hours. Henry and Joan were married on 4 September 1965, and went on to enjoy just over 50 years of married life together.

From 1965 to 1969, Henry was chief investigator of a collaborative project between the AEB, the Nuclear Fuels Corporation of South Africa (NUFCOR), and the French Atomic Energy Commission (CEA) on the production of uranium tetrafluoride (UF_4) from South African uranium concentrates in a high-temperature moving-bed reactor. During that period, he spent six months in France supervising test work at the Le Bouchet refinery of the CEA. The project culminated in the installation of a full-scale UF_4 reactor at NUFCOR works.

This was a very happy period for the young married couple, who got to see the sights and experience life in France for a while. Henry and Joan lived in Paris from June to November 1966, staying at the Hotel St Jacques, Rue Des Ecole, two blocks away from Sorbonne University.

From 1969 to 1971, Henry was chief investigator of a collaborative project between the AEB and NUFCOR on the techno-economic feasibility of establishing a commercial plant in South Africa for the production of uranium hexafluoride (UF_6) from UF_4. He was responsible for assessing overseas technology for the production of UF_4 and UF_6, with a view to selecting the optimum process route for South African conditions, and for gathering capital and operating cost information on complete process routes from the collection of ammonium diuranate slurry at the gold mines to the export of nuclear-grade UF_6.

Henry was the author of the final feasibility report submitted to an ad hoc committee of the AEB Board and representatives of the uranium industry. In 1971, Henry was appointed Deputy Director of the Extraction Metallurgy Division of the AEB, and from1971 to 1975 was involved in a supervisory capacity in the design, construction, and erection at Pelindaba of a large pilot plant for the production of UF_6 as feed material to the enrichment pilot plant of the Uranium Enrichment Corporation of South Africa.

In 1976, he was promoted to Director of the Extraction Metallurgy Division, and assumed responsibility for a wide range of research programmes in the field of uranium extraction. These were undertaken on a collaborative basis by the AEB, the National Institute for Metallurgy (NIM), and mining companies with interests in uranium production. One of the most successful projects undertaken during the period 1976 to 1980 was the transfer to industry of the technology associated with the recovery of uranium from unclarified Witwatersrand acid-leach liquors in the NIMCIX continuous upflow fluidized-bed ion-exchange contactor. The contactor was adopted by a number of mining companies for new full-scale uranium plants built between 1977 and 1980.

In 1978, Henry was invited by the International Atomic Energy Agency (IAEA) to chair a Consultants Panel charged with the task of writing a textbook on the extractive metallurgy of uranium. This book was published by the IAEA in 1980 under the title 'Significance of mineralogy in the development of flowsheets for processing uranium ores'. The project led to the establishment of an International Working Group on Uranium Extraction under the joint aegis of the IAEA and the Nuclear Energy Agency of the Organisation for Economic Co-operation and Development. Henry played an important role in defining the objectives of the Working Group and, as chairman from 1978 to 1980, guided its activities during its formative years. The most significant achievement of this Working Group was the publication in 1983 of a comprehensive book on the extractive metallurgy of uranium, entitled 'Uranium Extraction Technology'.

In 1980, he was appointed a Vice President of NIM, now Mintek. His duties as a member of Mintek's top-management team included responsibility for the policy aspects of manpower planning, development, and training; responsibility for safety at Mintek in terms of the Mines and Works Act; and responsibility for the Technical Services Division and the newly formed Techno-economics and Information Division, which undertook a wide range of projects in the area of techno-economics and provided services with respect to computerized information retrieval, publishing, conference organization, and public relations for Mintek. Another highlight of Henry's career was the Mintek 50 celebratory conference in 1984 that he managed so successfully. Henry made an invaluable contribution to the growth and development of what is one of the world's largest and leading research and development organizations.

Henry was registered as a Professional Engineer, and was elected as a Fellow of SAIMM on 20 February 1976. He first became a Council Member of the Institute in 1978/1979. One of his most difficult tasks on Council was his chairmanship of the Technical Programme and Publications Committee for the 12th CMMI Congress, which was held in 1982. The proceedings ran to two volumes and comprised more than a thousand pages.

Henry became President of SAIMM in 1985. His Presidential Address was entitled 'In search of a new development strategy for the beneficiation and export of South Africa's minerals'. This paper can be found at https://www.saimm.co.za/Journal/v085n09p309.pdf

Dr Louw Alberts (a past President of Mintek, and later Director General of the Department of Mineral and Energy Affairs) described the presentation as providing 'a wide-ranging yet very knowledgeable insight' into 'probably the most important topic that could be selected' for discussion on an SAIMM platform, covering 'the challenges required for a fuller exploitation of our most important natural resources in this country'. He described Henry as 'someone whom I have known for many years as an indefatigable enthusiast and worker in the fields that concern this Institute', and said that 'the address was presented with clarity and a thoroughness typical of the speaker and the research organization that he represents'.

Henry and Joan James felt privileged to attend the annual Banquets and annual Council dinners of SAIMM on a regular basis from 1985 to 2015 (30 years). These events not only became highlights in their social calendar but, more importantly, led to the building of enduring friendships with SAIMM members and their spouses. Because the SAIMM Banquet is generally held on the first Saturday evening of March, there were many occasions when the date fell on or very near to Joan's birthday.

Henry was awarded Honorary Life Fellowship of SAIMM on 23 June 1995.

Henry and Joan have two sons, Marc (1969) and Darrell (1974). In turn, Darrell and his wife Amanda (Mandy) (nee Gilman) also have two sons, Michael (2010) and Ethan (2015). Henry's grandsons were his pride and joy, and he loved showing pictures of them to his friends. Henry had a deep love for his family, and enjoyed exploring and documenting his family history.

Henry passed away on Friday 1 October 2021 at the age of 82.

Henry James is appreciated for his experience, his approach to problems, and his ability for hard work. He was admired for the way in which he cared about other people, and the genuine interest he showed in so many subjects. He was always an interesting person to talk to. He was a very fine man, and will be missed greatly.

R.T. Jones

Density: Bulk *in-situ* or SG?

K.G. Lomberg

Affiliation:
[1]Pivot Mining Consultants, South Africa.

Correspondence to:
K.G. Lomberg

Email:
ken@pivotmining.co.za

Dates:
Received: 12 Nov. 2020
Revised: 18 Jul. 2021
Accepted: 8 Oct. 2021
Published: September 2021

How to cite:
Lomberg, K.G. 2021
Density: Bulk *in-situ* or SG?
Journal of the Southern African Institute of Mining and Metallurgy, vol. 121, no. 9, pp. 469–474

DOI ID:
http://dx.doi.org/10.17159/2411-9717/1423/2021

This paper was first presented at the *SAMCODES 2020 Conference*, 17 November 2020 Misty Hills Conference Centre, Muldersdrift, Johannesburg, South Africa.

Synopsis

The density used to covert volume to tons is critical in determining the real *in-situ* tonnage of Mineral Resources. However, the methods used to determine density and the use of different technical terms are seen to be inconsistent throughout the industry. Probably the best discussion addressing the determination of density was presented by Lipton (2001). This paper does not try to replicate this excellent work, but rather to review current industry practice and present a comparison of the approach to density in public reporting. Some of the technical terms used in reporting and the common methods applied are also discussed.

Keywords
resource estimation, reporting, density measurement.

Introduction

While bulk density is a significant and critical component of a Mineral Resource estimation as it is a determinant of tonnage and metal content, it does not always get the same level of scrutiny as other data applied to the Mineral Resource estimation process. In the same way that a reliable estimate of grade is dependent on validated quality data and the use of a suitable and appropriate estimation methodology, so too is the appropriate estimation of the *in-situ* bulk density required. The underlying perceptions are that the *in-situ* bulk density is either not a critical factor, can easily be measured, or is constant in the deposit. None of these perceptions are true.

The Competent Person needs to understand the deposit, the need for density measurements, and the most appropriate method to apply to ensure that sufficient measurements are made to accurately estimate the density of the Mineral Resource. The aim of this paper is to highlight the important aspects of density and bulk density determination to provide the Competent Person with a reference as to the importance of density and how to apply it to Mineral Resource estimations. The paper does not provide the extensive details pertaining to the methods of density determination, as these have been previously published *e.g.* Lipton (2001), Lipton and Horton (2013).

Importance of *in-situ* bulk density

Dominy, Noppe, and Annels (2002) note that a Mineral Resource estimate should integrate a number of different facets, including:

- Geological data collection (drilling, mapping, *etc.*)
- Geotechnical data collection
- Sampling and assaying
- Bulk density determination
- Geological interpretation and modelling
- Grade/tonnage estimation
- Validation
- Resource confidence classification and reporting.

Each of these activities is associated with a level of inherent risk. Some of the risk can be mitigated if the right data is available and the appropriate estimation methodology is followed. It is noted that bulk density is one of the eight items highlighted and should be regarded and treated with the same level of diligence applied to the 'sampling and assaying' process.

Density: Bulk *in-situ* or SG?

A review of many mine reports, Competent Persons Reports, and Technical Reports compiled in accordance with NI 43-101 shows that the attention to detail in respect of bulk density is often absent. To demonstrate this very poor approach to density, a study of 50 Technical Reports filed on the System for Electronic Document Analysis and Retrieval (https://www.sedar.com/; SEDAR) was undertaken by Arseneau (2013). The results are represented in Table I and Figure 1. It was concluded that although sample density data is collected, it is seldom analysed or discussed in much detail when generating a robust and supportable estimate of the bulk density. Only 20% of the reports reviewed utilized a density-specific data-set with the data being used to estimate the density independently for each block of the block model, while 18% of the reports reviewed did not discuss density at all. Some 58% of these documents reported a simple average density value, not taking the distribution of the data into consideration. These statistics emphasise the lack of importance attributed to density in the reports reviewed.

The importance of bulk density is also noted as it is included in the CIM Mineral Exploration Best Practice Guidelines (CIM, 2018) and The AusIMM Guide to Good Practice Monograph 23 (AusIMM, 2001). The CIM Mineral Exploration Best Practice Guidelines not only includes a specific section on bulk density measurement, but also emphasise the need to have representative samples at appropriate intervals for the determination of the bulk density. Similarly, the AusIMM Monograph 23 includes a chapter on bulk density – the paper by Lipton (2001) that has become the reference paper for bulk density measurement as it relates to Mineral Resource estimation. This paper highlights the frequent lack of attention to the accurate determination of bulk density, the factors that affect the measurements, and provides guidelines on how to measure bulk density.

Bulk density *vs* specific gravity

The *in-situ* bulk density is the density of the material as it occurs naturally, including all the pore spaces, voids, alteration, oxidation, intrusions *etc.* Clearly, the density determined on relatively small samples will likely not incorporate these features which contribute to void and variability (Dominy, Noppe, and Annels, 2002). Typically, the density measured also needs to include the drying of the sample and/or the determination of the moisture content of the sample, since for Resource Estimation purposes a dry density is required. The dry *in-situ* bulk density is the density of the material when the water has been removed from the pores and voids of the material. The logic is that the density (and tonnage) for the Resource Estimate should be at the same moisture basis as the grade (typically dry), so that when the metal content is calculated there is not fictious metal calculated from differences in moisture content. In contrast to the density required for metalliferous deposits, the *in-situ* bulk density for coal deposits is reported inclusive of the water (Preston and Sanders, 1993), while tonnage and quality (assay) data for coal is generally calculated and reported to a variety of moisture contents (*in situ*, air dry, as received, as delivered, and even 'bone dry').

Specific gravity or relative density is the relative density or ratio of the density of the material compared to water at 4°C and is reported as a dimensionless number. The specific gravity does not take account of the pore spaces, voids, alteration, oxidation, intrusions *etc*. Measurements are typically made in the laboratory on samples collected, dried, and crushed, thus ignoring the *in-situ* bulk density requirement. Specific gravity is the appropriate measurement for metals and minerals when it may actually be equal to relative density, or may be thought of as the particle density (see also the pycnometer test). This is in distinct contrast to the case of natural rock samples which include various sources of voids.

What must be measured

The method of bulk density determination is often overlooked, but should be regarded as important as the assay technique

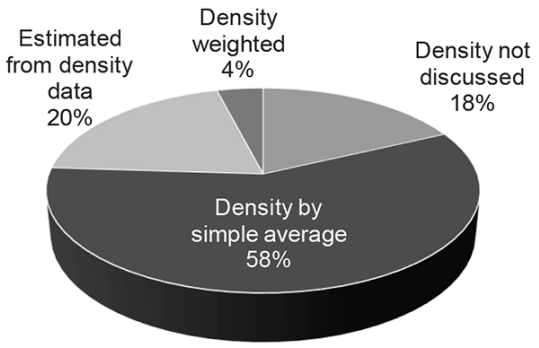

Figure 1—A summary of how density was reported in 50 SEDAR reports (Arseneau, (2013)

Table I

A summary of the approach to density in 50 SEDAR reports (Arseneau (2013)

Report type	Deposit type	Density not discussed	Density by simple average	Estimated from density data	Density weighted	Density as percentage of assay data
MRE	Precious metal	4	14	4	0	14%
PEA	Precious metal	0	2	0	0	3%
PFS	Precious metal	3	1	1	0	3%
MRE	Base metal	0	3	3	0	11%
PEA	Base metal	0	1	0	2	49%
PFS	Base metal	0	0	1	0	100%
MRE	Porphyry	1	4	1	0	5%
PEA	Porphyry	1	0	0	0	0%
MRE	Rare metal	0	4	0	0	24%
		9	29	10	2	23%

MRE - Mineral Resource Estimate
PEA - Preliminary Economic Assessment
PFS - Pre-Feasibility Study

used (Abzalov, 2013). The density of representative samples should be measured and recorded at appropriate intervals, using a method appropriate for the sample material. The determination used should recognize the type of material and mitigate the characteristics of the samples – core, drill chips, underground channel samples *etc*. Even a few per cent error in the bulk density determination could result in a significant change in the economic viability of the project or mine, particularly if it is a marginal project/mine. A fundamental understanding of what must be measured should be the basis for the method of measurement. The dry *in-situ* bulk density needs to be determined and reported as tons per cubic metre (t/m^3).

Methods of measurement

Due to the economic limitations of acquiring data, sophisticated estimation and interpolation methods to estimate the characteristics such as *in-situ* bulk density of the material are used based on sample density data occurring at known data-points. Importantly, the data at the known points must be reliable and measure the required parameter. If the wrong density measurement is made, or the data from different points is measured incorrectly because of variations in the deposit, methods of measurements, or poor moisture corrections, the interpolation between these points will not be valid. An assessment of the likely bias in sample selection for more solid sticks of core and the possible contribution of voids in the bulk rock mass also need to be considered and discussed in any bulk density estimate and reporting.

The use of a prescriptive approach to the method of density determination is not advocated (Lipton, 2001). It is noted that a deposit is seldom going to have a homogenous density, and this will change with the rock type, rock thickness, weathering, and oxidation encountered. The choice of methods of density determination for a particular deposit or project will depend on the physical characteristics of the mineralization, the type of samples that are available or may reasonably be collected, the equipment that is available, and the stage of advancement of the project (Lipton, 2001). The guiding premise should be that determination of the bulk density of the deposit and adjoining non-mineralized material is as important a part of the evaluation programme as determination of the volume or the grade of mineralization. Suitable Quality Assurance/Quality Control (QA/QC) procedures should be established to monitor and correct for anomalous readings and maintain a high-quality data-set. Lipton (2001) and Lipton and Horton (2014) present extensive guidance on sample collection and preparation, and measurement of sample density for use in bulk density estimates.

To accurately measure the sample density the volume and mass need to be accurately determined. As the samples being tested are generally small, the accuracy of measurement is very important. The most reliable material for the determination of sample density is core samples. However, the core may be inhomogeneous or more porous than expected, and this may lead to a bias in the selection of solid lengths of core or the incorrect application of a density measurement. Various methods could be used for density measurement, as described below.

Calliper

The volume of core is measured physically after dressing the core to represent a cylinder as closely as possible. The ends are cut square and the measurements made with precision devices such as simple outside callipers and Vernier callipers. The calliper method measures the dimensions of the core. This is potentially inaccurate as the core may not be regular in shape, with small variations is diameter as well as irregular ends. The method is very simple but depends on the ability to accurately dress the core to the shape of a cylinder. The mass is also relatively simple to determine, although care is required to ensure that the sample is dry before determining the dry bulk density.

Pycnometer

The advantage of this method is that the volume of an irregular sample can be determined directly. Gas pycnometers determine the volume by calculating the pressure change resulting from the displacement of gas by a solid object. Pycnometry is a very accurate method for the measurement of the density of a solid. As geological samples are pulverized before using a pycnometer the fabric of the rock is destroyed and any voids, pore spaces *etc*. are eliminated, making the pycnometer method generally unsuitable for the measurement of bulk density. Commonly, field geologists obtain details of laboratory procedures and select the density determination without consideration of the methodology used. This is on occasion a result of not having suitable equipment on site to accurately measure the bulk density and so relying on the laboratory to provide the necessary results.

Water displacement

Water displacement methods are very practical ways to determine bulk density as they overcome the most difficult requirement; that of determining the volume of an irregular shape, by measuring the volume of water displaced when the sample is immersed in water. There are a number of variations to the basic method depending on the physical characteristics of the sample, the porosity of the sample, the necessity to seal the sample, and the available equipment. Lipton (2001) presents six methods for the determination of sample density using water displacement. Commercially available equipment has made this method relatively simple to use. Generally, the core lengths are in the order of 10–20 cm, however larger equipment may allow longer sample lengths to be tested.

The method is based on the Archimedes Principle as the submerged sample experiences an upward force equal to the weight of fluid it displaces. In practice water is the best fluid to use. The volume is thus the difference of the weight of the sample as measured in water and as measured in air.

Practical aspects that should be considered are the nature of the sample, the water (composition and temperature), and air pressure. The accuracy of the measured density will depend on the ability of the water to infiltrate through any open pores/fractures within the samples structure. Of most significance is the nature of the sample and specifically whether there are voids, or if the sample is porous and permeable. Some preparation may be required such as the application of a wax or a quick-drying spray to seal the sample. The sample is weighed and then dipped in molten wax, and once dried, weighed again. Wrapping with clingwrap has been shown to change the buoyancy of the sample, which would affect the density measurement (Lipton and Horton 2014). The effect of temperature on the density of water is very small (Capano, 2000). Changes in temperature of the sample may produce measurable changes in its density because of volume changes in the sample (Capano, 2000). The effect of changes in atmospheric pressure is negligible (Capano, 2000). The density

of the water may be influenced by dissolved solids such as salt (seawater has a density of 1.02–1.05 t/m³). The use of pure water is therefore recommended. As for metalliferous deposits the dry bulk density is required, the contained moisture needs to be driven off prior to the density determination, or measured so that the dry density can be calculated.

Pycnometer vs water displacement methods

Jarman (2011) evaluated three different data-sets to demonstrate that there is a significant difference between the pycnometer and water displacement methods of sample density determination (Figure 2). The measurements are for the most part above the line that would indicate that the Archimedes and pycnometer values are the same, *i.e.* the pycnometer determination is higher than the real value. The differences showed that the pycnometer determined a bulk density higher by 5.28%, 5.55%, and 4.92%. This is in line with other determinations such as 7% for Eland Palatium Mine (Lomberg *et al.*, 2004) and 2% for Union mine (de Vries, 2013).

Density of tailings storage facilities

As tailings storage facilities (TSFs) and waste dumps are frequently re-mined, the determination of the density is important when considering the feasibility of the operation. Tailings densities are notoriously difficult to determine as the material has been dumped and, depending on the size distribution, includes voids. Tailings dumps are effectively dams filled with fine-grained material. The surface may be dry but immediately below the surface the material will be wet. The density determination poses many issues as the material can seldom be recovered without the drill-hole or excavation caving in or collapsing. The density is also expected to change with depth and position on the TSF, with the centre being finer graded than the perimeter. These aspects must be considered when selecting the method of bulk density determination.

It is generally best to determine the density on site by excavating a hole and measuring the volume directly. The weight can be determined by appropriate means, including a scale or weighbridge, depending on the size of the sample. The density will need to be corrected for moisture content.

A small hole (30 x 30 x 30 cm) on the surface with defined dimensions may be excavated and the material weighed on site with the moisture content, or alternatively the sample may be sealed, and the weight determined prior to drying of the material to determine the moisture content and thus allow the calculation of the dry bulk density. The hole should not be too big or else weighing the material is a potential problem. The hole dimensions can be determined by measurement, or the volume determined directly by lining with plastic/latex and filling with water.

Reliable dry bulk density database

The Competent Persons responsible for Mineral Resource estimation must ensure that the bulk density is reliable and robust. They must ensure that the sampling methodology is sound and appropriate for the deposit, that the process is overseen, and that various QA/QC procedures are implemented, and provide a discussion on the estimation of the bulk densities from the sample density results. If the determination of the dry sample density is included in the assay request form without any consideration to the method used and its implication, the final results may be compromised. It is suggested that a moisture determination is also made to assess the degree of drying, given that the dry bulk density is expected to be on the same basis as the dry assay grades.

It is expected that there will be some variability of bulk density within the volume that is being estimated. The variability is deposit-specific and may be complicated by the delineation of estimation domains, rock types, alteration, structural features, and degrees of weathering. Weathering or alteration, for instance, are likely to decrease the rock bulk density and increase the porosity. This may result in high variability in the host rock bulk density that will require the appropriate method of data collection, sample preparation, and proper attention when estimating the bulk density.

Typical hard rock bulk density values for *in-situ* deposits range from 1.8 t/m³ to 5 t/m³. An assessment of the database to ensure that there are no outliers is important. Outliers may be the result of transcription errors or faulty equipment. If the deposit being assessed is a TSF or dump, the range will be considerably different.

In some instances, such as iron ore deposits, it is necessary to determine the relationship between the haematite/magnetite and the bulk density as the iron content is the major component of the rock (> 50%). A regression curve may be used to determine the relationship (Figure 3). A similar approach is frequently applied between ash content and density for coal deposits.

Conclusions

Bulk density is an essential and critical component of a Mineral Resource estimation as it affects the determination of asset value through the calculation of tonnage and metal content. The sample-related data used for the dry bulk density determination and the methods used to measure and model the variably of the dry bulk density are seldom presented at the same level of detail or confidence as grade data, as the databases are frequently very different. It is stressed that density must be seen as a variable with the same status as a grade, given its use in estimating tonnage and contained metal.

The use of a prescriptive approach to the method of density determination is not advocated for deposits which have been drilled out with core drill-holes, provided an appropriate method is applied with referenced results. It is advocated that the choice of method(s) for determining the bulk density of a particular deposit is the responsibility of the Competent Person and will depend on the physical characteristics of the mineralization, rock types/characteristics, and the available sampling equipment.

References

Abzalov, M.Z. 2013. Measuring and modelling of dry bulk rock density for mineral resource estimation. *Transactions of the Institutions of Mining and Metallurgy: Section B. Applied Earth Science*, vol. 122, no. 1. pp. 16–29.

Arseneau, G.J. 2013. Estimation of bulk density for mineral resource reporting. Internal SRK Report

AusIMM. 2001. Mineral Resource and Ore Reserve estimation – The AusIMM guide to good practice. Edwards, A.C. (ed.). *Monograph* 23. Australasian Institute of Mining and Metallurgy: Melbourne.

CIM. 2018. Mineral Exploration Best Practice Guidelines. Prepared by the Canadian Institute of Mining, Metallurgy and Petroleum (CIM) Mineral Resource and Mineral Reserve Committee. Adopted by CIM Council November 23, 2018. Montreal.

Dominy, S.C., Noppe, M.A., and Annels, A.E. 2002. Errors and uncertainty in mineral resource and ore reserve estimation: The importance of getting it right. *Exploration and Mining Geology*, vol. 11, no. 1-4. pp. 77–98.

Density: Bulk *in-situ* or SG?

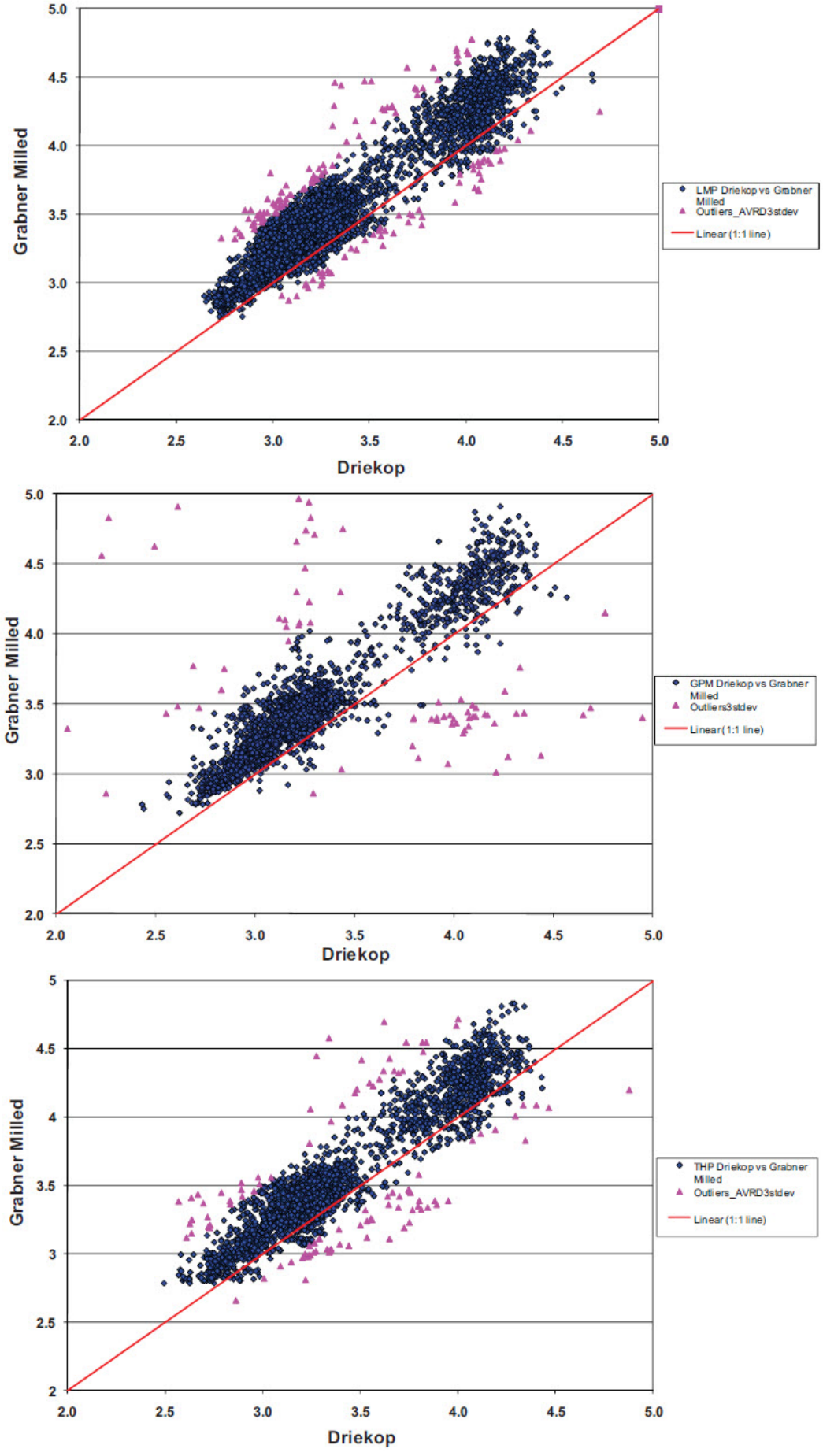

Figure 2—Graphical representation of the difference between pycnometer (y-axis – t/m³) and water displacement methods (x-axis – t/m³) (Jarman, 2011)

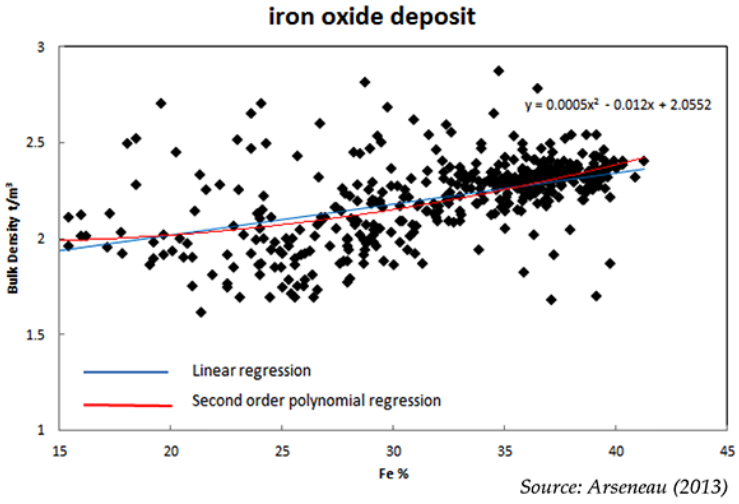

Figure 3—A typical regression curve for an iron ore deposit (Arseneau, 2013)

JARMAN, D.J. 2011. Comparison of rock density determination methods used in South African platinum mines for resource planning purposes. MSc thesis, University of Pretoria.

LIPTON, I.T. 2001. Measurement of bulk density for Resource Estimation. *Mineral Resource and Ore Reserve estimation – The AusIMM guide to good practice.* Edwards, A.C. (ed.). *Monograph* 23. Australasian Institute of Mining and Metallurgy, Melbourne. pp. 57–66

LIPTON, I.T. and HORTON, J.A. 2014. Measurement of bulk density for resource estimation – methods, guidelines and quality control. *Mineral Resource and Ore Reserve Estimation – The AusIMM Guide to Good Practice*. 2nd edn. *Monograph* 30. Australasian Institute of Mining and Metallurgy: Melbourne.

PRESTON, K.B. AND SANDERS, R.H. 1993. Estimating the *in situ* relative density of coal. *Australian Coal Geology*, vol 9. pp. 22–26. ◆

Decoupling the effects of alteration on the mineralogy and flotation performance of Great Dyke PGE ores

T. Dzingai[1], B. McFadzean[1], M. Tadie[2], and M. Becker[1]

Affiliation:
[1]Centre for Minerals Research, Department of Chemical Engineering, University of Cape Town, South Africa.
[2]Department of Process Engineering, University of Stellenbosch, South Africa.

Correspondence to:
M. Becker

Email:
megan.becker@uct.ac.za

Dates:
Received: 18 Jan. 2021
Revised: 15 Jul. 2021
Accepted: 22 Jul. 2021
Published: September 2021

How to cite:
Dzingai, T., McFadzean, B., Tadie, M., and Becker, M. 2021 Decoupling the effects of alteration on the mineralogy and flotation performance of Great Dyke PGE ores.
Journal of the Southern African Institute of Mining and Metallurgy, vol. 121, no. 9, pp. 475–486

DOI ID:
http://dx.doi.org/10.17159/2411-9717/1487/2021

ORCID:
M. Becker
http://orcid.org/0000-0002-7025-137X

M. Tadie
http://orcid.org/0000-0003-3111-5188

Synopsis

Ores from a single deposit may exhibit extensive variability in their mineralogy and texture. The ability to quantify this variability and link it to mineral processing performance is one of the primary goals of process mineralogy. This study focuses on the effect of alteration in three platinum group element ore samples from the Great Dyke in Zimbabwe – two of which were more pristine compared to the third, which was locally classified as 'oxidized' ore. These ores are known to be characterized by varying degrees of alteration, resulting in numerous challenges in flotation and affecting both grade and recovery. Alteration, by near-surface oxidation, of the valuable base metal sulphides and platinum group minerals resulted in lower flotation recoveries of Cu, Ni, Pt, and Pd. Evidence of incipient oxidation was more readily observed in the base metal sulphide assemblage than the platinum group mineral assemblage, even though the loss in recovery (because of oxidation) was most significant for Pd. Alteration through hydration resulted in a significant increase in mass pull and dilution of concentrate grade through the inadvertent recovery of naturally floating gangue comprising composite orthopyroxene and talc particles. In this study, the amount of naturally floating gangue was more strongly correlated with the talc grain size distribution than the grade of talc in the flotation feed. The oxidation and hydration alteration reactions are not necessarily mutually exclusive, although one may be more dominant than the other, giving rise to ore variability.

Keywords
Process mineralogy; platinum ores; hydration; oxidation; alteration; naturally floating gangue.

Introduction

The ability to manage ore variability is a major challenge faced by the mining industry at present. Many existing plants cannot necessarily deal with ore variability since their design specifications have historically focused on averaged ore characteristics (*e.g.* Powell, 2013). As design flexibility is not always an option for existing plants, the need for optimization of these operations based on process mineralogy is increasing (Lotter *et al.*, 2011, 2018; Baum, 2014). The major contributors to ore variability include hydrothermal alteration, oxidation, and weathering of a pristine ore deposit. The alteration of sulphide minerals by oxidation can lead to reduced recoveries of valuable minerals (Evans, 2002; Oberthür *et al.*, 2013; Sefako, Sekgarametso, and Sibanda, 2017). There is, therefore, a need for an understanding of the mineralogical aspects of ore variability, especially those arising from alteration, and the consequent assessment of how it can be managed. Some of the ways of managing ore variability include ore sorting, stockpiling and campaigning, blending, or the use of tailored reagent suites based on the mineralogy of the run-of-mine ore.

Great Dyke PGE ores

The Great Dyke in Zimbabwe is, after the Bushveld Complex in South Africa, the world's second-largest resource of the platinum group elements (PGE – Pt, Pd, Ir, Ru, Rh, Os), containing an estimated 8 680 t 4E (Pt, Pd, Rh, and Au) (Mudd, 2012; Oberthür *et al.*, 2013). The Great Dyke is a magmatic Ni-Cu-PGE stratiform intrusion stretching approximately 560 km in a NNE direction across Zimbabwe, with a width varying between 4 and 11 km. The Great Dyke is divided into two sections along strike, namely the North and South Chambers (see Wilson and Prendergast (2001) for a more comprehensive description of the Great Dyke). Economic PGE mineralization in the Great Dyke is stratabound and found in the Main Sulphide Zone (MSZ) and the Lower Sulphide Zone (Oberthür *et al.*, 2003). Sulphide ores are mined underground and processed at the Ngezi, Unki, and Mimosa mines by conventional

mineral processing and metallurgical methods which entail crushing and grinding, flotation, smelting, and matte production, as well as chemical refining (Jones, 2005; Oberthür *et al.*, 2013). These mines have combined resources of approximately 2 000 Mt at an average PGE grade of 3.6 g/t (Mudd, 2012). The oxidized ores occur closer to the surface and contain possible resources up to 250 Mt (Oberthür *et al.*, 2013). These oxidized ores are further divided into a spectrum according to the degree of oxidation from incipient to patchy to pervasively oxidized. The oxide ores are considered marginal to sub-economic and are not currently processed (*e.g.* Zimplats, 2019). Historical small-scale operations processing these oxidized ores by froth flotation were ultimately halted due to the low (less than 50%) PGE recoveries obtained (Evans, 2002). These oxide ores are therefore not being recovered to their full potential as oxidation and alteration present a 'mineralogical barrier' (Skinner, 1976).

In contrast to the majority of the ores from the Bushveld Complex in South Africa, which are relatively pristine with minor alteration, ores from the MSZ of the Great Dyke are characterized by more extensive alteration, resulting in numerous challenges in PGE recovery (Coghill and Wilson, 1993; Wilson and Prendergast, 2001; Oberthür *et al.*, 2013; Sefako, Sekgarametso, and Sibanda, 2017).

Before exploring some of the challenges posed by these altered ores from the Great Dyke and Bushveld Complex, and potential remedies, it is important to ensure that the appropriate nomenclature is used for describing the changes these ores have undergone. We have found that the terms 'alteration', 'weathering', and 'oxidation' are sometimes used interchangeably, particularly when engaging with practicing industry professionals, and will define the terms used in this paper.

Alteration and its effect on mineral processing

There are several types of alteration reactions that can occur in rocks, some of which are oxidation, hydrolysis, hydration, silicification, and decarbonation, among others (Guilbert and Park, 1986; Robb, 2005). All these reactions are capable of producing variability in mineralogy and texture. Of interest as regards ores from the Great Dyke are the oxidation, hydration, and hydrolysis reactions and their products (Figure 1). Oxidation typically results in the formation of secondary sulphides such as violarite, millerite, covellite, and chalcocite, as well as oxides and sulphates from the former primary base metal sulphide (BMS) mineral assemblage of pentlandite, pyrrhotite, and chalcopyrite. Hydrolysis refers to the addition of H^+, leading to the conversion of anhydrous silicates to hydrous ones, for example the conversation of plagioclase to muscovite. Hydration is the addition of water to the mineral, for example the alteration of orthopyroxene to talc, or olivine to serpentine. The latter reaction is known as serpentinization. Hydration and hydrolysis reactions can occur due to either hydrothermal alteration or deep weathering – in the case of hydrothermal alteration, the degree of alteration would increase with ore depth (like a typical porphyry ore), whereas weathering effects would decrease with ore depth.

The oxidation of Great Dyke ores as described in studies by Evans (2002), Locmelis, Melcher, and Oberthür (2010), and Oberthür *et al.* (2013) affects both the BMS and platinum group minerals (PGMs) in the near-surface environment. Oxidation leads to partial or complete oxidation and disintegration of the PGMs and BMS. This affects the attachment of reagents to these altered minerals as flotation collectors are mineral-specific. Even when partial oxidation occurs, the surface of the mineral would not necessarily have the same physico-chemical properties as the unaltered sulphide, thus affecting collector attachment. In addition, the PGMs may no longer be texturally associated with the BMS, preventing their recovery as composite particles using traditional thiol collectors (Becker, Wiese, and Ramonotsi, 2014). The PGMs, especially the fine particles, therefore become even harder to recover physically because of the challenges associated with fine particle flotation (Farrokhpay, Filippov, and Fornasiero, 2020). Furthermore, the base metals and PGE may have been mobilized from the supergene environment or redistributed into the silicate mineral assemblage. Consequently, these metals may not occur in the same host minerals as in unoxidized ores. Pd, in particular, may be completely mobilized out of the supergene

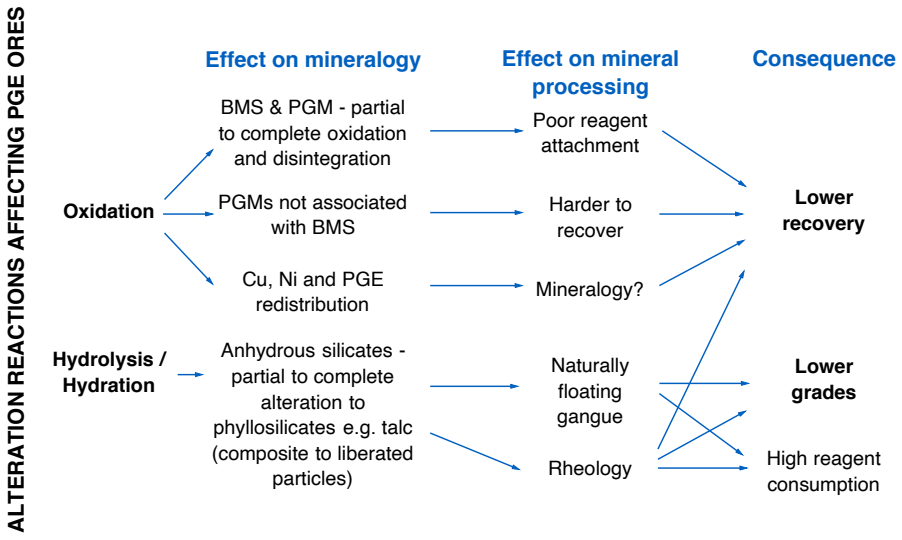

Figure 1—Potential challenges arising from the alteration of PGM ores, based on the findings of Evans, Buchanan, and Hall, 1994; Evans, 2002; Becker *et al.*, 2009; Locmelis, Melcher, and Oberthür, 2010; Oberthür *et al.*, 2013; Becker, Wiese, and Ramonotsi, 2014)

environment, and it has been estimated that up to 50% of the Pd may be lost (Evans, 2002; Oberthür *et al.*, 2013). PGE-bearing phyllosilicate minerals such as serpentine, smectite, and chlorite have also been reported in the Great Dyke (Locmelis, Melcher, and Oberthür, 2010) as well as in the Bushveld Complex (Chetty *et al.*, 2018). The combined effects of oxidation lead to a significant loss in pay metal recovery during processing. Altering the depressant type or dosage may not improve the recovery of the valuable minerals, but rather, more specific flotation collectors are needed to target these oxidized minerals (Becker, Wiese, and Ramonotsi, 2014; Sefako, Sekgarametso, ands Sibanda, 2017).

Hydration and hydrolysis reactions largely affect the primary silicate minerals in these ores, resulting in the formation of amphiboles as well as phyllosilicates such as mica, serpentine, talc, chlorite, and smectite (Locmelis, Melcher, and Oberthür, 2010; Chaumba, 2017). Talc, which is naturally hydrophobic, has a disproportionate effect on concentrate grade due to its inadvertent recovery in composite orthopyroxene-talc particles – these composites represent naturally floating gangue in these PGE ores (Becker *et al.*, 2009). Due to the anisotropic surface charge on talc and other phyllosilicate minerals, they also have the potential to create rheological challenges (Burdukova *et al.*, 2007; Becker *et al.*, 2013; Ndlovu *et al.*, 2014). Rheological complexity resulting from the higher amounts of phyllosilicate minerals in ores affects both the concentrate grade and the recovery (Bakker, Meyer, and Deglon, 2010; Patra, Nagaraj, and Somasundaran, 2011; Shabalala *et al.*, 2011; Farrokhpay, 2012; Zhang and Peng, 2015). The presence of ultrafine phyllosilicate minerals such as serpentine may also result in slime coating of the valuable minerals, further affecting flotation recovery (*e.g.* Bremmell, Fornasiero, and Ralston, 2005). The effects of both oxidation and hydration were observed by Becker, Wiese, and Ramonotsi (2014) in their work on an altered PGM ore from the Bushveld Complex in which there were high amounts of oxides as well as talc in the feed; this implies that the different types of alteration are not mutually exclusive. Changing the depressant type and dosage could in this case improve the flotation performance, as this reduces the amount of the naturally floating gangue reporting to the concentrate. Apart from reducing the valuable mineral grades in the concentrate, the inadvertent recovery of Mg-bearing minerals such as talc, serpentine, and pyroxene to the concentrate may also lead to smelting penalties (Lotter *et al.*, 2008). Overall, the alteration of the silicate minerals through hydration and hydrolysis reactions appears to have a greater effect on concentrate grade than on recovery (Figure 1).

Motivation and objective

Although current mining activities on the Great Dyke focus on sulphide ore, the run-of-mine ore may contain material with varying degrees of alteration. Recently, there has been renewed interest in the potential for the hydrometallurgical treatment of oxidized PGM ores, both in Zimbabwe and South Africa (Kraemer *et al.*, 2015; Sefako, Sekgarametso, and Sibanda, 2017; Mpinga *et al.*, 2018). However, modifying the operating conditions on an existing flotation plant presents an opportunity for managing ore variability when processing blends of pristine and oxidized ore, or even possibly for tailings retreatment. This could be followed by further downstream hydrometallurgical treatment for complex ores (Liddell and Adams, 2012; Sefako, Sibanda, and Sekgarametso, 2019).

In this paper we investigate the mineralogy of three different ores sampled across the Great Dyke, and compare their batch flotation responses. This information is used to develop a better understanding of the key mineralogical factors that affect the response of these ores to flotation, the effects of alteration, and the variability thereof. An improved understanding of these effects ultimately enables better management of processing performance.

Material and methods

Samples and sample preparation

Three 100–150 kg ore samples were obtained from different locations in the North and South chambers of the Great Dyke. Ores 1 and 2 were sampled from underground operations and represent sulphide ores that are currently processed. Ore 3 was obtained from a nearby open-pit source belonging to the operation from which ore 2 was sourced and represents what is classified as 'oxide ore'. Ores 1 and 2 were notably grey whereas ore 3 was a distinctive reddish colour, suggesting some degree of incipient oxidation. Samples were prepared on-site by crushing to 100% passing 3 mm and shipped to the Centre for Minerals Research laboratories at the University of Cape Town (UCT). Upon arrival, each sample was blended and split using a rotary riffle splitter into representative 1 kg portions.

Each 1 kg sample was milled to 65% passing 75 μm (resulting in a similar particle size distribution) in a 1 kg stainless steel rod mill charged with 20 stainless steel rods of varying diameter (6 x 25 mm, 8 x 20 mm, and 6 x 16 mm), at 66 wt.% solids, using synthetic plant water (Wiese, Harris, and Bradshaw, 2005). All milling and batch flotation experiments were conducted using a standard synthetic plant water recipe made up from distilled water with the addition of various salts (supplied by Merck). The divalent cations in the plant water are essential for the effective adsorption of the depressants onto talc (Khraisheh *et al.*, 2005).

Mineralological and chemical characterization

A combination of wet and dry screening was used to separate the mill product into various size classes (–25, +25 –53, +53 –75, and +75 μm). The discrete size fractions were split into smaller aliquots with a rotary microriffler and mixed with graphite before preparation as 30 mm diameter polished sections for measurement of their bulk mineralogical composition, sulphide liberation, and association by Quantitative Evaluation of Minerals by Scanning Electron Microscopy (QEMSCAN) using an FEI 650F instrument equipped with two Bruker 6130 silicon drift energy-dispersive spectrometers. All QEMSCAN analyses were run at 25 kV and 10 nA using the particle mineralogical analysis (PMA) and specific mineral search (SMS) routines to obtain the bulk mineralogy and sulphide liberation, respectively. The trace mineral search (TMS) routine was run on polished blocks of unsized sample for the PGM searches. The relative error of the mineral grades was calculated using the method of Van der Plas and Tobi (1965).

Aliquots of the bulk samples were also prepared for quantitative X-ray diffraction (XRD) with a McCrone micronizing mill, then analysed on a Bruker D8 Advance powder diffractometer with a Vantec detector and fixed divergence and receiving slits with Co-Kα radiation. The step size was 0.01° 2θ per second over the range 10 to 90°, with a measurement run time of 90 minutes. Phase quantification was performed by Rietveld refinement with the Bruker Topas software. The goodness of fit and Rwp of the phase quantification were approximately 4.2% and 9%, respectively. X-ray fluorescence

(XRF) spectrometry was performed using a Panalytical Axios wavelength-dispersive instrument with a 4 kW Rh tube. Calibration standards include natural element SARMs (South Africa Reference Materials) and USGS (US Geological Survey) standards. The QEMSCAN mineralogy of the various samples was validated by comparison with quantitative XRD, XRF, and the measured loss on ignition (LOI, performed in conjunction with the XRF analysis). (The full set of results of these analyses can be found in Dzingai (2017).

Batch flotation tests

Reagents were chosen based on those used at the Great Dyke PGE operations. The depressant of interest was characterized at the Centre for Minerals Research Polymer Characterization Laboratory at UCT. It is of high purity (97.6%), an intermediate degree of substitution (0.7), and intermediate molecular weight (251 430 g/mol). The depressant dosages used in the tests were 100 g/t (by active content). Collector (sodium isobutyl xanthate) and frother (SasFroth 200) dosages were 300 g/t and 75 g/t respectively, which were chosen based on the existing flow sheets from Great Dyke operations.

For batch flotation tests, the collector was added to the mill charge before milling. The milled slurry from the sample preparation stage was transferred to a Barker 3 L batch flotation cell and made up with synthetic plant water to a solids concentration of 35% by mass. The impeller speed was set at 1200 r/min, and the pulp level was controlled manually. Air supply was maintained at 7 L/min and the froth height was kept constant at 1 cm. A feed sample was taken before commencement of the flotation procedure. The depressant was added to the slurry in the flotation cell and a conditioning time of 2 minutes was allowed. The frother was then added and conditioning continued for 1 minute, after which the air supply was opened. Four concentrates were collected by scraping the froth every 15 seconds into a collecting pan at 2, 6, 12, and 20 minutes (C1, C2, C3, and C4 respectively). A tailings sample was also collected after each flotation test. The amount of water recovered was measured during each test.

The flotation feeds, concentrates, and tailings were filtered, dried, and weighed before analysis. Batch flotation tests at each condition were conducted in duplicate and the standard error calculated. The dried flotation feed, concentrate, and tailings samples were analysed for Cu, Ni, S, Pt, and Pd. Cu and Ni were measured on loose powders using a Bruker S4 Explorer XRF spectrometer, while S analysis was done using a LECO DR423 sulphur analyser. The average relative standard error of the recalculated Cu and Ni feed grades was 2.4 and 1.8%, respectively. All internal assays used a variety of standard reference materials, including SARM standards. Pt and Pd were concentrated by fire assay (Pb collection) and analysed by inductively coupled plasma optical emission spectrometry (ICP-OES) by an external accredited service provider.

The results of all batch flotation tests were analysed by comparing the solids mass and water recoveries, as well as Cu, Ni, S, Pt, and Pd grades and recoveries. Also, the amount of floating gangue was determined using the method described in Wiese (2009). In this method, it is assumed that the only material recovered at high depressant dosage (500 g/t in this study) is via entrainment, whereas at a standard depressant dosage (100 g/t in this study) the recovery of gangue is through both entrainment and true flotation. The cumulative mass of gangue at the 500 g/t depressant condition (that is, the full concentrate mass excluding PGMs and sulphide minerals) is then plotted against the amount of water recovered. The slope of the line is equivalent to an 'entrainability factor' which is then used to calculate the amount of entrained gangue at the standard depressant dosage conditions (see Equation [1]). The total mass of gangue less the mass of entrained gangue gives the amount of floating gangue (Equation [2]). Bulk mineralogy, liberation, and association analyses were carried out on the +38 –75 μm size fraction of the flotation concentrates and are considered representative of recovery by true flotation rather than recovery by entrainment (Savassi, 1998; Becker *et al.*, 2009; Wang *et al.*, 2015).

$$Mass\ of\ Entrained\ Gangue = Mass\ of\ Total\ Water\ Recovered \times Entrainability\ factor \quad [1]$$

$$Mass\ of\ Floating\ Gangue = Mass\ of\ Total\ Gangue - Mass\ of\ Entrained\ Gangue \quad [2]$$

Results and discussion

Elemental and mineral grades of flotation feeds

The feed ore samples were assessed mineralogically and chemically (Tables I to III) to investigate what factors would contribute to differences in flotation responses, if any, given the use of a uniform reagent suite for all three ores.

All three ore samples were pyroxene-rich (73–85 wt.% combined orthopyroxene and clinopyroxene, Table I), with lesser amounts of plagioclase (2.7–7.1 wt.%). Ores 1 and 2 had similar contents of phyllosilicate alteration minerals (approximately 10 wt.%) whereas ore 3 had the lowest phyllosilicate content (5.4 wt.%). In all three ores, talc was the most common phyllosilicate alteration mineral. High phyllosilicate concentrations (particularly talc, chlorite, and serpentine) are indicators of hydrothermal alteration in these magmatic Ni-Cu-PGE ores (Li *et al.*, 2008; Chaumba, 2017).

Table I

Bulk mineralogy of the three samples measured by QEMSCAN (wt.%). Ni and Cu sulphides are primarily pentlandite and chalcopyrite, respectively. 'Other sulphides' mainly comprises galena. Quartz is a major constituent of 'Other'. The relative error (%) for the mineralogical analyses at the 2σ standard deviation is given in parentheses

	Ore 1	Ore 2	Ore 3
Ni sulphides	0.5 (0.8)	0.3 (0.7)	0.2 (1.0)
Cu sulphides	0.4 (0.8)	0.3 (0.8)	0.3 (0.8)
Pyrrhotite	0.5 (0.6)	0.2 (0.7)	0.1 (1.2)
Pyrite	0.1 (1.9)	0.1 (1.2)	0.3 (1.0)
Other sulphides	< 0.1 (9.3)	< 0.1 (13.2)	< 0.1 (8.7)
Olivine	1.8 (0.3)	1.4 (0.3)	1.3 (0.4)
Orthopyroxene	64.8 (< 0.1)	78.1 (< 0.1)	82.1 (< 0.1)
Clinopyroxene	8.5 (0.2)	2.7 (0.2)	3.3 (0.2)
Serpentine*	0.1 (1.8)	0.2 (0.7)	0.1 (1.3)
Talc*	8.4 (0.1)	9.1 (0.1)	4.9 (0.2)
Chlorite*	1.3 (0.4)	0.6 (0.4)	0.3 (0.6)
Mica*	0.5 (0.6)	0.2 (0.7)	0.1 (1.1)
Amphibole	3.8 (0.2)	1.8 (0.2)	1.5 (0.3)
Plagioclase	7.1 (0.2)	2.7 (0.2)	3.2 (0.2)
Calcite	0.2 (0.9)	0.3 (0.6)	< 0.1 (1.7)
Chromite	0.2 (1.3)	0.3 (0.7)	0.2 (1.2)
Fe oxides/hydroxides	0.9 (0.5)	0.9 (0.4)	1.6 (0.4)
Other	0.9 (0.4)	0.8 (0.4)	0.5 (0.5)
Total	100.0	100.0	100.0

* Phyllosilicate minerals

Ore 1 had the highest BMS content (1.5 wt.%), with ores 2 and 3 containing similar but lesser amounts (0.9 wt.%) as shown in Table I. One of the hallmarks of oxidation is the formation of secondary sulphides, hence the deportment of Cu and Ni was further investigated. Chalcopyrite was the major host of Cu in all three ores (Table II), although in ores 2 and 3 secondary sulphides comprising chalcocite and covellite hosted 2.6% and 10.8% of the Cu respectively. Pentlandite was the major host of nickel in all three ores, with some minor pyrrhotite-hosted Ni (Table II). Ore 3, however, notably contained some Ni hosted in the secondary sulphide violarite (8.6%). Pyrrhotite was the major Fe sulphide in ores 1 and 2, whereas pyrite was more common in ore 3 (Table I). The Fe oxide content of ore 3 was almost double that of the other two samples (Table I). This is consistent with the reddish colour of this sample, which suggests a degree of incipient oxidation.

To further distinguish differences between the three samples their feed elemental Cu, Ni, Pt ,and Pd grades were analysed, as summarized in Table III. The Pt feed grade of ore 3 was higher than that of ores 1 and 2, whereas its Pd grade was lower, resulting in a Pt/Pd ratio of 2.3 for the former compared to approximately 1.2 for the latter samples. A higher Pt/Pd ratio is one of the distinguishing characteristics of an oxidized PGE ore due to the mobilization of Pd (Evans, 2002; Locmelis, Melcher, and Oberthür, 2010; Oberthür *et al.*, 2013). The Pt/Pd ratio and composition of ore 3 are similar to those reported by Kraemer *et al.* (2015) and Oberthür *et al.* (2013) for oxidized PGE ores from the Great Dyke.

BMS and PGM mineralogy, liberation, and association

An understanding of the BMS and PGM mineralogy, liberation, and associations is an essential component in exploring the mineralogical variability of these ores, as well as facilitating the interpretation of the flotation behaviour. Liberation is defined here as particles comprising greater than 90% of the mineral of interest by particle area and is reported for the BMS as a group rather than for discrete Cu or Ni sulphides because of the bulk sulphide flotation process used. The liberation of BMS is similar for ores 1 and 2 (almost 90%) and only slightly lower in ore 3 (86% liberated, Figure 2). Unliberated BMS in all three ores show some association with pyroxene, the phyllosilicate alteration minerals, and Fe oxides. In ore 3 the association with Fe oxides is slightly greater (7%) than in ores 1 and 2 (approx. 2%), which is another indicator of incipient oxidation (Figure 2).

Table II

Deportment of Cu and Ni in each of the three ore feeds, determined using QEMSCAN. Note that Ni deportment excludes the contribution of Ni in silicate minerals

Cu distribution (%)	Ore 1	Ore 2	Ore 3
Chalcopyrite	99.9	97.3	88.4
Other Cu sulphides	0.1	2.6	10.8
Cu oxides	–	–	–
Cu silicates	–	0.1	0.7
Fe oxides/hydroxides	–	–	0.1
Ni distribution (%)	**Ore 1**	**Ore 2**	**Ore 3**
Pentlandite	98.1	98.3	90.6
Pyrrhotite	1.5	1.0	0.7
Violarite	0.4	0.7	8.6
Millerite	–	–	0.1

Table III

Valuable element (Cu, Ni, Pt, and Pd) feed grades and Pt/Pd ratios. The standard error of replicate Cu, Ni feed assays is given in parentheses

Feed	Cu (g/t)	Ni (g/t)	Pt (g/t)	Pd (g/t)	Pt/Pd
Ore 1	1407 (39)	2657 (41)	1.64	1.29	1.26
Ore 2	809 (25)	1987 (47)	1.45	1.19	1.22
Ore 3	1373 (20)	2745 (37)	2.08	0.91	2.29

The mineralogy of the discrete PGMs analysed for these ores is summarized in Table IV, with results reported in terms of both the distribution by area and grain count percentage. The PGE bismuthotellurides are the dominant mineral group in all three ores, with moncheite-maslovite and kotulskite representing the main phases. Overall, the PGM mineralogy of ores 2 and 3 is more similar to one another than to ore 1 (especially with respect to the PGE-arsenides). This is likely because ores 2 and 3 were sampled from the same operation (and the same chamber of the MSZ). The presence of the PGE sulphides and PGE arsenides is also significant in ore 1 (5.2 and 31.7% respectively by area). For ore 2, gold and the PGE sulphides are more common (8.3 and 23.7% respectively by area). In ore 3, however, PGE alloys are the most dominant group after the PGE bismuthotellurides (25.1% by area) due to the presence of a single approx. 30 µm ferroplatinum particle skewing the distribution. On a grain count

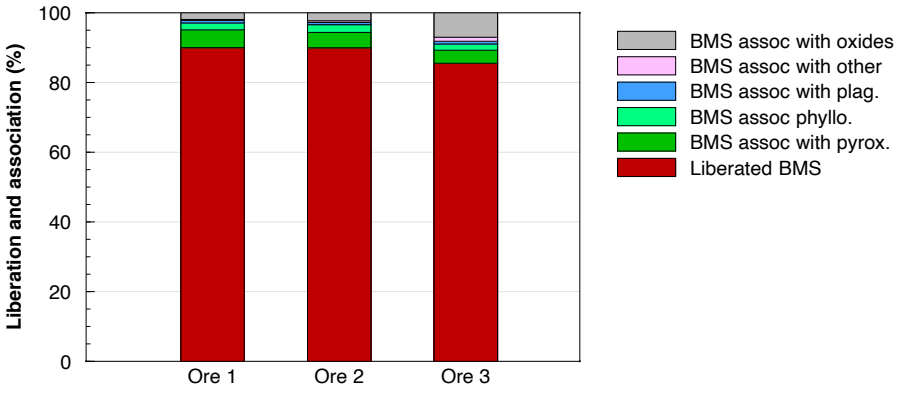

Figure 2—Base metal sulphide liberation and association for the three ores. A liberated BMS particle represents a particle with >90% by area comprising BMS. The mineral association is provided for unliberated BMS. BMS association with 'phyllo' represents association with talc, chlorite, serpentine, and mica. Number of particles analysed: 12 470 for ore 1, 8 620 for ore 2, and 12 260 for ore 3

Table IV

PGM distribution in each of the three ore feeds as determined by QEMSCAN. The main minerals analysed within each PGM group are also listed. Results are reported both in terms of normalized area distribution (%) and normalized grain count distribution (%) given the presence of an approx. 30 µm ferroplatinum particle in ore 3. The total number of PGM-bearing particles is also provided

Distribution (area %)	Ore 1	Ore 2	Ore 3
Gold	5.8	8.3	4.3
PGE sulphides (cooperite, braggite)	5.2	23.7	6.8
PGE sulpharsenides (hollingworthite)	2.4	0.1	< 0.1
PGE arsenides (sperrylite)	31.7	4.4	4.6
PGE bismuthotellurides (moncheite-maslovite, kotulskite)	50.5	57.2	59.0
PGE bismuthides (Pt, Pd- bismuthide)	3.5	0.9	0.2
PGE alloys (ferroplatinum)	0.9	5.5	25.1*
Distribution (grain count %)	**Ore 1**	**Ore 2**	**Ore 3**
Gold	2.7	6.0	8.9
PGE sulphides (cooperite, braggite)	11.2	12.1	11.3
PGE sulpharsenides (hollingworthite)	4.0	0.3	< 0.1
PGE arsenides (sperrylite)	10.6	3.4	4.8
PGE bismuthotellurides (moncheite-maslovite, kotulskite)	66.2	71.2	64.2
PGE bismuthides (Pt, Pd- bismuthide)	1.9	2.8	2.0
PGE alloys (ferroplatinum)	3.4	4.2	8.9
No. of PGM grains	624	614	293
No. of PGM-bearing particles	128	109	96

basis, however, the PGE sulphides, PGE arsenides, as well as the PGE alloys are the most common PGM groups in ore 3 after the PGE bismuthotellurides.

The PGMs in ores 1 and 2 are 55 and 48% liberated respectively, compared to ore 3 where the PGM liberation is 74% (Figure 3). PGM liberation is defined here as greater than 80% of the mineral of interest by area consisting of PGMS. In the case of ore 3, the data reported excludes a single liberated ferroplatinum nugget (that would increase the liberation up to 83%). When considering the effective PGM liberation (liberated PGMs plus PGMs in liberated BMS) the difference in the liberation between ores 1 and 2 compared with ore 3 is only around 14%. The balance of the unliberated PGMs are mostly associated with the silicates and phyllosilicates (talc, chlorite, serpentine) either as enclosed or attached grains. The relative differences in PGM grain size distribution are consistent with the trends in liberation data; the d_{50} of ores 1, 2, and 3 being 8.1, 7.1, and 9.3 µm, respectively (the most liberated ore has the coarsest grain size distribution).

Batch flotation performance

The flotation performance of the ores was assessed by comparing the Cu, Ni, Pt' and Pd recoveries with the mass recovery of solids. This was followed by an assessment of the mass of naturally floating gangue as well as the key indicators of valuable mineral recoveries using Cu, Ni, Pt, and Pd.

Grade and recovery

The Cu, Ni, Pt, and Pd recoveries from the batch flotation tests at 100 g/t depressant are shown in Figure 4. Grades and recoveries at 500 g/t depressant are not reported here, since these high depressant dosages were used purely for the calculation of floating gangue and are not representative of actual plant operating conditions (where such high depressant dosages are extremely unlikely to be used on a single rougher bank, which the batch flotation test represents). The highest Cu and Ni recoveries were obtained for ore 1 (87.3 and 67.0% respectively), whereas for Pt and Pd, the recoveries were similar for ores 1 and 2 (approx. 86 and 85% respectively). Consistently lower recoveries were obtained in the flotation of ore 3 for all four metals (Figure 4). This is despite ore 3 having the highest head grades of Pt and Ni (Table II) – it is generally accepted that flotation recovery increases with increasing head grade (Napier-Munn, 1998).

These differences in recovery can be correlated with the observations from the characterization of the flotation feed material, which indicated the incipient oxidation of the BMS in ore 3 – a red colour coupled with the slightly higher Fe oxide/hydroxide content in the feed as well as slightly higher association of unliberated BMS with the Fe oxide/hydroxides. Although the association of the BMS with the Fe oxide/hydroxides may quantitatively be very low, the possibility that surface rims may occur as nano-coatings on the sulphide minerals (not visible using QEMSCAN) significantly reducing floatability, should not be discounted. The presence of secondary Cu minerals (chalcocite, covellite) and Ni sulphides (violarite) is another indicator of the incipient oxidation of ore 3. These

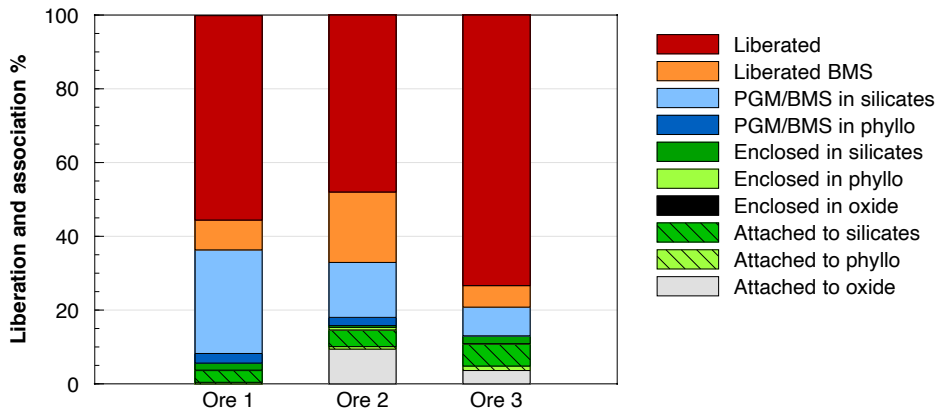

Figure 3—PGM liberation and association in the three feed samples. Liberated PGM particles comprise greater than 80% PGMs by particle area. Liberated BMS represents locked or attached PGMs inside a liberated BMS particle. PGM/BMS in silicates represents locked PGMs inside a locked or attached BMS particle in silicates, and so forth. 'Phyllo' represents the phyllosilicates – talc, chlorite, serpentine, mica. Number of PGM particles analysed (N) is 128 for ore 1, 109 for ore 2, and 95 for ore 3. Ore 3 liberation data excludes the approx. 30 µm single liberated ferroplatinum particle

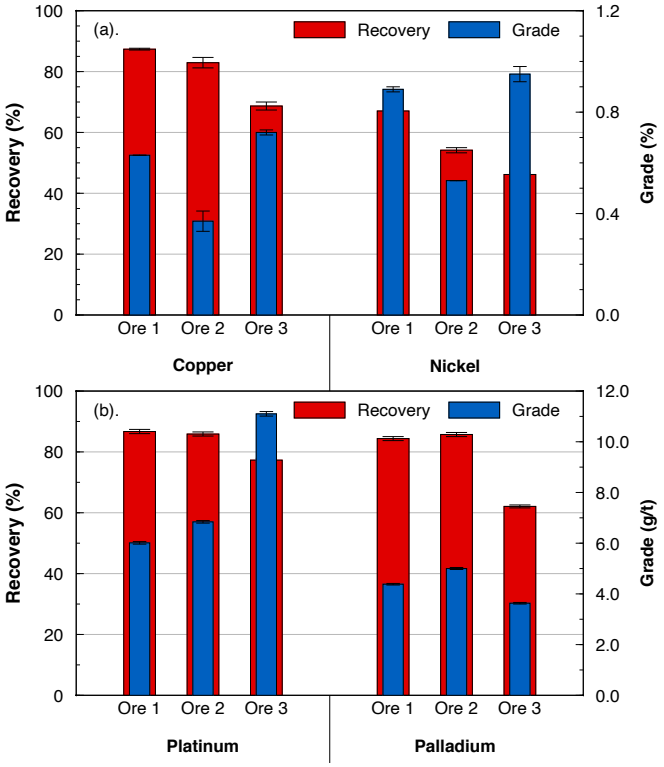

Figure 4—Cumulative recovery and grade in batch flotation tests at 100 g/t depressant dosage for the three samples. Recovery and grade provided for Cu-Ni (a), and Pt-Pd (b). Note the difference in the y-axis scale for grade between Cu-Ni and Pt-Pd. The error bars represent the standard error

secondary copper minerals are not readily floatable with the current SIBX collector (Grobler, Sondashi, and Chidley, 2005; Lee *et al.*, 2009; Lotter, Bradshaw, and Barnes, 2016).

In the PGM mineralogical characterization, however, the indications of oxidation were not as clear in ore 3 (other than the increased Pt/Pd ratio of the feed, Table II) as they were for the BMS. The PGM mineralogy reported here (Table IV) for all three ores is more similar to that reported for pristine sulphide ores (where the PGE bismuthotellurides are the dominant phases) than for the oxidized ores considered by Locmelis *et al.* (2010) and Oberthür *et al.* (2013), in which PGE oxides/hydroxides were recognized. The PGE deportment of the Great Dyke ores, however, is known not to be limited to discrete PGMs, and Oberthür *et al.* (2013) estimated that approximately 95% of the Pt budget is hosted by discrete PGMs, with the balance in solid solution with the BMS in pristine sulphide ores. For Pd however, only approximately 20% of the Pd was estimated to be hosted in discrete PGMs, and the balance in solid solution in pentlandite. In this case, the comparative decoupling of the trends in Pt and Ni recovery for ore 3 relative to the behaviour of ores 1 and 2 may be a further indication of incipient oxidation and mobilization of Pd in ore 3. In terms of PGM liberation, the fact that the PGM grain size and liberation were greatest in ore 3, yet the Pt and Pd recoveries were the lowest, also suggests that some of the PGE may be hosted in some of the more exotic phases *(e.g.* PGE oxides/hydroxides) that are not recoverable with thiol collectors. For ores 1 and 2 however, the similarity in Pt-Pd recoveries was consistent with the liberation data when considering the combined categories of liberated PGMs and PGMs hosted by liberated BMS (Figures 3, 4).

Ore 3, however, yielded the highest flotation concentrate grades for Cu, Ni, and Pt. Little difference in Pd concentrate grade was observed between the three ores (Figure 4). The associated increase in grade that usually accompanies a decrease in mass pull is noted in Figures 4 and 5, resulted in dilution of the concentrate grade for ores 1 and 2. A second point worth noting is the differences in the mass pull between the ores for the same cell operating and reagent conditions (Figure 5). This suggests that if operating conditions were optimized to increase the mass pull for ore 3, increases in recovery may be realized, although this would be at the expense of grade. To further understand the mechanisms for concentrate dilution in these ores, the role of the naturally floating gangue should be explored.

Naturally floating gangue

Naturally floating gangue in PGE ores ideally represents only hydrophobic minerals such as talc which are expected to be recovered during flotation. However, in practice, naturally floating gangue in these ores typically consists of composite particles of talc and orthopyroxene. These particles were formed through the hydration of orthopyroxene to talc. Ore 1 had the greatest amount of naturally floating gangue, followed by ore 2 and ore 3 respectively (Figure 6). This was also the order of decreasing solids recovery. Based on comparison of the feed bulk mineralogy, the initial expectation would be that ore 2 contained the greatest amount of naturally floating minerals due to its higher orthopyroxene content (with a talc content comparable to that of ore 1), although this was not the case.

To further understand why ore 1 yielded the greatest mass of floating gangue, a mineralogical analysis of the naturally floating material in the +38 –75 μm size class of the concentrate was carried out. In order to aid the interpretation, the results reported in Table V are shown as absolute concentrate masses obtained during flotation tests on the 1 kg feed sample. It is noteworthy that the mass of talc recovered from ore 1 was the lowest, despite this ore containing the highest mass of naturally floating gangue. Analysis of the mineral liberation and association showed that the talc in the ore 1 concentrate was mostly locked (less than 30% liberated, Figure 7) and strongly associated with pyroxene (Figure 8). The associated talc grain size distribution within the same size fraction showed that the talc in the ore 1 concentrate was more finely disseminated than in ore 2 (Figures 9, 10).

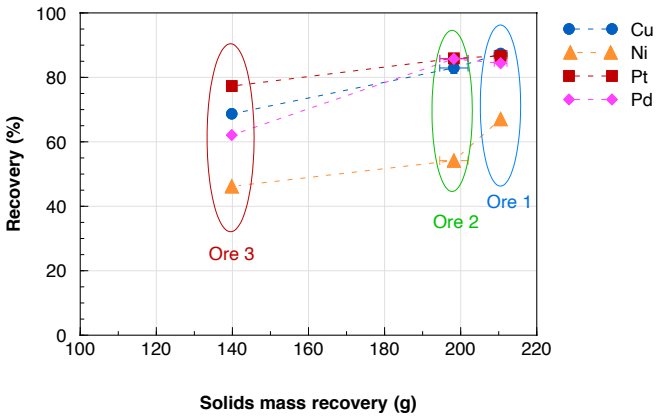

Figure 5—Recovery of Cu, Ni, Pt, and Pd as a function of mass pull for the three ores at 100 g/t depressant dosage. The error bars represent the standard error. The ellipses are shown for ease of reference to discriminate between ores 1, 2, and 3

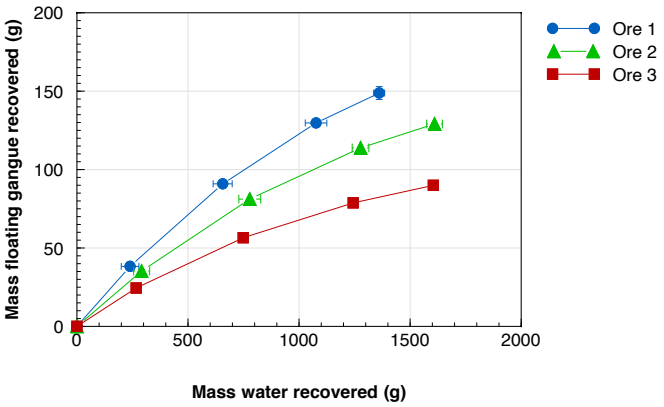

Figure 6—Cumulative mass of floating gangue recovered plotted against cumulative mass of water recovered at 100 g/t depressant dosage. The error bars represent the standard error. Details on the calculation of floating gangue are given in the section 'Batch flotation tests'

This difference is likely due to the difference in the extent of the hydrothermal hydration (alteration) reaction, with coarser grained talc indicating more extensive alteration (Figure 10). The results indicate that even low amounts of talc finely dispersed in pyroxene particles lead to the inadvertent flotation and recovery of the pyroxene resulting in greater amounts of naturally floating gangue. In this case, a simple upfront quantification of talc mineral content may not necessarily be entirely sufficient to predict the amount of naturally floating gangue. Mineral textural information that quantifies the talc liberation, grain size distribution, and relationship to orthopyroxene will be more revealing.

Table V

Simplified mineralogical composition of +38 –75 μm fraction of the batch flotation concentrates analysed by QEMSCAN. (BMS = Cu + Ni + Fe-sulphides, Pyroxene = Orthopyroxene + clinopyroxene; Other phyllosilicates = Serpentine + chlorite + mica; Oxides = Fe oxides + chromite; 'Other' is made up mainly of quartz in this case)

Phases	Mass in ore 1 (g)	Mass in ore 2 (g)	Mass in ore 3 (g)
BMS	0.9	1.2	2.0
Pyroxene	18.8	18.1	12.1
Talc	1.4	3.2	3.3
Other phyllosilicates	1.7	1.3	0.6
Plagioclase	0.6	0.2	0.3
Oxides	2.2	1.5	1.6
Other	0.3	0.2	0.2
Total	25.9	25.7	20.0

Conclusions

The primary objective of this investigation is to understand the effects of mineralogical variability due to alteration on the flotation response of three Great Dyke PGE ore samples. To do so involves decoupling the different types of alteration that these ores have undergone, as well as articulating what the indicators

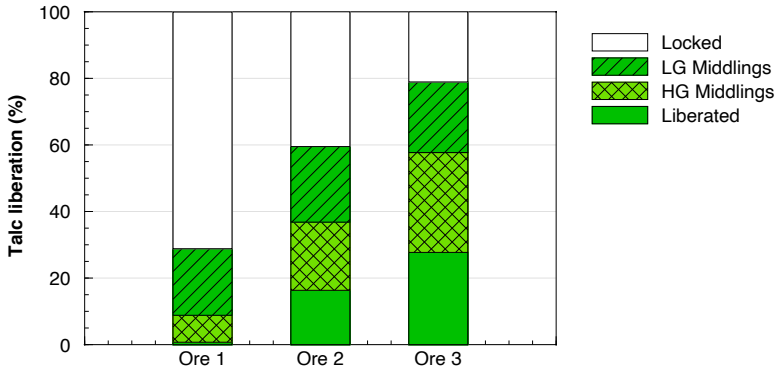

Figure 7—Talc liberation in the +38 –75 μm fraction of the batch flotation concentrates. Liberated represents > 90% talc by area, high-grade middlings 60–90%, low-grade middlings 30–60%, and locked <30%. Number of particles analysed (N) = 4 619 for ore 1, 3 787 for ore 2, and 5 155 for ore 3

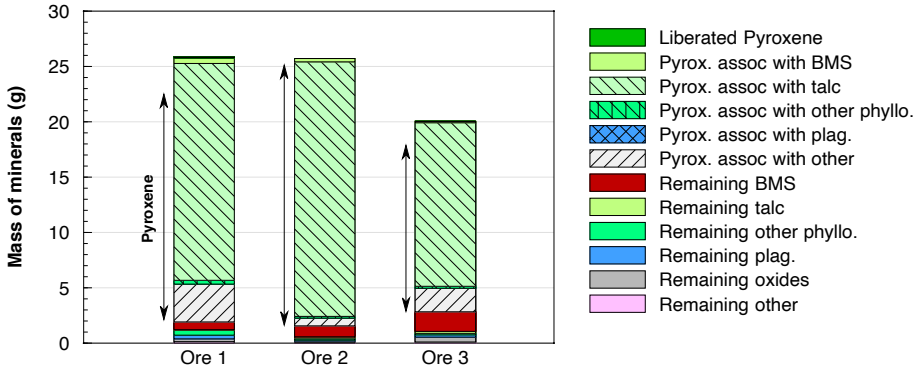

Figure 8 – Mass of minerals in the in the –75 +38 μm fraction of the batch flotation concentrates of the three ores. ('assoc' is short for associated; e.g. pyroxene assoc with BMS = total mass of pyroxene associated with BMS + mass of BMS in these composites. Remaining BMS = mass of BMS not within these pyroxene-BMS composites. 'Other' is mainly quartz)

Decoupling the effects of alteration on the mineralogy and flotation performance

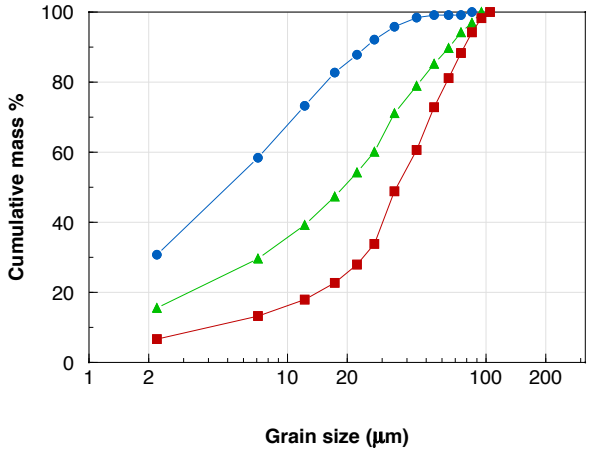

Figure 9—Talc grain size distribution in the –75 +38 µm fraction of the batch flotation concentrates. Number of particles analyzed (N) = 4 619 for ore 1, 3 787 for ore 2, and 5 155 for ore 3. The grain sizes represent the equivalent circle diameter

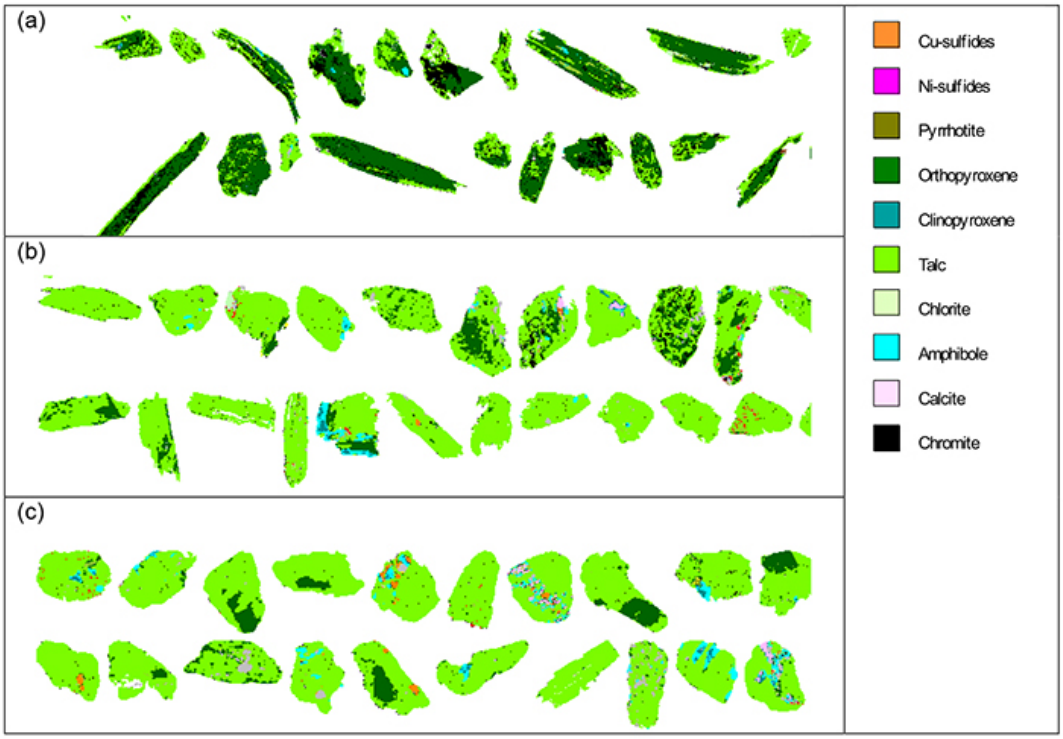

Figure 10 – QEMSCAN false colour images of selected particles in the –75 +38 µm fraction of the batch flotation concentrates, illustrating the variation in texture of talc grains in (a) ore 1, (b) ore 2, and (c) ore 3. Number of particles analysed (N) = 4 619 for ore 1, 3 787 for ore 2, and 5 155 for ore 3

of alteration are through quantitative mineralogical analysis. Although on first inspection mineralogical analyses did not reveal any major differences between the three ores studied, closer investigation allowed those subtle differences that have a significant effect on flotation performance to be further identified.

Alteration through oxidation of the valuable BMS and PGMs resulted in significantly lower flotation recoveries of Cu, Ni, Pt, and Pd in ore 3 compared to ores 1 and 2. Evidence of incipient oxidation was more readily observed in the BMS assemblage (association of unliberated BMS with Fe oxide/hydroxides, presence of minor secondary Cu and Ni-sulphides) than the PGM assemblage. Further investigation of the PGM assemblage with improved sampling statistics and instrumental analysis would ideally be required to visualize the effect of the incipient oxidation and confirm the PGE distribution in both conventional and unconventional phases (*e.g.* PGE oxides/hydroxides or PGE silicates).

The alteration of orthopyroxene to talc through hydration resulted in significant differences in mass pull and dilution of concentrate grade through the inadvertent recovery of naturally floating gangue comprising composite orthopyroxene and talc particles. The greatest amount of naturally floating gangue was recovered from ore 1, despite it not having the highest amount of talc in the feed. However, talc in ore 1 was the least liberated, with the finest grain size distribution (more finely disseminated). In this case quantification of the talc mineral textural characteristics would be required to predict which ore types will need active grade management through the use of depressant.

Oxidation and hydration reactions are not necessarily mutually exclusive in these magmatic Ni-Cu-PGE ores, although one may be more dominant, giving rise to ore variability. Continual assessment of the mineralogy of both the valuable and gangue fractions of the ore is needed to enable a better understanding of the repercussions and application of the appropriate measures to ensure consistent grades and recoveries. Such measures could include, but are not limited to, ore blending strategies, use of different reagent suites, optimized mass pull, and even the design of reagents that target the more oxidized valuable minerals.

Acknowledgements

Our appreciation goes to Senmin (Pty) Ltd, the National Research Foundation (NRF) of South Africa, and the University of Cape Town for their support and funding of this research. Our thanks go to Mimosa Mining Company (Pvt) Ltd and Zimplats Holdings Ltd for the ore samples. Useful discussions with Thomas Oberthür are also acknowledged. Grateful thanks to staff in the Centre for Minerals Research for their assistance, especially Gaynor Yorath and Keshree Pillay. This work is based on the research supported in part by the National Research Foundation of South Africa (Grant Number 86054). Any opinions, findings, and conclusions or recommendations expressed in any publication generated by NRF-supported research is that of the authors, and the NRF accepts no liability whatsoever in this regard.

Author contributions

Conceptualization – MB, BM; Methodology – DZ, BM, MT, MB; Formal analysis - DZ, BM, MT, MB; Writing of original draft – DZ, MB; Review and editing - BM, MT, MB; Supervision - BM, MT, MB; Funding acquisition – MB.

Supplementary data

The raw data is available at: https://doi.org/10.25375/uct.13580378

References

Bakker, C.W., Meyer, C.J., and Deglon, D.A. 2010. The development of a cavern model for mechanical flotation cells. *Minerals Engineering*, vol. 23, no. 11–13. pp. 968–972. doi: 10.1016/j.mineng.2010.03.016

Baum, W. 2014. Ore characterization, process mineralogy and lab automation: A roadmap for future mining. *Minerals Engineering*, vol. 60. pp. 69–73. doi: 10.1016/j.mineng.2013.11.008.

Becker, M., Harris, P.J., Wiese, J.G., and Bradshaw, D.J. 2009. Mineralogical characterisation of naturally floatable gangue in Merensky Reef ore flotation. *International Journal of Mineral Processing*, vol. 93, no. 3–4. pp. 246–255. doi: 10.1016/j.minpro.2009.10.004

Becker, M., Yorath, G., Ndlovu, B., Harris, M., Deglon, D., and Franzidis, J.P. 2013. A rheological investigation of the behaviour of two Southern African platinum ores. *Minerals Engineering*, vol. 49. pp. 92–97. http://www.sciencedirect.com/science/article/pii/S0892687513001489

Becker, M., Wiese, J., and Ramonotsi, M. 2014. Investigation into the mineralogy and flotation performance of oxidised PGM ore. *Minerals Engineering*. vol. 65. pp. 24–32. http://www.sciencedirect.com/science/article/pii/S0892687514001198

Bremmell, K.E., Fornasiero, D., and Ralston, J. 2005. Pentlandite–lizardite interactions and implications for their separation by flotation. *Colloids and Surfaces A: Physicochemical and Engineering Aspects*, vol. 252, no. 2–3. pp. 207–212. doi: http://dx.doi.org/10.1016/j.colsurfa.2004.10.100

Burdukova, E., Becker, M., Bradshaw, D.J., and Laskowski, J.S. 2007. Presence of negative charge on the basal planes of New York talc. *Journal of Colloid and Interface Science*, vol. 315. pp. 337–342.

Chaumba, J.B. 2017. Hydrothermal alteration in the Main Sulfide Zone at Unki Mine, Shurugwi Subchamber of the Great Dyke, mineral chemistry. *Minerals*, vol. 7. p. 127. doi: 10.3390/min7070127

Chetty, D., Carelse, C., Mogoru, J., Pebane, M., and Ngoasheng, M. 2018. Mineralogical factors affecting platinum group element recovery from oxidised chromite of the middle group, western Bushveld Complex. *Proceedings of Process Mineralogy '18, Cape Town. Minerals Engineering International*, Falmouth, UK.

Coghill, B.M. and Wilson, A.H. 1993. Platinum-group minerals in the Selukwe Subchamber, Great Dyke, Zimbabwe: Implications for PGE collection mechanisms and post-formational redistribution. *Mineralogical Magazine*, vol. 57. pp. 613–634.

Dzingai, T. 2017. A process mineralogical study on the effect of alteration on the flotation of Great Dyke platinum group element (PGE) ores. MSc thesis, University of Cape Town.

Evans, D. 2002. Potential for bulk mining of oxidized platinum-group element deposits. *Applied Earth Science*, vol. 111. pp. 81–86.

Evans, D.M., Buchanan, D.L., and Hall, G.E.M. 1994. Dispersion of platinum, palladium and gold from the Main Sulphide Zone, Great Dyke, Zimbabwe. *Transactions of the Institution of Mining and Metallurgy. Section B: Applied Earth Science*. vol. 103 (Jan-Apr). pp. 57-67.

Farrokhpay, S. 2012. The importance of rheology in mineral flotation: A review. *Minerals Engineering*, vol. 36–38. pp. 272–278. doi: 10.1016/j.mineng.2012.05.009

Farrokhpay, S., Filippov, L., and Fornasiero, D. 2020. Flotation of fine particles: A review. *Mineral Processing and Extractive Metallurgy Review.* doi: 10.1080/08827508.2020.1793140

Grobler, W.A., Sondashi, S., and Chidley, F. 2005. Recent developments in flotation reagents to improve base metal recovery. *Proceedings of the 3rd Southern African Base Metals Conference*. Kitwe, Zambia. Southern African Institute of Mining and Metallurgy, Johannesburg. pp. 185–190.

Guilbert, J. and Park, C. 1986. The Geology of Ore Deposits. W.H. Freeman, New York.

Jones, R. 2005. An overview of Southern African PGM smelting. *Proceedings of Nickel and Cobalt 2005: Challenges in Extraction and Production*, Calgary, Alberta, 21-24 August. Donald, J. and Shoneville, R. (eds). Canadian Institute of Mining, Metallurgy and Petroleum, Montreal. pp. 147–178.

Khraisheh, M., Holland, C., Creany, C., Harris, P., and Parolis, L. 2005. Effect of molecular weight and concentration on the adsorption of CMC onto talc at different ionic strengths. *International Journal of Mineral Processing*. vol. 75. pp. 197–206.

Kraemer, D., Junge, M., Oberthür, T., and Bau, M. 2015. Hydrometallurgy improving recoveries of platinum and palladium from oxidized platinum-group

element ores of the Great Dyke, Zimbabwe, using the biogenic siderophore Desferrioxamine B. *Hydrometallurgy*. vol. 152. pp. 169–177. doi: 10.1016/j.hydromet.2015.01.002

Lee, K., Archibald, D., McLean, J., and Reuter, M. 2009. Flotation of mixed copper oxide and sulphide minerals with xanthate and hydroxamate collectors. *Minerals Engineering*, vol. 22. pp. 395–401.

Li, C., Ripley, E.M., Oberthür, T., Miller, J.D., and Joslin, G.D. 2008. Textural, mineralogical and stable isotope studies of hydrothermal alteration in the main sulfide zone of the Great Dyke, Zimbabwe and the precious metals zone of the Sonju Lake Intrusion, Minnesota, USA. *Mineralium Deposita*, vol. 43. pp. 97–110.

Liddell, K.S. and Adams, M.D. 2012. Kell hydrometallurgical process for extraction of platinum group metals and base metals from flotation concentrates. *Journal of the Southern African Institute of Mining and Metallurgy*, vol. 112, no. 1. pp. 31–36.

Locmelis, M., Melcher, F., and Oberthür, T. 2010. Platinum-group element distribution in the oxidized Main Sulfide Zone, Great Dyke, Zimbabwe. *Mineralium Deposita*, vol. 45. pp. 93–109. doi: 10.1007/s00126-009-0258-y

Lotter, N.O., Bradshaw, D.J., Becker, M., Parolis, L.A.S., and Kormos, L.J. 2008. A discussion of the occurrence and undesirable flotation behaviour of orthopyroxene and talc in the processing of mafic deposits. *Minerals Engineering*, vol. 21, no. 12–14. doi: 10.1016/j.mineng.2008.02.023

Lotter, N.O., Kormos, L., Oliveira, J., Frangomeni, D., and Whiteman, E. 2011. Modern process mineralogy: Two case studies. *Minerals Engineering*, vol. 24. pp. 638–650.

Lotter, N.O., Bradshaw, D.J., and Barnes, A.R. 2016. Classification of the major copper sulphides into semiconductor types, and associated flotation characteristics. *Minerals Engineering*. vol. 96–97. pp. 177–184. doi: 10.1016/j.mineng.2016.05.016

Lotter, N.O., Baum, W., Reeves, S., Arrué, C., and Bradshaw, D.J. 2018. The business value of best practice process mineralogy. *Minerals Engineering*, vol. 116, April. pp. 226–238. doi: 10.1016/j.mineng.2017.05.008

Mpinga, C.N., Eksteen, J.J., Aldrich, C., and Dyer, L. 2018. Atmospheric leach process of high-chromitite PGM-bearing oxidized mineralized ore through a single-stage and two-stage techniques. *Minerals Engineering*, vol. 125. pp. 165–175. doi:10.1016/j.mineng.2018.05.007.

Mudd, G.M. 2012. Key trends in the resource sustainability of platinum group elements. *Ore Geology Reviews*, vol. 46. pp. 106–117. doi: 10.1016/j.oregeorev.2012.02.005

Napier-Munn, T.J. 1998. Analysing plant trials by comparing recovery-grade regression lines. *Minerals Engineering*, vol. 11. pp. 949–958.

Ndlovu, B., Forbes, E., Farrokhpay, S., Becker, M., Bradshaw, D., and Deglon, D. 2014. A preliminary rheological classification of phyllosilicate group minerals. *Minerals Engineering*, vol. 55. pp. 190–200. http://www.sciencedirect.com/science/article/pii/S0892687513001921

Oberthür, T., Weiser, T.W., Gast, L., and Kojonen, K. 2003. Geochemistry and mineralogy of platinum-group elements at Hartley Platinum Mine, Zimbabwe: Part 2: Supergene redistribution in the oxidized Main Sulfide Zone of the Great Dyke, and alluvial platinum-group minerals. *Mineralium Deposita*, vol. 38, no. 3. pp. 344–355. doi: 10.1007/s00126-002-0337-9

Oberthür, T., Melcher, F., Buchholz, P., and Locmelis, M. 2013. The oxidized ores of the Main Sulphide Zone, Great Dyke, Zimbabwe: Turning resources into minable reserves–mineralogy is the key. *Journal of the Southern African Institute of Mining and Metallurgy*, vol. 113. pp. 191–201.

Patra, P., Nagaraj, D.R., and Somasundaran, P. 2011. Impact of pulp rheology on selective recovery of value minerals from ores. *Proceedings of the XII International Seminar on Mineral Processing Technology* (MPT-2011), Udaipur, India. pp. 1223–1231. http://eprints.nmlindia.org/4122

Powell, M.S. 2013. Utilising orebody knowledge to improve comminution circuit design and energy utilisation. *Proceedings of the 2nd AUSIMM International Geometallurgy Conference*, Brisbane, Australia. Australasian Institute of Mining and Metallurgy, Melbourne. pp. 27–35.

Robb, L. 2005. Introduction to Ore Forming Processes. Blackwell, Malden.

Savassi, O.N. 1998. Direct estimation of the degree of entrainment and the froth recovery of attached particles in industrial flotation cells. PhD thesis, University of Queensland.

Sefako, R., Sekgarametso, K., and Sibanda, V. 2017. Potential processing routes for recovery of platinum group metals from southern African oxidized PGM ores: A review. *Journal of Sustainable Metallurgy*, vol. 3, no. 4. pp. 797–807. doi: 10.1007/s40831-017-0146-0

Sefako, R., Sibanda, V., and Sekgarametso, K. 2019. PGM extraction from oxidized ores using flotation and leaching. *Journal of the Southern African Institute of Mining and Metallurgy*, vol. 119, no. 11. pp. 929–936. doi: 10.17159/2411-9717/287/2019

Shabalala, N.Z.P., Harris, M., Leal Filho, L.S., and Deglon, D.A. 2011. Effect of slurry rheology on gas dispersion in a pilot-scale mechanical flotation cell. *Minerals Engineering*, vol. 24, no. 13. pp. 1448–1453. doi: 10.1016/j.mineng.2011.07.004

Skinner, B. 1976. A second Iron Age ahead? The distribution of chemical elements in the earth's crust sets natural limits to man's supply of metals that are much more important to the future of society than limits on energy. *American Scientist*, vol. 64, no. 3. pp. 258–269.

Van der Plas, L. and Tobi, A. 1965. A chart for judging the reliability of point counting results. *American Journal of Science*, vol. 263. pp. 87–90.x

Wang, L., Peng, Y., Runge, K., and Bradshaw, D. 2015. A review of entrainment: Mechanisms, contributing factors and modelling in flotation. *Minerals Engineering*, vol. 70. pp. 77–91. doi: 10.1016/j.mineng.2014.09.003

Wiese, J. 2009. Investigating depressant behaviour on the flotation of selected Merensky ores. MSc thesis, University of Cape Town..

Wiese, J.G., Harris, P.J., and Bradshaw, D.J. 2005. The influence of the reagent suite on the flotation of ores from the Merensky Reef. *Minerals Engineering*, vol. 18. pp. 189–198.

Wilson, A.H. and Prendergast, M.D. 2001. Platinum-group element mineralisation in the Great Dyke, Zimbabwe, and its relationship to magma evolution and magma chamber structure. *South African Journal of Geology*, vol. 104. pp. 319–342.

Zhang, M. and Peng, Y. 2015. Effect of clay minerals on pulp rheology and the flotation of copper and gold minerals. *Minerals Engineering*, vol. 70. pp. 8–13. doi: 10.1016/j.mineng.2014.08.014.

Zimplats. 2019. Integrated Annual report. ◆


We do integrated mining...
As a maverick organisation, Ukwazi offers unique mining solutions, seamlessly integrating key activities and disciplines in the mining value chain; working with our clients for low-cost quartile, safe and sustainable mines and projects.
UKWAZI
www.ukwazi.com

Investigation into the dephosphorization of ferromanganese alloys for the production of advanced high-strength steel

M.P. Maphutha[1,2], J.D. Steenkamp[1], and P.C. Pistorius[2,3]

Affiliation:
[1]Mintek, Randburg, South Africa.
[2]University of Pretoria, South Africa.
[3]Carnegie Mellon University, Pittsburgh PA, United States of America.

Correspondence to:
M.P. Maphutha

Email:
Patriciam@mintek.co.za

Dates:
Received: 9 Feb. 2021
Revised: 25 Aug. 2021
Accepted: 26 Aug. 2021
Published: September 2021

How to cite:
Maphutha, M.P., Steenkamp, J.D., and Pistorius, P.C. 2021 Investigation into the dephosphorization of ferromanganese alloys for the production of advanced high-strength steel. Journal of the Southern African Institute of Mining and Metallurgy, vol. 121, no. 9, pp. 487–496

DOI ID:
http://dx.doi.org/10.17159/2411-9717/1510/2021

ORCID:
J.D. Steenkamp
https://orcid.org/0000-0003-0635-7927
P.C. Pistorius
https://orcid.org/0000-0002-2966-1879

Synopsis

Advanced high-strength steels (AHSS) are sophisticated materials being developed by the steel industry to mitigate challenges related to the performance of motor vehicles. To meet the requirements of AHSS, the ferromanganese alloys (FeMn) utilized in the production of the steel are required to contain acceptable levels of unwanted impurities, *i.e.* P, S, N, H, and C. The focus of the current study was to investigate dephosphorization of ferromanganese to produce a low-P alloy that could be effectively utilized in the production of AHSS. The study involved conducting laboratory-scale testwork to study the efficiency of CaO-based slag systems to dephosphorize FeMn alloys. The addition of Na_2O, CaF_2, and BaO to MnO-CaO-SiO_2 slag was considered. The test work was carried out in a 25 kW induction furnace at temperatures of 1350°C, 1400°C, and 1450°C. The P partition coefficient (L_p) remained small at <1, which is an indication that dephosphorization had not been achieved. The baseline slag, comprising 40%CaO-40%SiO_2-20%MnO, reported higher L_p values. Addition of Na_2O and CaF_2 did not show any further benefit. Substituting half of the CaO by BaO, resulted in similar L_p values to those of the baseline slag under conditions of 1350°C and 1450°C at 30 minutes. In summary, based on the L_p values obtained, the conditions investigated with the CaO-based slags appeared to have been unfavourable for dephosphorization of FeMn alloys, as most of this impurity element remained in the alloy.

Keywords
ferromanganese, dephosphorization, advanced high-strength steel.

Introduction

In the automotive industry the drive towards lightweight, high-strength steel grades to mitigate the challenges around the escalating energy crisis and environmental problems is a priority. It has been estimated that a 10% weight reduction in automobiles would reduce fuel consumption by between 3% and 7% (Demiri, 2013). This has led to the development of advanced high-strength steels (AHSS) (Baluch, Udin, and Abdullah, 2014).

AHSS steels are a group of special steel grades which offer excellent strength, allowing the use of thinner gauges to reduce the weight of vehicles. As the manganese (Mn) content in AHSS can be up to 25%, these steels could potentially be a significant market for manganese ferroalloys (Safarian and Kolbeinsen, 2013). The challenge lies in the maximum allowable phosphorus (P) content of <0.01% in the steel grades (Bernhard *et al.*, 2019).

P has a detrimental effect on the strength, brittleness, ductility, and fracture toughness of steel. As a result, the quality of the steel could become compromised, especially in the case of AHSS where the Mn content can be up to 25%. As a consequence, FeMn alloys utilized in the production of AHSS are required to contain low P levels (You, Lee, and Pak, 1999; Chaudhary and Roy, 2001).

During carbonaceous reduction of Mn ores to produce FeMn alloys, almost all the P is reduced to the alloy phase. The P originates mainly from the Mn ores, and is intimately associated with iron (Fe) and Mn, making it difficult to remove by mineral processing routes (Chaudhary and Goel, 2007). South African Mn ores are, however, generally low in P compared to ores from other countries such as China. The P content in the typical South African ores, namely Gloria ore and Nchwaning ores, varies between

0.02% and 0.05% (Visser *et al.*, 2013; Olsen *et al.*, 2007). When using low-P ore, the P present in the slag and the alloy originates mainly from the carbonaceous reductants used (Olsen *et al.*, 2007). To produce FeMn alloys containing P at levels acceptable to AHSS producers, methods have to be developed to lower the P levels in the alloy.

Background

Mechanisms of dephosphorization

Dephosphorization of the molten alloy under oxidizing conditions can be described by the following ionic reaction (Chaudhary Minj, and Goel, 2007; Nasaralla, Fruehan, and Min, 1991; Simeonov and Sano, 1985):

$$\frac{3}{2}(O^{2-}) + [P] + \frac{5}{2}[O] = (PO_4^{3-}) \quad [1]$$

where:

[X]: species dissolved in the alloy
(Y): species dissolved in the slag.

The equilibrium constant can be expressed as follows:

$$K_1 = \frac{a_{(PO_4^{3-})}}{a_P \cdot a_{[O]}^{5/2} \cdot a_{(O^{2-})}^{3/2}} \quad [2]$$

Based on the above expression, it can be deduced that the removal of P from the alloy can be aided by the following (Chaudary and Goel, 1994):

- Higher oxygen activity in the alloy
- High activity of basic oxide ($a_{O^{2-}}$) in the slag
- Low activity coefficient of phosphate ($\gamma_{PO_4^{3-}}$) in the slag
- High *K* values, which can be achieved at low temperatures since the reaction is of exothermic nature.

Slag basicity is associated with the degree of polarization of oxygen in the slag. Highly basic slag contains more free oxygen ions (O^{2-}) and less bridging and terminal oxygen. Slag basicity can therefore be defined by the activity of oxygen ions in slags (Liu *et al.*, 1998). As indicated by Equation [1], high concentrations of O^{2-}, and therefore basic slags, are efficient for dephosphorization (Wagner, 1975).

Dephosphorization of FeMn can also be carried out with basic slag under reducing conditions to form a phosphide species. The reaction is shown below (Chaudhary and Goel, 2007):

$$[P] + \frac{3}{2}(O)^{2-} = P^{3-} + \frac{3}{4}O_2 \quad [3]$$

Based on Equation [3], it can be deduced that the removal of P from the alloy under these conditions can be aided by a high activity of basic oxide ($a_{O^{2-}}$) in the slag. A relatively lower oxygen partial pressure is required for reducing conditions, and CO gas is typically used. Metallics such as Ca, typically added as calcium silicide or CaC_2, would dissolve into the metal and react with P to form phosphide. The reducing reaction occurs through the reaction between CaO in the flux and Si in the melt (for SiMn alloy), and also through the transfer of Ca from the calcium silicide introduced into the melt. An example is shown below (Karbowniczek *et al.*, 2014):

$$[Si] + 2(CaO) = 2[Ca] + (SiO_2) \quad [4]$$

$$3[Ca] + 2[P] = (Ca_3P_2) \quad [5]$$

The reaction product from Equation [5] is phosphide, which in the presence of atmospheric moisture produces toxic phosphene. Dephosphorization of FeMn alloy under reducing conditions is therefore not desirable.

P removal in vapour form, as phosphine gas, by the reaction of P with hydrogen dissolved in the metal can occur (Chaudary and Goel, 1994):

$$[P] + 3[H] = PH_3\ (g) \quad [6]$$

The reaction product (phosphine) would not be environmentally tolerable when released into the atmosphere (Chaudary and Goel, 1994). Based on Equation [6], it can be deduced that the removal of P from the alloy under these conditions can be aided by higher hydrogen activity in the alloy. Dephosphorization under gaseous conditions may also result in loss of Mn, which has a higher vapour pressure than P. Application of the technique is deemed undesirable for dephosphorization of FeMn alloys (Chaudary and Goel, 1994).

Considering the abovementioned reaction mechanisms, dephosphorization of liquid FeMn alloy by basic slags for selective removal of P over Mn under oxidizing conditions is deemed the most viable route (Chaudary and Goel, 1994).

The study aimed at investigating the use of CaO-bearing, synthetic slag systems – similar to the systems applied in dephosphorisation of iron – for the dephosphorization of FeMn alloys commercially produced in South Africa.

Method

The study involved conducting preliminary thermochemical FactSage calculations followed by experimental laboratory tests to investigate the dephosphorization of South African FeMn alloys by different synthetic CaO-based slag systems, similar to the systems applied in dephosphorization of iron.

FactSage calculations

FactSage™ version 7.3 was utilized. The package is a fully integrated thermodynamic database computing system developed in 1976 by a joint research project between McGill University and École Polytechnique de Montréal (Canada). FactSage provides access to several databases, including pure substances, oxides, solutions, and alloy databases. The tool is widely applied to study thermochemistry for different chemical and metallurgical processes (Bale *et al.*, 2016).

The calculations were conducted in the Equilib module. In all calculations, the pure substance database (FactPS), which is suitable for pure solids, liquids, and gases, was utilized. As solution databases, FToxid was utilized to describe the slag system and FSstel the alloy system. FToxid includes a wide range of components such as Al_2O_3, As_2O_3, B_2O_3, CaO, CoO, CrO, Cr_2O_3, Cu_2O, FeO, Fe_2O_3, GeO_2, K_2O, MgO, MnO, Na_2O, NiO, PbO, SiO_2, SnO, TiO_2, Ti_2O_3, ZnO, and ZrO_2. Furthermore, FToxid contains many solid solution databases, which include those listed below (Bale *et al.*, 2009):

- Wollastonite: $CaSiO_3$ (+$FeSiO_3$, $MgSiO_3$, $MnSiO_3$)
- Olivine: (Ca^{2+}, CO^{2+}, Fe^{2+}, Mg^{2+}, Mn^{2+}, Ni^{2+}, Zn^{2+})$_2SiO_4$
- α'-Ca_2SiO_4: α'-Ca_2SiO_4 (+Fe_2SiO_4, Mg_2SiO_4, Mn_2SiO_4)
- Monoxide: CaO-MgO-MnO-CoO-NiO-FeO (+Fe_2O_3-Al_2O_3-ZnO-Cr_2O_3)
- Corundum: Al_2O_3-Cr_2O_3-Fe_2O_3

FSstel is a steel database covering a wide range of compositions related to steelmaking processes (Bale *et al.*, 2009).

Although thermodynamic data exists for HCFeMn, it does not contain equilibrium data on P (Tang and Olsen, 2006). FSstel has been proven in the past to represent equilibrium conditions in SiMn production, and as it contained data on P, was selected for the calculations presented here (Steenkamp, Pistorius, and Tangstad, 2015).

As pure species, all liquids and solids were selected except the Mn phosphide phases. As pure ideal gas species, only O_2 and Ar were selected. For solution systems, all solution phases were selected, except in cases where more than one option existed. Solution phases that were suppressed were SlagD Slag? MeOB, MeP_? cPyrB, and cPyr?. SlagA model was selected over Slag? model because SlagA provides much more reasonable L_P values for steelmaking than does Slag?, which overestimates P removal. Since MeOB, does not include BaO as a solute, this solution phase was not selected. MeP? cPyrB, and cPyr? were not selected because more than one option existed.

The calculations were done to investigate the phosphorus partition coefficient (L_P) between slag and alloy. The expression for L_P is

$$\frac{\text{Wt\%P\_FToxid\_SLAGA}}{\text{Wt\%P\_FSstel\_Liqu}} \quad [7]$$

The typical HCFeMn and MCFeMn compositions obtained from the literature (see Table I) were utilized for the dephosphorization thermochemical calculations.

The slag systems in Table II were utilized. To determine the L_P for the different slag-alloy systems, 100 g of the alloy was reacted with 10 g of slag, *i.e.* the slag-to-alloy mass ratio was maintained constant at 0.1 (but equilibrium is essentially independent of the relative masses, other than the effect of equilibration of Mn and Si between metal and slag). A small amount of Ar (0.01 g) was also added to allow for reactions to converge (Steenkamp, Pistorius, and Tangstad, 2015). The temperature range considered was 1300–1700°C at 50°C intervals.

Table I

Typical compositions of HCFeMn and MCFeMn alloys (mass%) utilized in thermodynamic calculations (Olsen, 2007)

Alloy	Mn	C	Si	P	Fe
HCFeMn	78.00	7.50	0.30	0.18	14.00
MCFeMn	80.00	1.50	0.60	0.20	17.70

Table II

Target chemical compositions of different slag systems

Slag label	Slag systems							Total
	MnO	CaO	SiO_2	CaF_2	Na_2O	BaO	BaF_2	
A	20.0	40.0	40.0					100.0
B	25.0	37.5	37.5					100.0
C	15.0	42.5	42.5					100.0
D	20.0	40.0	20.0		20.0			100.0
E	20.0	20.0	40.0		20.0			100.0
F	20.0	40.0	20.0	7.5	12.5			100.0
H	20.0	20.0	40.0			20.0		100.0
I	20.0					60.0	20.0	100.0
Basicity 0.7	20.0	34.0	46.0					100.0
Basicity 1.3	20.0	46.0	34.0					100.0

Materials and equipment

Two FeMn alloys were utilized for the dephosphorization experiments, namely MCFeMn and HCFeMn alloys. The MCFeMn and HCFeMn alloys were sourced from an industrial producer in South Africa. HCFeMn was utilized in only a few cases to investigate experimentally which of the two alloys would be easier to dephosphorize. Table III summarizes the average chemical composition of the MCFeMn alloy and HCFeMn master alloy. Because a graphite crucible was used for the experiments, these alloys converged on a similar carbon concentration after the reaction.

The slag reagents utilized in the study were sourced from the commercial suppliers Sigma Aldrich and ACE chemicals. Analytical grade CaO, SiO_2, MnO_2, CaF_2, $BaCO_3$, Na_2CO_3, and BaF_2 were utilized. Different synthetic slags were prepared. The slag components, *i.e.* CaO, SiO_2, Na_2CO_3, and $BaCO_3$, were calcined separately at 1000°C for 2 hours in air to remove volatile matter. Decomposition of the carbonaceous matter for Na_2CO_3 and $BaCO_3$ was, however, not successful at 1000°C. The calcined materials were then weighed and blended in a ring mill to generate a homogeneous mixture and charged into a graphite crucible. The crucible charges were subsequently heated in an induction furnace at 10°C/min to 1600°C and maintained at the temperature for 1 hour under an inert atmosphere using Ar gas. The molten materials were allowed to cool to room temperature under an inert atmosphere. The slags were then retrieved from the crucibles, crushed, milled, and decarburized at 1200°C for 2 hours in air, using alumina crucibles to burn off the residual carbon. The decarburized slags were analysed to determine their elemental compositions.

The MnO_2 reagent was not added during the melting stage of the synthetic slags to avoid reaction with the graphite crucibles. The component was incorporated after the decarburizing stage. $BaCO_3$ was also only added to the decarburized slags. The inclusion of $BaCO_3$ during the melting stage resulted in the erosion of the graphite crucibles.

Equipment

The dephosphorization tests were conducted in a 25 kW induction furnace Figure 1 presents the schematic diagram of the furnace. The furnace operates by radiation heating from a graphite susceptor heated by magnetic induction created by a water-cooled copper coil. The furnace power is switched on by using an on/off button on the control panel. The power was adjusted manually; the temperature was controlled by manually increasing the power setpoint at an interval of 30 minutes until the target temperature was reached. As it is generally difficult

Table III

Average bulk chemical composition of the industrial MCFeMn alloy and HCFeMn master alloys utilized in the study (mass%)

Element	Industrial MCFeMn	Industrial HCFeMn
Mn	78.70	75.80
Fe	18.62	17.00
Si	0.43	0.33
C	1.56	6.77
P	0.07	0.06
S	0.01	0.01
Total	99.17	99.90

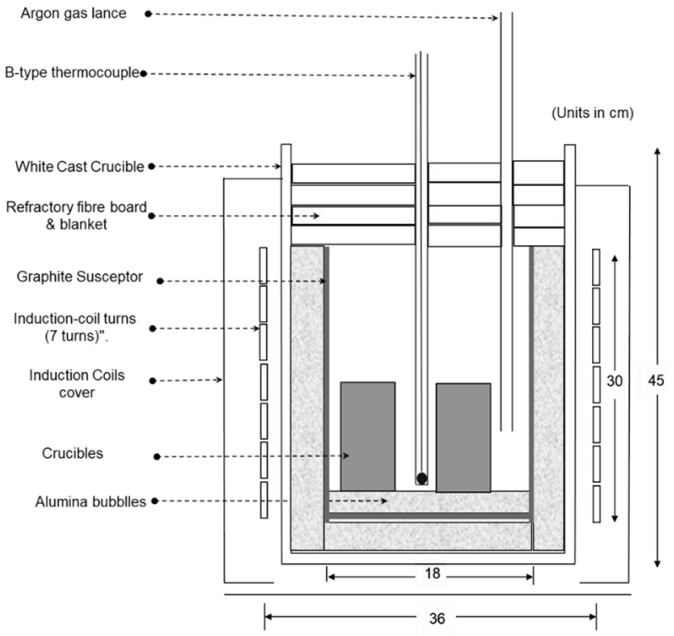

Figure 1—Schematic diagram of the induction furnace

to maintain a constant furnace temperature, a range of 10°C above and 10°C below the target temperature was maintained. Increasing the power setpoint at an interval of 30 minutes is the standard approach to ensure that the operating temperature is not overshot excessively.

Recipe design

Baseline CaO-based slag (Slag A)

In the current study, the slag system comprising 20%MnO-40%CaO-40%SiO_2 was adopted as a baseline slag. The basic oxide CaO was selected to provide free oxygen (O^{2-}) when dissolved in the liquid slag (refer to Equation [1]). MnO was added to provide the oxidizing condition in the system. The acidic SiO_2 was selected as a flux to reduce the melting point of the high-melting, basic MnO-CaO binary system. Figure 2 presents the MnO-SiO_2-CaO phase diagram, showing the fluxing strategy chosen and the expected change in slag liquidus temperature at 40% SiO_2 addition. As shown in Figure 2, the baseline slag has a liquidus temperature of 1320°C.

Na_2O-CaF2 addition (Slag D, Slag E, and Slag F)

The addition of Na_2O has proven to enhance the ability of CaO-based slags to dephosphorize liquid iron (van Niekerk and Dippenaar, 1998; Nassaralla and Fruehan, 1992). CaF_2, on the other hand, is added during hot metal treatment to maintain the fluidity of lime-based slags. Both additives have been reported to influence the phosphate capacities of basic slags (Fujita *et al.*, 1988) and were therefore investigated in the current study. CaO was partially replaced with Na_2O and CaF_2, while the MnO content was maintained constant.

BaO addition (Slag H)

Chaudhary and Roy (2001) found the BaO-BaF_2-MnO slag system to be effective for the dephosphorization of FeMn alloys, as well as liquid iron when BaO was utilized. The effect of BaO addition was investigated in the current study by replacing a fraction of the CaO with BaO.

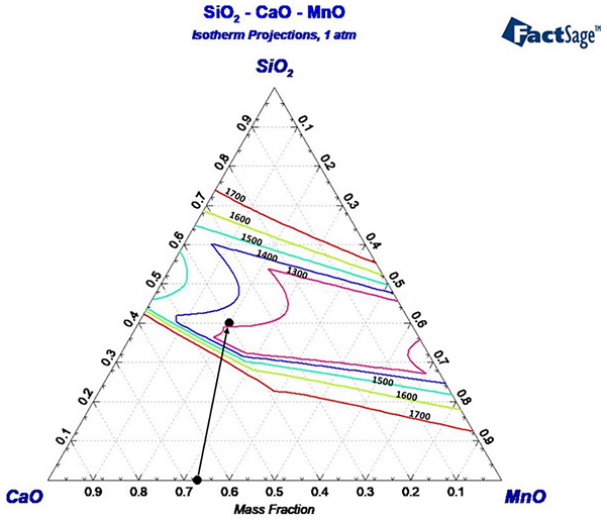

Figure 2—Liquidus isotherms for the system CaO–SiO_2–MnO, showing the desired slag composition achievable with the addition of SiO2 (calculated with FactSage)

BaO-BaF_2 addition (Slag I)

Replacing both the lime and silica by BaO and BaF_2 flux was also investigated. This slag system has been reported to be effective for dephosphorization of high-carbon FeMn alloy (Chaudary, Goel, and Minz, 2008; (Fujita *et al.*, 1988; (Dashevski *et al.*, 1998). The use of BaO-based slag without CaO posed numerous challenges during the current test work. The slag was very wetting towards the graphite crucible and spilled from the crucible due to what is assumed to have been the Marangoni effect. This slag could therefore not be investigated further.

Basicity changes to baseline CaO-based slag

The effect of changes in basicity, %CaO/%SiO_2, on the P partition coefficient was also investigated. The basicities investigated were 0.7, 0.9, and 1.3 using baseline slag A with the MnO content constant.

Table IV presents the chemical compositions of the prepared master slags. The results indicate that FeO, MgO, S, P, and Al_2O_3 were the major impurities. The slag reagents used contained significant amounts of impurities. The FeO was introduced mainly by the MnO_2 reagent. The target MnO, SiO_2, and CaO contents in the master slags were not entirely attained, owing mainly to the FeO content in the slag. The total chemical compositions of the slags are also generally lower than 100%. This was attributed to the expression of Mn as MnO instead of MnO_2 and the presence of carbonaceous matter introduced by $BaCO_3$ and Na_2CO_3. These slags were utilized in the dephosphorization tests.

Dephosphorization test procedure

All tests used the same test preparation method, which entailed weighing the required amounts of the slag and alloy, followed by homogenization of the feed charges in a ring mill for about 30 seconds. About 10 g of both the starting alloy and slag was used for the experiments. The charge was then packed into the graphite crucible. Packing was done such that a dense, compact solid charge was formed to promote the interaction of solid particles in the crucible. Graphite crucibles sere used to avoid attack of the crucible by the different slag systems. The crucibles were also selected with the intention of maintaining the slag chemistries during the tests without interference by the crucible.

Table IV

Bulk chemical compositions of the prepared master slags (mass%)

	S	P_2O_5	Al_2O_3	SiO_2	CaO	MnO	FeO	BaO	MgO	Na2O	CaF_2	Total
Target				40.0	40.0	20.0						
Slag A	0.029	0.18	0.74	40.3	35.0	16.9	3.72		0.60			97.46
Target				40.0	20.0	20.0				20.00		
Slag E	0.008	0.13	0.49	36.9	16.9	15.6	3.37		0.39	15.99		89.8
Target				40.0	20.0	20.0				12.50	7.50	
Slag F	<0.005	0.25	0.55	36.7	18.0	16.4	3.43		0.44	11.60	5.16	92.52
Target				40.0	20.0	20.0		20				
Slag H	<0.005	0.12	0.61	40.3	19.1	17.2	3.90	14.30	0.45			96.01
Target				37.5	37.5	25.0						
Slag B	<0.005	0.12	0.30	36.0	34.0	22.9	4.47		1.00			98.79
Target				42.5	42.5	15.0						
Slag C	<0.005	0.12	0.31	42.0	40.5	12.8	2.73		1.05			99.51
Target				34.0	47.0	20.0						
*Basicity 1.3	<0.005	0.12	0.28	31.0	40.5	17.5	2.75		0.95			93.11
Target				47.0	34.0	20.0						
*Basicity 0.7	<0.005	0.13	0.261	44.7	31.0	16.5	3.57		0.49			96.62

* %CaO/%SiO²

The charged crucibles were weighed and placed in the furnace chamber. The furnace chamber was covered with high-temperature refractory blankets (Fiberfrax) to prevent air ingress and preserve heat in the chamber. An alumina tube piped argon gas into the furnace chamber to create an inert environment for the duration of each test. An alumina sheath encased the Type B control thermocouple. The same thermocouple monitored the sample temperature.

The furnace was heated gradually by incrementally increasing the power input until the target test temperature was reached. The typical heating rate was 8–10°C/min under an inert atmosphere. The argon flow rate was maintained at around 2 L/min for the duration of the test. The samples were maintained at the target temperature for retention times of 30 minutes and 60 minutes. A lower retention time of 5 minutes was also investigated, but the analysis of the samples could not be completed due to poor separation of the slag and alloy at 1350°C. Upon completion of each test, the furnace power was switched off and the refractory blankets slightly moved to allow removal of the graphite crucibles from the furnace chamber. The hot crucibles were removed from the furnace using steel tongs and immediately quenched in a water-and-ice bath to ensure rapid cooling of the molten slag and alloy and maintain the phase chemistry in both the slag and alloy at the specific test conditions. The quenched crucibles were then dried at 105°C overnight in a drying oven. The dried sample was weighed and broken to retrieve the slag and alloy.

The alloy and slag were separated manually, weighed, and pulverized for analysis. The bulk chemical compositions of the feed materials and products were determined by Inductively coupled plasma-optical emission spectroscopy (ICP-OES). C and S were determined by combustion (LECO). P was determined using wet chemical analysis by ICP. Table V represents a summary of the completed test matrix. Test work using slag D was unsuccessful because the slag has a high liquidus temperature of about 1800°C and separation of slag and alloy was not possible at the experimental temperatures. This slag was therefore not investigated further. Slag I was aggressive towards the graphite crucible, resulting in crucible erosion and leakage of the contents.

Table V

Matrix of tests completed

Slag	Alloy	Basicity*	Sampling times (min)	Temperature (°C)
Slag A	MCFeMn	1	30,60	1350, 1400,1450
Slag A	MCFeMn	1.3	30	1450
		0.7		
Slag A, E, F, H	HCFeMn	1	60	1350
Slag B	MCFeMn	1	30	1450
Slag C	MCFeMn	1	30	1450
Slag E	MCFeMn	1	30,60	1350, 1400,1450
Slag F	MCFeMn	1	30,60	1350, 1400,1450
Slag H	MCFeMn	1	30,60	1350, 1400,1450

* $\%CaO/\%SiO_2$

Results and discussion

FactSage calculations

Phosphorus partition coefficient

The L_p values obtained from the thermochemical calculations are presented in Figure 3 for HCFeMn and Figure 4 for MCFeMn. The calculations generally predict that dephosphorization of both alloys will not be possible with the CaO slags as the L_p values obtained were well below unity. The results generally showed an increase in L_p for most of the slag-alloy systems as the temperature is increased. The increase in L_p with increasing temperature was unexpected, as the dephosphorization reaction is exothermic (Chaudary and Goel, 1994; Simeonov and Sano, 1985).

The addition of BaO in conjunction with CaO caused a detrimental effect, with lower predicted L_p values obtained as indicated by slag H. Replacing both CaO and SiO_2 with BaO and BaF_2 flux in slag I resulted in higher L_P values, above unity. The FactSage predictions concerning the BaO-BaF_2-MnO slag system agree with the observations made by various researchers (Fujita, *et al.*, 1988;Chaudhary, Minj, and Goel, 2007; Dashevski *et al.*, 1998). The effect of temperature on L_P

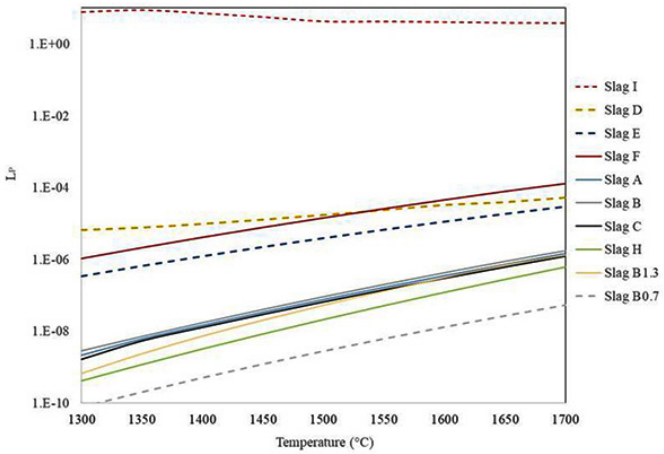

Figure 3—Predicted equilibrium P distribution coefficient (on a logarithmic scale) for the different slags when reacted with the HCFeMn alloy

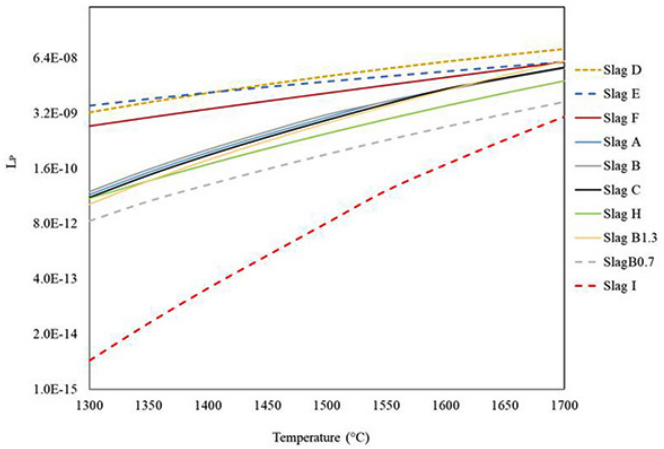

Figure 4—Predicted equilibrium P distribution coefficient (on a logarithmic scale) for the different slags when reacted with the MCFeMn alloy

for slag I is small compared to the opposite effect for most of the other slags. Comparing the results obtained from the two alloys, the prediction by FactSage show that the BaO-based slag will not dephosphorize the MCFeMn alloy, and lower L_p values were obtained with MCFeMn alloy.

In conclusion, the results obtained from the FactSage calculations predicted that none of the CaO-based slags would yield significant dephosphorization. The L_p predictions for CaO-based slags were very low and not in agreement with findings in the literature that L_p decreases as temperate is increased (Chaudhary and Goel, 2007; Fujita *et al.*, 1988). Based on the results, it appears that FactSage does not accurately predict dephosphorization ratios for FeMn calculations. Experimental test work was thus necessary to serve as a check on the FactSage results.

Dephosphorization test work

Phosphorus partition coefficient: effect of temperature and reaction time

Figures 5 and 6 show the L_p values obtained from the different slags at different temperatures for reaction times of 30 minutes and 60 minutes, respectively. The results show that the baseline slag CaO-SiO_2-MnO slag (slag A) appeared to yield higher L_p values than the other slags at the temperatures and reaction times investigated. The results also show that at higher temperatures, generally lower L_p values were obtained. Slag H, however, gave slightly higher values at 1450°C. This anomaly may be attributed to the analytical errors for samples from either the 1400°C or 1450°C experiments. Liu *et al.* (1995) similarly observed lower L_p values as the temperature was increased during dephosphorization of FeMn alloy with BaO-containing slags.

Effect of changing MnO content of baseline slag

Figure 7 shows the L_p values obtained at the three initial MnO slag contents at 1450°C, 30 minutes reaction time. Figure 8 represents the L_p *versus* the final MnO slag contents, which increase in the final slags. The loss of Mn from the alloy is influenced by the oxygen partial pressure in the system. Factors that may have contributed to the loss of Mn include possible air ingress during the tests and the exposure of the alloys to oxygen during quenching, as Mn has a high affinity for oxygen. Liu *et al.* (1995) observed that the use of CaO, SiO_2, and CaF_2 to dephosphorize ferromanganese melts resulted in increased Mn losses to the slag. Watanabe *et al.* (1993) reported that MnO in basic slag acts as a diluent which may lessen the basic effect of the slag, reducing the capacity of the slag to remove P from the alloy. The presence of MnO in the slag is important to provide the required oxygen, although high MnO content can lead to low dephosphorization (Chaudhary and Roy, 2001).

The L_p results show that there was an increase in L_p from 15% to 20% MnO, followed by a reduction in the partition ratio. High amounts of MnO may affect the activity of the basic oxides such as CaO and BaO in the slag and can reduce the capacity of the slag to absorb P. Chaudhary, Minj, and Goel (2007) observed that an increase in the MnO content to above 20% (in BaO-containing slag) resulted in poor P removal. In the HCFeMn dephosphorization studies by Liu *et al.* (1995), it was observed

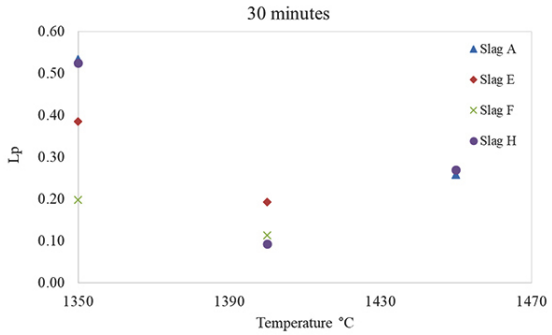

Figure 5—*Lp* values obtained at different temperatures for MCFeMn alloy; 30 minutes reaction time

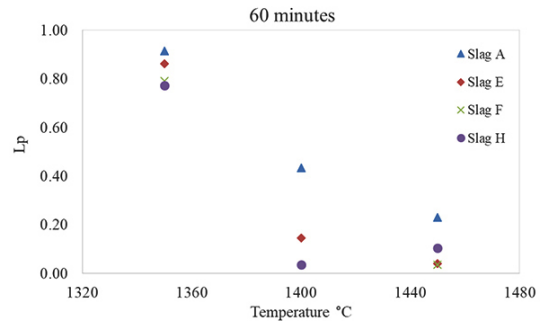

Figure 6—*Lp* values obtained at different temperatures for MCFeMn alloy; 60 minutes reaction time

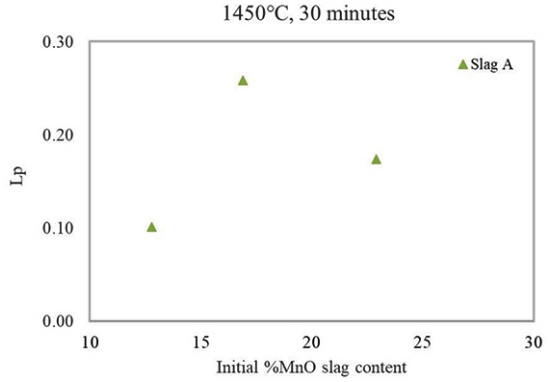

Figure 7—Effect of initial MnO content in the slag on *Lp* at 1450°C and 30 minutes retention time

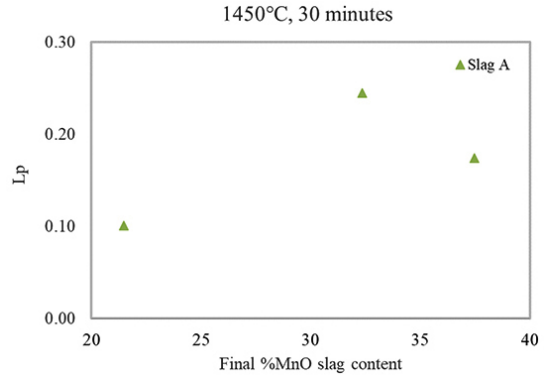

Figure 8—*Lp versus* the final MnO in slags at 1450°C and 30 minutes retention time

that an increased concentration of MnO in slag had a negative influence on the phosphate capacity of BaO-MnO-$BaCl_2$ slag. It was, therefore concluded from the investigations that an MnO content above a certain value is detrimental to the capability of the slag to dephosphorize FeMn alloys. In the current study, the high MnO slag contents may have adversely affected the P capacity of the slags.

Effect of adding Na_2O and CaF_2

Na_2O is a more basic oxide than CaO, so it was expected that dephosphorization would be improved by Na_2O additions. The results represented in Figures 5 and 6 generally show that the addition of Na_2O, indicated by slag E, generally did not provide any added benefit as low L_p values were still obtained. The literature indicates that the addition of Na_2O to CaO-based slags improves the dephosphorization of liquid iron; however, Na_2O can be reduced by either C or Mn, producing CO/MnO. The instability of Na_2O can therefore have a detrimental effect on the dephosphorization of FeMn alloys due to loss of Mn (Tabuchi and Sano, 1985). In the current study, the loss of Mn from the alloy was observed even with the Na_2O-free slags, so it is not possible to establish the effect of Na_2O on Mn loss. Fujita *et al.* (1988) also observed that low degrees of dephosphorization were achieved when using Na_2CO_3 flux on FeMn alloy.

The fluoride ion (F^-) from CaF_2/BaF_2 is reported to stabilize the phosphate ion (PO_4^{3-}) during the ionic dephosphorization reaction in molten slag under oxidizing conditions, and thus contribute positively to dephosphorization (Liu *et al.*, 1998). However, Ca^{2+} binds fluoride ions much more strongly than Ba^{2+} does, because of the difference in the ionic radius of the two cations. Therefore, fewer free fluoride ions would be available when using CaF_2 to enhance dephosphorization (Liu *et al.*, 1998). Liu *et al.* observed that the addition of CaF_2 to MnO-BaO-BaF_2 slag reduced L_p and increased the Mn capacity of the slag, *i.e.* Mn losses to the slag. In the current study, the addition of CaF_2 (slag F) showed no improvement in terms of L_p.

Effect of adding BaO

The use of BaO in conjunction with CaO (slag H), also resulted in no improvement. Similar L_p values to those of slag A were obtained under conditions of 1350°C and 1450°C at 30 minutes. Slag A was, however, not outperformed by slag H under any of the other conditions. Nasaralla, Fruehan, and Min (1991) investigated the use of BaO as an additive in CaO-based flux for dephosphorizing Fe-C-P alloy. It was observed that amounts of BaO < 40% had no effect on the phosphate capacity of the slag. A larger increase in the phosphate capacity was only observed after increasing the BaO content of the CaO-CaF_2 slag to above 40%. The researchers also later observed that the L_p increased significantly, by a factor of 4.6, when a high BaO content of 30% was utilized in the CaO-Al_2O_3-CaF_2 slag system (Nassaralla and Fruehan, 1992). During the current study, a BaO content of 20% was utilized. The lower L_p values obtained could be attributed to the low concentration of the basic oxide and uncertainties in the analysis of P, as well as the dilution of the slag by MnO.

Effect of slag basicity

Increasing the slag basicity (%CaO/%SiO_2) to 1.3 caused the slag liquidus temperature to increase to about 1500°C. This led to difficulties in melting the slag and resulted in poor slag separation during the experiment at 1450°C, due to the alloy being entrained in the slag. This had a detrimental effect on the ability of the slag to remove P. As the reaction occurs in a liquid phase, a lower L_p was obtained by increasing the basicity to 1.3, as shown in Table VI. At the lower %CaO/%SiO_2 ratio of 0.7, the P concentration in the slag was below the detection limit (<0.005%) and L_p could not be calculated. The results, therefore, show an initial increase in L_p value from a basicity of 0.7 to 1.0, followed by a slight reduction in L_p.

Effect of initial alloy composition

Figures 9 and 10 show the L_p values obtained with HCFeMn at 1350°C and 1400°C respectively. Dephosphorization of HCFeMn by the respective slags was also not significant, as lower $L_p$values of <1 were generally obtained.

Comparison between the results shows that at 1350°C, relatively higher L_p values were obtained from MCFeMn, and lower values at 1400°C. As noted earlier, both the HCFeMn and the MCFeMn alloy would have reached carbon saturation during the experiments. The studies on the effect of initial C, Mn, and Si content on dephosphorization have shown that a high Mn in the alloy decreases the activity coefficient of P, and L_p increases

Table VI

Effect of %CaO/%SiO_2 ratio on L_p at 1450°C and 30 minutes retention time

%CaO/%SiO_2	L_p
0.7- 0.90.26 1.30.13	

-: P slag analysis <0.005%

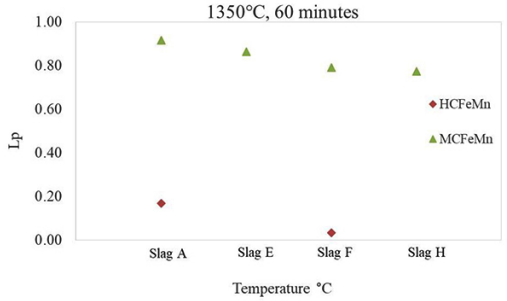

Figure 9—Comparison of phosphorus distribution between MCFeMn and HCFeMn and slag at 1350°C, 60 minutes reaction time

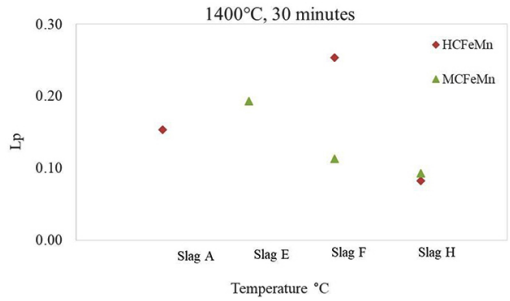

Figure 10—Comparison of phosphorus distribution between MCFeMn and HCFeMn and slag at at 1400°C, 30 minutes reaction time

Table VII

Comparison between the results obtained in the current study and in the literature

Variables	What did they find?	Current results
MnO content of baseline slag	Chaudhary, Minj, and Goel (2007) conducted dephosphorization tests using graphite crucibles in an induction furnace. An increase in the MnO content to above 20% in the BaO slag system resulted in poor P removal. In dephosphorization of HCFeMn studies, Liu *et al.* (1995) observed that increased MnO in the slag had a negative influence on the phosphate capacity. Watanabe *et al.* (1993) reported that MnO in basic slag acts as an acidic oxide which may counter the basic effect of the slag, reducing its capacity to remove P from the alloy.	The results showed increased MnO contents in the final slags. There was a slight increase in L_p from the initial MnO slag content of 15% to 20%, followed by a reduction in the partition ratio.
Na_2O and CaF_2	(Simeonov and Sano (1985) studied the equilibrium P distribution ratio between additions $MnO-SiO_2-CaO-CaF_2$ slag and carbon-saturated iron containing 4.6–5.5% Mn and 0.025–0.06% P. The addition of Na_2O increased the phosphate capacity of the slag. (Fujita *et al.* (1988) obtained low dephosphorization rates using Na_2CO_3 flux with FeMn alloy. Liu *et al.* (1998) studied the effect of different additives (CaO, MgO, SiO_2, CaF_2, and Al_2O_3) in $BaO-BaF_2$-MnO slags on the L_p . The addition of CaF_2 to $MnO-BaO-BaF_2$ slag reduced L_p.	The addition of Na_2O to $CaO-MnO-SiO_2$ slags generally did not provide any added benefit as low L_p values were still obtained. With additions of CaF_2, similar L_p values to those of slag A were obtained at 1350°C and 1450°C at 30 minutes. However, the CaF_2-containing slag did not outperform the base slag (slag A) under any of the other conditions
BaO additions	(Nasaralla, Fruehan, and Min (1991) investigated the use of BaO as an additive in CaO-based flux to dephosphorize Fe-C-P alloy. A small amount of BaO (<40%) had no effect on the phosphate capacity of the slag. A larger increase in the phosphate capacity was observed with >40% BaO in the $CaO-CaF_2$ slag. Nassaralla and Fruehan (1992) observed that L_p increased, by a factor of 4.6 when a high BaO content of 30% was used in the $CaO-Al_2O_3-CaF_2$ slag system.	A BaO content of 20% was utilized. The use of BaO in conjunction with CaO showed no improvement. Similar L_p values to those of slag A ($CaO-MnO-SiO_2$) were obtained at 1350°C and 1450°C at 30 minutes, but slag with BaO did not outperform slag A. The lower L_p values could be attributed to the low concentration of the basic oxide and also the uncertainties in the analysis of P, as well as dilution of the slag by MnO.
Slag basicity	Simeonov and Sano (1985) investigated the equilibrium P distribution ratio between carbon-saturated iron with a high Mn content and lime-based slags contained MnO, Na_2O, and BaO. The slag systems included $MnO-SiO_2-CaO-CaF_2$, $MnO-SiO_2-CaO$ CaF_2-BaO, and $MnO-SiO_2-CaO-Na_2O$. The results illustrated that a higher basicity increased the P equilibrium distribution	Increasing the slag basicity ($\%CaO/\%SiO_2$) to 1.3 increased the slag liquidus temperature to about 1500°C. This caused difficulties in melting the slag and resulted in poor slag separation during the experiment- at 1450°C, due to alloy entrainment in the slag. This had a detrimental effect on the efficiency of the slag to remove P. At the lower $\%CaO/\%SiO_2$ ratio of 0.7, the P in the slag was below detection limit (<0.005%) and L_p could not be calculated. The results therefore show an initial increase in L_p value from basicity of 0.7 to 1.0, with a slight decrease in L_p beyond this.
Initial alloy composition	The studies by (Chaudary, Goel, and Minz (2008) and Bhardwaj (2014) on the effect of initial C, Mn, and Si on dephosphorization showed that high Mn in the alloy decreases the activity coefficient of P and L_p increases with increasing initial C content until the C saturation point. High initial Si (>0.2%) is not favourable for dephosphorization as Si oxidizes during the dephosphorization, leading to increased SiO_2 in the slag, which consumes the high basic oxides and ultimately reduces the capacity of the slag to remove P.	The molten MCFeMn absorbed C from the crucible, forming HCFeMn, and the final average compositions of the alloys were similar after dephosphorization. The initial Si contents in both alloys were similar at about 0.4%; Si is reported to be undesirable for dephosphorization of FeMn alloys.

with increasing initial C content until the C saturation point. High initial Si (>0.2%) is not favourable for dephosphorization as the Si is oxidized during dephosphorization, leading to increased SiO_2 in the slag, which consumes the high basic oxides and ultimately reduces the capacity of the slag to remove P (Chaudary, Goel, and Minz, 2008; Bhardwaj, 2014). During the current study, the molten MCFeMn absorbed C from the crucible, forming HCFeMn, and the final average compositions of the alloys appeared to be similar after dephosphorization. The initial Si in both alloys was similar at about 0.4%, which is reported to be undesirable for dephosphorization of FeMn alloys.

Conclusion

The FactSage calculations indicated that none of the CaO-based slags would result in significant dephosphorization.

The results generally showed that L_p remained small (<1): a significant proportion of P remained in the alloy, and thus dephosphorization was not favoured. The $CaO-SiO_2$-MnO (slag A) slag system yielded higher values of L_p. The addition of Na_2O (slag E) generally did not show any added benefit. Substituting half of the CaO by BaO (slag H) resulted in similar L_p values to those of slag A under conditions of 1350°C and 1450°C at 30 minutes. Slag H did not outperform slag A under any of the other conditions. Increasing the temperature generally resulted in lower L_p values. This may be attributed to the exothermic nature of the reaction which should be favourable at lower temperatures. Increasing the $\%CaO/\%SiO_2$ ratio of the starting slag gave an initial increase in L_p value from a basicity of 0.7 to 1.0, followed by a slight reduction in the partition ratio. The latter results were not expected, as a higher basicity is expected

to improve the P capacity of the slag. Increasing the basicity increased the slag liquidus temperature, which negatively affected dephosphorization.

In summary, based on the L_p values obtained, the conditions investigated are unfavourable for the removal of P from South African MCFeMn and HCFeMn industrial alloys, as significant amounts of P remained in the alloy. The experimental results are in line with FactSage predictions that the CaO slags are not suitable for dephosphorization of FeMn alloys.

Below is a summary of the shortcomings of the current study and recommended future work (Table VIII).

Due to the unsuccessful removal of P from the FeMn alloys by the CaO-based slag systems, it is recommended that further investigations be considered on the use of BaO-based slags with no CaO addition. BaO slags are reported in the literature to be effective for dephosphorization of FeMn alloys. However, during the current study experimental challenges were encountered with the BaO-based slag. Further test work should be conducted with highly pure slag reagents that do not introduce P as an impurity in the master slags. It is also recommended that various other slags be investigated, with which higher basicity can be achieved at lower temperatures.

Acknowledgment

The paper is published with the permission of Mintek. The authors wish to thank Mintek for financial support.

References

Bale, C., Bélisle, E., Chartrand, P., Decterov, S.A., Eriksson, G., Hack, K., Jung, I.-H., Kang, Y.-B., Melançon, J., Pelton, A.D., Robelin, C., and Petersen, S. 2009. FactSage thermochemical software and database-recent development. *Calphad*, vol. 33, no. 2. pp. 295–311.

Bale, C. Bélisle, E., Chartrand, P., Decterov, S., Eriksson, G., Gheribi, A., Hack, K., Jung, I., Kang, Y-N., Melancon, J., Pelton, A., Petersen, S., Robelin, C., Sangster, J., Spencer, P., and van Ende, M-A. 2016. Reprint of: FactSage thermochemical software and databases, 2010-2016. *Calphad*, vol. 55, no. 1. pp. 1–19.

Baluch, N., Udin, Z.M., and Abdullah, C.S. 2014. Advanced high strength steel in auto industry: An overview. *Engineering Technology and Applied Science Research*, vol. 4, no. 4. pp. 686–689.

Bernhard, C., Linzer, B., Presoly, P., Watzinger, I., and Watzinger, J. 2019. Evaluation of AHSS concepts with a focus on the product properties and appropriate casting characteristics of Arvedi ESP thin slab casters. *IOP Conference Series - Materials Science and Engineering*, vol. 529, no. 1. *Joint 5th International Conference on Advances in Solidification Processes (ICASP-5) & 5th International Symposium on Cutting Edge of Computer Simulation of Solidification, Casting and Refining (CSSCR-5)*, Salzburg, Austria, 17–21 June 2019. pp. 1–10.

Bhardwaj, B.P. 2014. Production of ferroalloys. *The Complete Book on Ferroalloys*. NCPS, Delhi, India. pp. 300–309.

Chaudhary, P.N. and Goel, R.P. 1994. Dephosphorization of liquid ferromanganese. *4th Refresher Course on Ferro Alloys*, Jamshedpur, India, 12-14 January 1994. National Metallurgical Laboratory, Jamshedpur. pp. 1-11.

Chaudhary, P.N., Goel, R.P., and Minz, R.K. 2008. An improved process for dephosphorization of high carbon ferromanganese. *Patent no*. 217812. Council of Scientific and Industrial Research, New Delhi.

Chaudhary, P.N., Minj, R.K., and Goel, R.P. 2007. Development of a process for dephosphorisation of high carbon ferromanganese. *INFACON 8. Proceedings of the 11th International Ferroalloys Congress*, New Delhi. pp. 288-295. https://www.pyrometallurgy.co.za/InfaconXI/288-Chaudhary.pdf

Chaudhary, P.N. and Roy, G.G. 2001. Dephosphorization of HCFeMn using $BaCO_3$ based fluxes. *Ionmaking & Steelmaking*, vol. 29, no. 5. pp. 396–403.

Dashevskii, V.Y.. Kashin, V.I., Lyakishev, N.P., Velichko, B.F., and Koval, A.V. 1998. Desphosphorization of manganese ferroalloys with CaO and MnO based slag-forming mixtures. *Proceedings of INFACON VIII*, Beijin, China. pp. 300-301. https://www.pyrometallurgy.co.za/InfaconVIII/300-Dashevskii.pdf

Fujita, M., Katayama, H., Yamamoto, A., and Mutsuo, M. 1988. Dephosphorization of Fe-Mn-C alloy with $BaCO_3$. *Tetsu-to-Hagane*, vol. 74, no. 5. pp. 816–822.

Karbowniczek, M., Michaliszym, A., Wcislo, Z., and Slezak, W. 2014. Dephosphorization of ferromanganese. *Acta Metallurgica Slovaca-Conference*, vol 4. pp. 138–144. doi:10.12776/amsc.v4i0.252

Liu, X., Wijk, O., Selin, R., and Edstrom, J.O. 1998. Effects of additives in $BaO-BaF_2$-MnO slags on phosphate and manganese capacities. *ISIJ International,* vol. 38, no. 1. pp. 36–45.

Liu, X., Wijk, O., Selin, S.R., and Edstrom, J.O. 1995. Phosphorus equilibrium between $BaO-BaF_2$-MnO fluxes and ferromanganese melts. *Steel Research*, vol. 66, no. 3. pp. 96–102.

Nasaralla, C., Fruehan, R.J., and Min, D.J. 1991. A thermodynamic study of dephosphorization using $BaO-BaF_2$, $CaO-CaF_2$, and $BaO-CaO-CaF_2$ systems. *Metallurgical Transactions B*, vol. 22, no. 1. pp. 33–38.

Nassaralla, C. and Fruehan, R.J. 1992. Phosphate capacity of $CaO-AI_2O_3$ slags containing CaF_2, BaO, Li_2O, or Na_2O. *Metallurgical Transaction B*, vol. 23, no. 2. pp. 117–123.

Olsen, S.E., Olsen, S., Tangstad, M., and Lindstad, T. 2007. Manganese ores. *Production of Manganese Ferroalloys*. Tapir Academic Press, Trondheim, Norway. pp. 19–26.

Safarian, J. and Kolbeinsen, L. 2013. Purity requirements for Mn-alloys for producing high manganese TRIP and TWIP steels. *Proceedings of the Thirteenth International Ferro-Alloys Congress*, Almaty, Kazakhstan, 9-13 June 2013. pp. 175–183. https://pyrometallurgy.co.za/InfaconXIII/0175-Safarian.pdf

Simeonov, S.R. and Sano, N. 1985. Phosphorus equilibrium distribution between slags containing MnO, CaF_2 and Na_2O and carbon-saturated iron for hot metal pretreatment. *Transactions of the Iron and Steel Institute of Japan*, vol. 25, no. 10. pp. 1031–1035.

Steenkamp, J.D. BamII; W.G., Ringdalen, E., MushwanaI; M., Hockaday, S.A.C., and Sithole, N.A. 2018. Working towards an increase in manganese ferroalloy production in South Africa - A research agenda. *Journal of the Southern African Institute of Mining and Metallurgy*, vol. 118, no. 6. pp. 645–654.

Steenkamp, J.D., Pistorius, P.C., and Tangstad, M. 2015. Chemical wear analysis of a tap-hole on a SiMn production furnace. *Journal of the Southern African Institute of Mining and Metallurgy*, vol. 115, no. 3. pp. 199–208.

Tabuchi, S. and Sano, N. 1985. Thermodynamics of phosphate and phosphide in $CaO-CaF_2$ melts. *Metallurgical Transactions B*, vol. 15, no. 2., pp. 351–356.

Tang, K. and Olsen, S.E. 2006. Computer simulation of equilibrium relations in manganese ferroalloy production. *Metallurgical ad Materials Transactions B*, vol. 37, no. 4. pp. 599–606.

Van Niekerk, W.H. and Dippenaar, R.J. 1998. Phosphorus distribution between carbon-saturated iron at 1350°C and lime-based slags containing Na_2O and CaF_2. *Metallurgical and Materials Transactions B*, vol. 29, no. 1. pp. 147–153.

Visser, M., Smith, H., Ringdalen, E., and Tangstad, M. 2013. Properties of Nchwaning and Gloria ores in the production of Mn Ferro-alloys. *Proceedings of the Thirteenth International Ferroalloys Congress*, Almaty, Kazakhstan, 9-13 June 2013. pp. 553–566. https://www.pyrometallurgy.co.za/InfaconXIII/0553-Visser.pdf

Wagner, C. 1975. The concept of the basicity of slags. *Metallurgical Transactions B*, vol. 6, no.3. pp. 405–409.

Watanabe, Y. Kitamura, K., Rachev, I.P., Tsukihashi F., and Sano, N. 1993. Thermodynamics of phosphorus and sulfur in the BaO-MnO flux system between 1573 and 1673 K. *Metallurgical Transactions B*, vol. 24, no. 2. pp. 339–347.

You, B., Lee, B., and Pak, J. 1999. Manganese loss during the oxygen refining of high-carbon ferromanganese melts. *Metals and Materials*, vol. 5, no. 5. pp. 497–502. ◆

Table VIII

Summary of the shortcomings of the current study and recommended future work

	Shortcoming	Future work
1.	The analytical grade reagents used appeared to not be free of impurities. Some of the reagents (e.g. MnO_2 used as a source of MnO) introduced a significant amount of P to the master slag,	Conduct the dephosphorization test work with highly pure slag reagents that do not introduce P as an impurity in the master slags.
2.	The $BaO-BaF_2$-MnO slag system is reported to be effective for dephosphorization of ferromanganese alloys. However, the slag reacted with the graphite crucible in the current study.	The slag should be investigated using different $BaO–MnO-BaF_2$ compositions.
3.	Oxidation of Mn occurred during the experiment due to possible air ingress as well as exposure of the alloys to air during quenching	Use a furnace that is gas-tight. The drop-quenched furnace set-up can be improved.

8TH SULPHUR AND SULPHURIC ACID CONFERENCE | 2022

16 MAY 2022 - WORKSHOP
Sulfuric Acid Catalysis - Key Parameters to Increase Efficiency and Lower Costs

17-18 MAY 2022 - CONFERENCE
19 MAY 2022 - TECHNICAL VISIT

THE VINEYARD HOTEL, NEWLANDS, CAPE TOWN, SOUTH AFRICA

BACKGROUND

The production of SO_2 and sulphuric acid remains a pertinent topic in the Southern African mining and metallurgical industry, especially in view of the strong demand for, and increasing prices of, vital base metals such as cobalt and copper.

The electric car revolution is well underway and demand for cobalt is rocketing.

New sulphuric acid plants are being built, comprising both smelters and sulphur burners, as the demand for metals increases. However, these projects take time to plan and construct, and in the interim sulphuric acid is being sourced from far afield, sometimes more than 2000 km away from the place that it is required.

The need for sulphuric acid 'sinks' such as phosphate fertilizer plants is also becoming apparent.

All of the above factors create both opportunities and issues and supply chain challenges.

To ensure that you stay abreast of developments in the industry, the Southern African Institute of Mining and Metallurgy invites you to participate in a conference on the production, utilization, safe transportation and conversion of sulphur, sulphuric acid, and SO_2 abatement in metallurgical and other processes, to be held in 19 May 2022 in Cape Town.

FORMAT OF THE EVENT

At this point in time, the event is planned as a full contact conference with international participation through web links. It is also planned to hold technical visits to nearby facilities.

The situation will be constantly reviewed, and if it appears that the effects of the pandemic are still such as to pose a threat to the health and safety of delegates, this will be changed to a digital event.

OBJECTIVES

- To expose delegates to issues relating to the generation and handling of sulphur, sulphuric acid, and SO_2 abatement in the metallurgical and other industries.
- Provide an opportunity to producers and consumers of sulphur and sulphuric acid and related products to be introduced to new technologies and equipment in the field.
- Enable participants to share information about and experience in the application of such technologies.
- Provide an opportunity for role players in the industry to discuss common problems and their solutions.

WHO SHOULD ATTEND

The Conference will be of value to:

- Metallurgical and chemical engineers working in the minerals and metals processing and chemical industries
- Metallurgical/chemical/plant management
- Project managers
- Research and development personnel
- Academics and students
- Technology providers and engineering firms
- Equipment and system providers
- Relevant legislators
- Transportation

EXHIBITION AND SPONSORSHIP

There are a number of sponsorship opportunities available. Companies wishing to sponsor or exhibit should contact the Conference Co-ordinator.

FOR FURTHER INFORMATION, CONTACT:

Camielah Jardine,
Head of Conferencing
E-mail: camielah@saimm.co.za
Tel: +27 11 834-1273/7
Web: www.saimm.co.za

WORKSHOP SPONSOR

BASF
We create chemistry

SAIMM
THE SOUTHERN AFRICAN INSTITUTE OF MINING AND METALLURGY

Determination of the optimal transition point between a truck and shovel system and a semi-mobile in-pit crushing and conveying system

M. Shamsi[1] and M. Nehring[2]

Affiliation:
[1]School of Mining Engineering, Faculty of Engineering, University of Tehran.
[1]School of Mechanical and Mining Engineering, Faculty of Engineering, University of Queensland.

Correspondence to:
M. Nehring
M. Shamsi

Email:
m.nehring@uq.edu.au
shamsi.miner@gmail.com

Dates:
Received: 9 Mar. 2021
Revised: 14 Aug. 2021
Accepted: 24 Aug. 2021
Published: September 2021

How to cite:
Shamsi, M. and Nehring, M. 2021 Determination of the optimal transition point between a truck and shovel system and a semi-mobile in-pit crushing and conveying system. Journal of the Southern African Institute of Mining and Metallurgy, vol. 121, no. 9, pp. 497–504

DOI ID:
http://dx.doi.org/10.17159/2411-9717/1564/2021

ORCID:
M. Shamsi
https://orcid.org/0000-0001-7555-8568
M. Nehring
https://orcid.org/ 0000-0002-0404-5332

Synopsis

One of the most challenging aspects in semi-mobile in-pit crushing and conveying (SMIPCC) system design is determining the optimum depth at which to change from a purely truck-based haulage system to a conveyor-based haulage system. We used scenario analysis to determine the optimum transition depth between a truck and shovel (TS) system and a SMIPCC system. Traditional pit-limit algorithms were used to generate the final pit limit on a copper deposit, which was then divided into four pushbacks. The final operating pushbacks (phases) were designed for both TS and SMIPCC. The end depths for each phase are viewed as candidate transition points to switch from the TS to SMIPCC haulage system. Economic calculations were applied for five different scenarios, including adopting SMIPCC from the outset (pure SMIPCC), after the first, second, and third phases, and finally not using the SMIPCC system (pure TS) at all. The analysis indicates that the second scenario, at a depth of 335 m, results in the lowest cumulative discounted cost (CDC). In this case, the CDC is 17.6% lower than that for the pure TS scenario and 10.7% lower than for the pure SMIPCC system scenario.

Keywords
Open-pit mining, mining transportation systems, in-pit crushing and conveying, truck and shovel, transition point.

Introduction

Mining is considered a cost-intensive industry that will yield a profit when the revenue from selling the valuable product exceeds the cost of producing it across the mine life. For maximum profit, designers are looking to increase precision and the ability to optimize production processes throughout the life of mine (Samavati *et al.*, 2018). One way to enhance profits from mining is to identify expensive production processes and provide operational solutions to reduce the cost of these processes.

Transportation costs have always been a significant part of operating costs in large open-pit mines. This is illustrated in Figure 1, which shows a typical operating cost distribution for a large, deep open-pit mine using the conventional truck and shovel (TS) system. Transportation costs are very variable, depending on pit configuration and geographical location. However, the haulage component is often about 45% of operating costs on a life of mine basis (Tutton and Streck, 2009). As the pit depth increases, the greater the distance and cycle time for trucks hauling material out of the pit. As a result, more trucks are required to transport a specified volume of material. Fluctuations in fuel, tyre, and spare parts prices, and greenhouse gas emissions due to the truck and shovel system, may increase operating costs and cause environmental impacts.

Due to the depletion of many high-grade and near-surface mineral sources, mining operations have expanded to exploit mostly low-grade and deeper deposits (Osanloo, 2012). Thus, it is necessary to use methods that entail lower extraction costs in addition to greater environmental compatibility so that low-grade and deep mineral resources can be extracted viably.

The concept of using a conveyor belt to transport material from the pit was first mooted at an open pit mine in Germany in 1956, due to the wet and soft ground conditions which made it difficult to use trucks (Koehler, 2003; Utley, 2011). Due to the limited range of materials sizes that could be transported by conveyors (Terezopoulos, 1988), a mobile in-pit crusher system was used for crushing the extracted material. The in-pit crushing and conveying (IPCC) system is a combination of these two types of equipment (conveyor and crusher). Although this system was first used because of poor road conditions, today, advances in the design and construction of conveyors receive more attention. IPCC

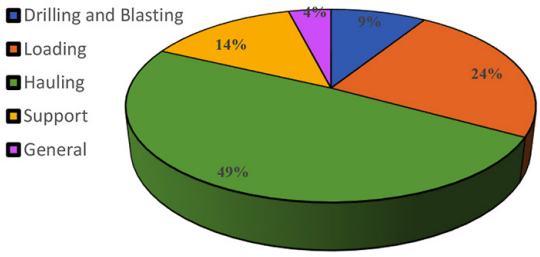

Figure 1—Typical operating costs distribution in large open-pit mines throughout the life of mine, based on a 600 kt/d operation examples in Chile using the TS system (Tutton and Streck, 2009)

systems have lower operating costs than TS systems because of their continuous operating regime, reduced labour requirements, and lower energy consumption. However, they require a higher capital cost and are less flexible (Nehring *et al.*, 2018).

In conventional TS mining the extracted materials are loaded into trucks after blasting. Waste materials are sent to a waste dump while ore is sent for primary crushing before being stored on a run-of-mine (ROM) pad prior to feeding into the processing plant. In this method, the crusher is located outside the final pit limit. Due to the short transportation distance in the initial years of mine life, the haulage cycle time is short. However, as the mine life matures and the depth of the mine increases, the distance that material needs to be transported increases. This causes the truck cycle time to lengthen. As shown in Figure 2, the incremental increase in haulage distance reduces the hourly throughput of trucks. This generally results in the need for more trucks, and in turn a significant capital reinvestment. It also increases operating costs. Accordingly, reducing the truck haulage distance may be a good method for decreasing haulage costs (on a tons per hour basis).

In the IPCC haulage system, extracted material is transported from within the pit by conveyor belts. To do so, materials are initially crushed by an in-pit crusher to a size range that allows efficient transportation to their destination. If the extracted material feeds into conveyors after passing through the crusher, the haulage system is termed a fully-mobile in-pit crushing and conveying (FMIPCC) system. Similarly, if the conveyor belt is fed by trucks, the haulage system is a semi-mobile in-pit crushing and conveying (SMIPCC) system (Frizzell and Martin, 1992). In the SMIPCC system, the transfer of waste or ore from the upper and lower benches to the in-pit crusher is carried out by trucks. This system combines a continuous (conveyor belt) and discontinuous (truck) system and has the advantages of both systems (Paricheh, Osanloo, and Rahmanpour, 2017). In the case of a breakdown in the system (trucks or conveyors), the transportation process may often continue, albeit at a reduced capacity. The SMIPCC system is therefore viewed as a lower risk system and is often thus preferred over FMIPCC, which is a purely continuous system.

Because the transportation route is shorter, a smaller fleet of trucks is required; however, the number of loading machines is the same as for the TS system. To avoid increasing the haulage distance, the crusher(s) location may be changed at regular intervals (Rahmanpour *et al.*, 2014). Using this method can save costs and improve the economics of the operation (Kochanowsky, 1961; Terezopoulos, 1988; Zimmermann and Kruse, 2006; Szalanski, 2010; Dean *et al.*, 2015; Nehring *et al.*, 2018; Paricheh and Osanloo, 2019a; Nunes *et al.*, 2019; Hay *et al.*, 2020). Reduced fuel requirements, energy consumption,

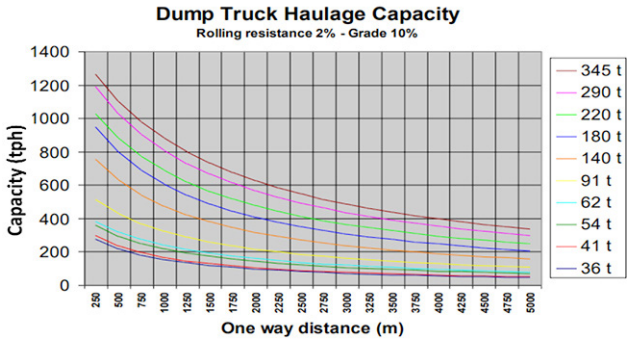

Figure 2—Effect of transportation distance on hourly throughput of trucks with different capacities (Zimmermann and Kruse, 2006)

and pollutant gas emissions are further benefits of this system (Norgate and Haque, 2013; Purhamadani, Bagherpour, and Tudeshki, 2021).

Numerous researchers have investigated use of an in-pit crusher (Hays, 1983; Huss, 1983), conveyors (Kesimal, 1997; Paricheh and Osanloo, 2019b), and high-angle conveyor (dos Santos, 1984; Mitchell and Albertson, 1985; dos Santos and Stanisic, 1986; dos Santos, 2016; Liu and Pourrahimian, 2021). Others have addressed the problem of optimally locating the crusher (Tudeshki *et al.*, 2004; Konak, Onur, and Karakus, 2007; Roumpos *et al.*, 2014; Paricheh, Osanloo, and Rahmanpour, 2017, 2018; Abbaspour *et al.*, 2019; Paricheh and Osanloo, 2019a, 2019c), and economic advantages and disadvantages. Nevertheless, insufficient research has been done concerning the optimal transition point (time or depth) between a TS system and SMIPCC.

In open-pit mining operations in most developing countries, the material transportation cycle is mainly discontinuous and carried out using the conventional TS system. Due to the superiority of IPCC, if one wants to use this system, the first major question is when or at what depth to shift from the TS to the IPCC system. In this paper we present an innovative approach whereby the end of each pushback/phase is considered as a potential point in the operation to switch the haulage system. Considering five potential transition point scenarios, economic calculations (determining operating and capital costs) are performed for both systems.

Subject modelling

Six main steps have been defined and carried out in this study to achieve accurate and consistent comparisons. Figure 3 shows a flow chart of the various aspects of the process used to generate and evaluate the use of IPCC as part of the mine planning process.

- Step 1: Geological and exploratory review to determine and assess the deposit location and the topography of the area, volume, tonnage, grade, density, and grade-tonnage relationship.
- Step 2: With these new estimations, the possibility of open pit mining is investigated. If the conditions for open pit mining are favourable, the final pit limits and extraction scheduling are then determined. In the case of unfavourable conditions for open pit mining, underground mining methods should be evaluated.
- Step 3: After defining the final pit limit and extraction sequence, operating costs are calculated. According to

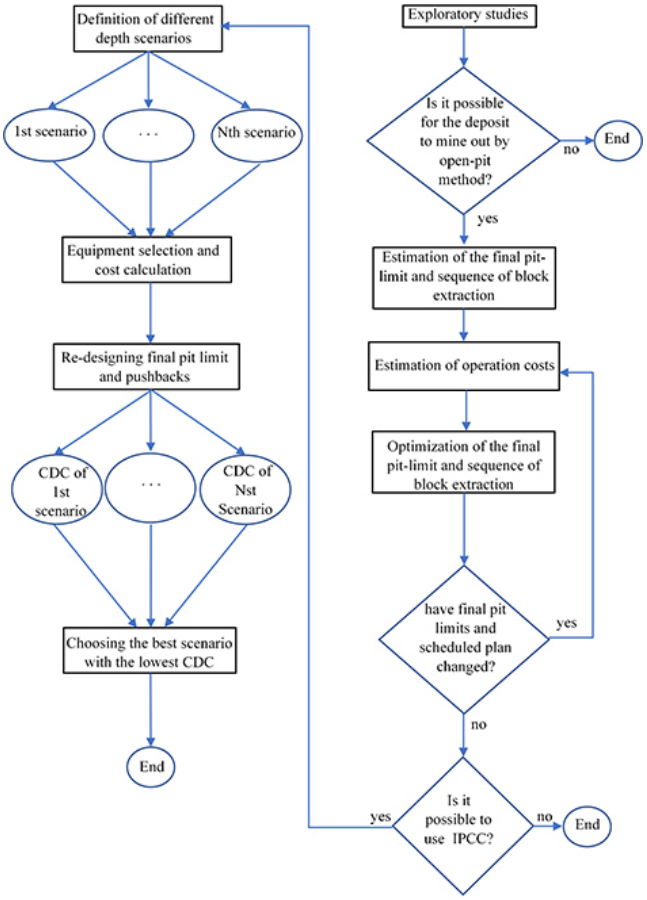

Figure 3—Flow chart of investigation for the implementation of IPCC

operational expenses, the final pit limit and schedule may change to achieve the most optimal plan.

- Step 4: At this stage, the utilization of the IPCC system is subjected to a detailed feasibility study. Influencing factors in decision-making include production rate, mine life, topography, weather conditions, environmental laws, access to fuel and energy resources, availability of required machinery, strength and hardness of the rock, *etc*. Based on these factors, if the implementation of IPCC is not feasible for any reason, the decision part of the flow chart will end. Otherwise, different scenarios are determined to transition the haulage system to IPCC as the depth increases.
- Step 5: At this stage, research is carried out on the equipment for each haulage system (conveyor belt type, width, slope, belt count, and cost of the conveyor belt system, crusher cost, cost of trucks, and truck count). Furthermore, each pushback and final pit limit are re-designed according to conveyor exit restrictions and crusher location.
- Step 6: According to the cost parameters, the CDC of each scenario is calculated. The lowest CDC option should be selected as appropriate to change the method.

Assumptions

A number of assumptions were made in this research as follows:

1. Crushing costs are the same for both in-pit (in IPCC system) and out-of-pit crushers (in the TS system).
2. The same system (TS or SMIPCC) is used for both waste and ore.
3. There is no mixing of ore and waste materials as a result of using the SMIPCC system. In this case, there are separate crusher and conveyor systems for waste and for ore handling.
4. There is only one crusher for ore and one crusher for waste in the SMIPCC system. In the TS system, there is only one fixed ore crusher outside of the final pit limit, while waste material does not need crushing and is delivered to the waste dump directly by truck.
5. Uncertainty related to all parameters such as operating costs (electricity, fuel, crusher movement, *etc*.) and capital costs (conveyor, crusher, truck, and spreader) has not been considered.
6. The same mathematical final pit limit (not the operating final pit limit) in both TS and SMIPCC systems is assumed. In this case, there is no significant difference between the final pit limits of the SMIPCC and TS systems.
7. The tonnage-grade distribution of the deposit is the same across both systems. Therefore, when considering a constant ore price, the income per ton of ore is the same in both systems. As such, the economic investigation is carried out based on cumulative discounted operating and capital costs.

Case study

As a case study, a conceptual cylinder-shaped copper deposit has been used. The average radius and depth of the orebody are 345 m and 670 m respectively, with 20 m of overburden. A block model of the orebody was initially constructed, and nested pits were generated based on different product prices. Technical and economic information that forms the basis of this investigation is provided in Table I. Figure 4 describes the amount of ore, waste, and stripping ratio located within the final pit limit for different copper prices. As the copper price increases, the amounts of ore and waste inside the final pit limit increase. However, the stripping ratio may increase or decrease, depending on (1) increasing the rate of new ore due to conversion of waste to ore as the price increases and cut-off grade decreases; (2) increases in new waste when the final pit is extended and more overburden is required to be removed.

A minimum working bench width of 80 m is applied, which in this case generates four pushbacks to fully exploit the pit limit. Figures 5 shows a schematic view of the pushbacks and final pit

Table I

Parameters required for estimating the reserve and designing of the final pit

Parameter	Amount (unit)
Ore density	2.6 (t/m³)
Waste density	2.3 (t/m³)
Copper price	5 900 US$/t)
Selling cost	356 (US$/t)
Mining cost	2 (US$/t)
Stripping cost	1.8 (US$/t)
Dilution	5%
Mining recovery	95%
Milling and flotation cost	7.0 (US$/t)
Processing recovery	85%
Maximum stable pit slope	45 (degrees)
Minimum pit floor width	50 (m)

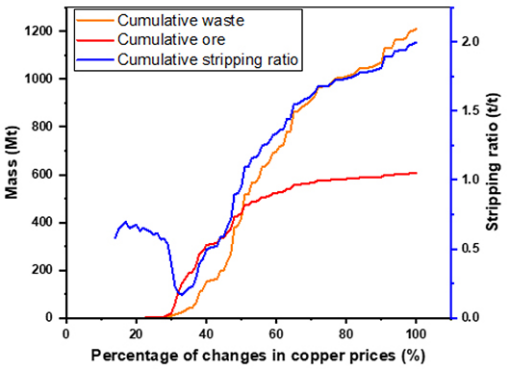

Figure 4—Stripping ratio along with ore and waste extraction in the nested pits for various prices of copper

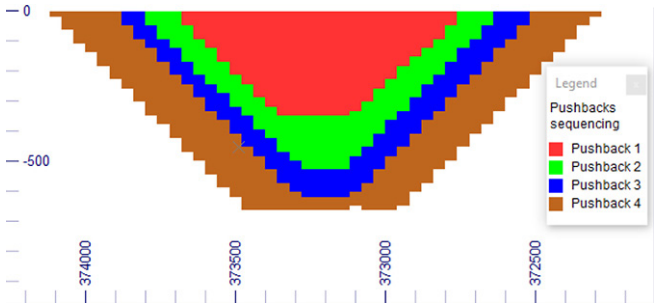

Figure 5—East-west section of pushback sequencing

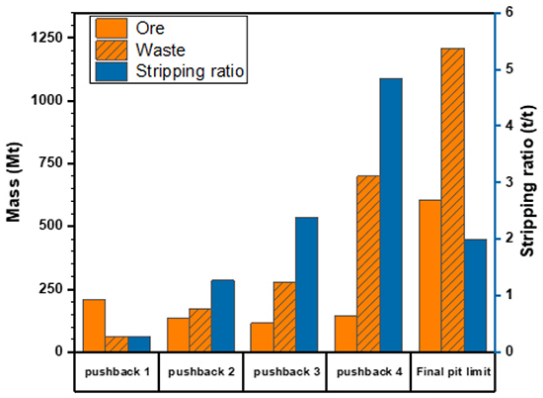

Figure 6—Ore and waste in each pushback and final pit

limit, which is determined based on maximizing profit. Figure 6 shows the ore, waste, and stripping ratio associated with each pushback and final pit limit.

After determining the pushbacks, the mine production capacity of 20 Mt per year was derived using Taylor's equation. The final depth of each pushback is considered a potential transition point of the haulage system from TS to IPCC. The centre of gravity of ore and waste for each pushback was used to best locate the in-pit crusher.

Five scenarios are considered in total, as follows:

1. SMIPCC used from the outset (SMIPCC only)
2. Transition to SMIPCC after pushback 1
3. Transition to SMIPCC after pushback 2
4. Transition to SMIPCC after pushback 3
5. SMIPCC not used (TS only).

The operating pushbacks (phases) and final pit limit were designed for both systems with a bench height of 15 m and a face slope angle of 65 degrees. Figures 7 to 10 show the plan view of four pushbacks using TS and SMIPCC.

The final operating pit limit of scenarios 1 to 4 is the same, with the amount of waste of these four scenarios increasing by approximately 90 Mt compared to the fifth scenario (pure TS), and 100 Mt compared to the optimal final pit shell. This increase is due to the additional waste generated during construction of new ramps for the conveyor path and switchbacks in the truck ramp to avoid intersecting the conveyor and truck roads. Details of the increasing waste in each designed phase of the two systems (compared to the optimal pit shell) are described in Table II. The total amount of waste in the final pit limit is increased by 7.4% under the SMIPCC scenario compared to TS. However, the amount of ore does not change.

Due to the characteristics of the mine, the need for trucks with high capacity is evident. Caterpillar 793C trucks (Caterpillar, 1998) with a capacity of 221 t were found to be suitable. According to the performance of this truck, the cycle time was calculated for each phase.

The centre of gravity of waste and ore was used to measure transportation time in the TS system along the path length. In the SMIPCC system, four centres of gravity were considered – two for ore blocks above and below the crusher, and two for waste blocks. Transportation time was calculated using the abovementioned centres of gravity and the specific paths for hauling ore and waste from each of them. Table III contains the information used for calculating the efficiency of the TS system.

Using this information, efficiency was calculated at 62% for each shovel and 70% for each truck. Data for calculating the required number of trucks is presented in Table IV.

As shown in Table II, the amount of stripping required increases from the first to the fourth pushback. As such, the number of machines for executing each phase needs to gradually increase. Since ore production capacity has been set at 20 Mt/a, the capacity of the conveyor for ore extraction will remain consistent.

Considering three 8-hour work shifts and 310 working days in a year (55 days for repair, replacement, daily and monthly servicing), the required capacity of the ore conveyer was

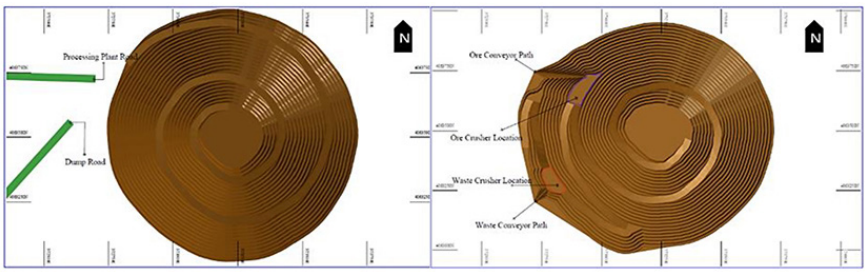

Figure 7—Pit appearance after extraction of first pushback with two haulage systems (left: TS and right: SMIPCC)

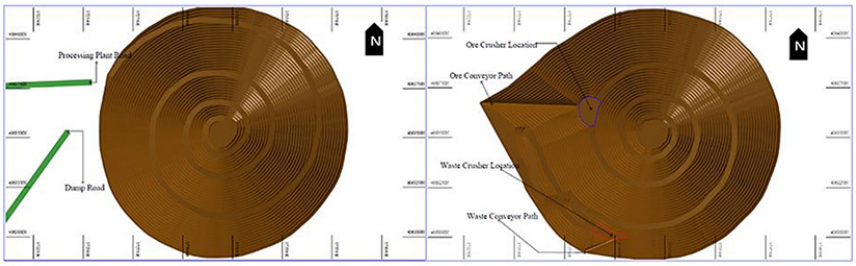

Figure 8—Pit appearance after extraction of second pushback with two haulage systems (left: TS and right: SMIPCC)

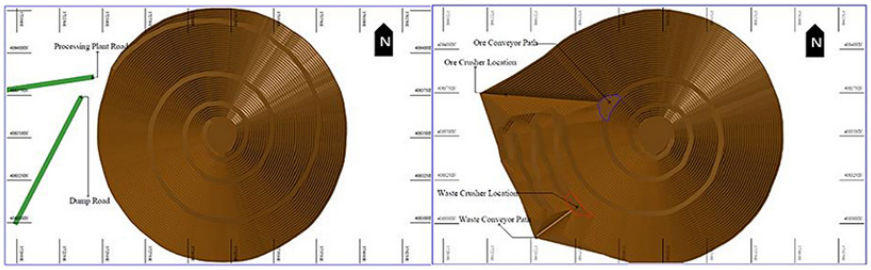

Figure 9—Pit appearance after extraction of third pushback with two haulage systems (left: TS and right: SMIPCC)

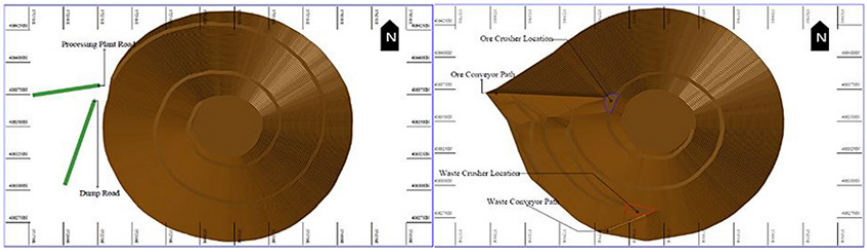

Figure 10—Pit appearance after extraction of fourth pushback with two haulage systems (left: TS and right: SMIPCC)

Table II

Increasing waste in pushbacks for TS and SMIPCC systems compared to optimal pit shell

Increase in waste	TS (Mt)	SMIPCC (Mt)	Difference (Mt)
Phase 1	61.8	71.8	10
Phase 2	205.6	223	17.4
Phase 3	266.8	297.8	31
Phase 4	684.7	716.1	31.4
Final operating pit limit	1218.9	1308.7	89.8

Table III

Information on Idle times of truck and shovel equipment

Cause of delay	Amount
Bad weather	20 days per year
Shift change	0.5 hours per shift
Truck breakdown and repair	15 days per year
Shovel breakdown and repair	30 days per year
Unpredictable idle time	10%

estimated at 2690 t/h. The capacity of the stripping conveyor, however, will differ in each phase. Thus, the equipment required in each phase needs to be computed separately. A brief description of the machines required for each phase is provided in Table V. For example, if it is decided to mine using the third scenario, the machinery for the first two phases will be chosen from the TS system and for the remaining two phases from the SMIPCC system.

Table IV

Information required to calculate the number of needed equipment items

Parameters	Value
Ore density	2.6 t/m^3
Waste density	2.3 t/m^3
Ore load fill factor	0.85
Waste load fill factor	0.9
Delay time factor	0.95
Shovel loading cycle	30 seconds per cycle
Truck waiting time	30 seconds per cycle
Truck manoeuver time	30 seconds per cycle

Based on economic analysis of the various scenarios, it is apparent that the purchase of single large waste conveyors and spreaders is preferred over multiple lower capacity sets of equipment. Therefore, the required machinery for each scenario has been selected based upon the lowest CDC. Capital and operating costs of the equipment of both systems are calculated using InfoMine cost tables and are presented in Table VI. Different components of the SMIPCC haulage system for each scenario are presented in Table VII. Economic studies for each scenario are presented in Table VIII. The most economical haulage option is chosen between the TS and SMIPCC alternatives.

Table V

Machines required for the execution of each phase

System type	Required components	Phase 1	Phase 2	Phase 3	Phase 4
SMIPCC	Sloped waste conveyor length (m)	100	200	312	420
	Sloped waste conveyor capacity (t/h)	900	4150	7650	14 800
	Sloped ore conveyor length (m)	260	590	807	1030
	Horizontal waste conveyor length (m)	870	800	700	700
	Horizontal ore conveyor length	980	580	430	216
	Shovel count	2	3	4	6
	Truck count	5	9	18	29
TS	Shovel count	2	3	4	6
	Truck count	8	21	38	79

Table VI

Haulage equipment capacity with corresponding economic information

Equipment type and capacity	Capital cost (US$ million)	Annual operating cost (US$ million)
Truck – 221 t	4.86	2.10
Spreader – 1270 t/h	7.57	3.53
Spreader – 3628 t/h	9.60	4.78
Spreader – 4525 t/h	10.89	5.54
Horizontal conveyor – 454 t/h (1615 m length)	4.50	3.65
Horizontal conveyor – 907 t/h (1615 m length)	5.10	4.32
Horizontal conveyor – 3629 t/h (1615 m length)	8.40	7.72
Sloping conveyor – 454 t/h (610 m length)	1.97	1.56
Sloping conveyor – 907 t/h (610 m length)	22.38	1.96
Sloping conveyor – 3629 t/h (610 m length)	4.30	3.28

Table VII

SMIPCC equipment for each scenario

Phase	Scenario 1		Scenario 2	
	Conveyor belt	Spreader	Conveyor belt	Spreader
1	One 907 t/h belt	One 4535 t/h spreader	-	-
2	One 3629 t/h belt	-	One 3629 t/h and one 907 belt	One 4535 t/h spreader
3	One 3629 t/h belt	One 3629 t/h spreader	One 3629 t/h belt	One 3629 t/h spreader
4	Two 3629 t/h belts	Two 3629 t/h spreaders	Two 3629 t/h belts	Two 3629 t/h spreaders
	Scenario 3		Scenario 4	
1	-	-	-	-
2	-	-	-	-
3	Two 3629 t/h and one 454 t/h belt	One 3629 t/h and one 4535 t/h spreader	-	-
4	Two 3629 t/h belts	Two 3629 t/h spreaders	Four 3629 t/h and one 454 t/h belt	Three 4535 t/h and one 1270 spreader

The sensitivity of the optimal scenario and transition point to discount rate is shown in Figure 11. As indicated, the optimal transition point between TS and SMIPCC systems is not reasonably related to the discounted rate. The second scenario, with a depth of 335 m for transition from TS to SMIPCC, has the lowest CDC across all discount rates. A comparison between pure TS and pure SMIPCC shows that the pure SMIPCC system has a higher economic advantage (lower CDC) than the pure TS system at a zero discounted rate. This advantage continues up to the 10% discounted rate. At a discounted rate of 10% or more, the pure TS system has a lower CDC than pure SMIPCC because the operating costs do not affect the CDC significantly at a high discounted rate in the latter periods of mine life. Therefore, the pure TS system with a lower capital cost than the SMIPCC will be selected as the optimum system. Choosing between pure TS and pure SMIPCC systems is highly sensitive to the discount rate, but the optimum transition point is not.

Conclusion

The SMIPCC system is one of the most appropriate options for mining deeper and lower-grade deposits due to its lower operating costs, which can thus reduce the cut-off grade. However, a greater capital investment is required in comparison to conventional truck and shovel systems. Whether or not the greater initial capital investment can be recouped throughout the mine life from lower operating costs should be the subject of technical and feasibility studies in order to identify the most appropriate system(s) and the point at which a transition may occur.

For the case study that was presented, a depth of 335 m was determined as the optimum transition point from TS to SMIPCC based on a CDC analysis. It was also found that the transition point is not sensitive to the discount rate. However, because the operating costs do not influence the CDC substantially in the

Table VIII

Summary of economic analysis (costs in million US$)

Phase	Parameter	Scenario 1	Scenario 2	Scenario 3	Scenario 4	Scenario 5
First	Number of required trucks	5	8	8	8	8
	Capital cost for purchasing trucks	24.30	38.88	38.88	38.88	38.88
	Operational cost of trucks (per year)	10.50	16.80	16.80	16.80	16.80
	Capital cost for purchasing conveying system	10.07	0	0	0	0
	Operational cost of conveying (per year)	10.07	0	0	0	0
	Capital cost for purchasing crusher	20.00	0	0	0	0
	Capital cost for purchasing spreader	10.89	0	0	0	0
	Operational cost of spreader (per year)	5.45	0	0	0	0
	Additional stripping costs (per year)	0.37	0	0	0	0
	Transportation SMIPCC cost at the end of phase	2.00	0	0	0	0
Second	Number of required trucks	4	1	13	13	13
	Capital cost for purchasing trucks	19.44	4.86	63.18	63.18	63.18
	Operational cost of trucks (per year)	18.90	18.90	44.10	44.10	44.10
	Capital cost for purchasing conveying system	8.29	17.46	0	0	0
	Operational cost of conveying (per year)	14.51	14.32	0	0	0
	Capital cost for purchasing crusher	0	20.00	0	0	0
	Capital cost for purchasing spreader	0	10.89	0	0	0
	Operational cost of spreader (per year)	5.45	5.45	0	0	0
	Additional stripping costs (per year)	0.97	0.97	0	0	0
	Transportation SMIPCC cost at the end of phase	2.00	2.00	0	0	0
Third	Number of required trucks	9	9	0	17	17
	Capital cost for purchasing trucks	43.74	43.74	0	82.62	82.62
	Operational cost of trucks (per year)	37.80	37.80	37.80	79.80	79.80
	Capital cost for purchasing conveyor system	8.60	8.60	22.49	0	0
	Operational cost of conveying (per year)	21.52	21.33	20.03	0	0
	Capital cost for purchasing crusher	10.00	10.00	30.00	0	0
	Capital cost for purchasing spreader	9.60	9.60	20.49	0	0
	Operational cost of spreader (per year)	10.23	10.23	10.23	0	0
	Additional stripping costs (per year)	2.38	2.42	2.42	0	0
	Transportation SMIPCC cost at the end of phase	3.00	3.00	3.00	0	0
Fourth	Number of required trucks	11	11	8	0	41
	Capital cost for purchasing trucks	53.46	53.46	38.88	0	199.26
	Operational cost of trucks (per year)	60.90	60.90	60.90	60.90	165.90
	Capital cost for purchasing conveyor system	16.72	13.08	16.65	38.10	0
	Operational cost of conveying (per year)	35.55	32.02	33.99	34.05	0
	Capital cost for purchasing crusher	20.00	20.00	20.00	50.00	0
	Capital cost for purchasing spreader	19.20	19.20	16.80	40.24	0
	Operational cost of spreader (per year)	19.78	19.78	19.78	19.89	0
	Additional stripping costs (per year)	1.94	1.94	1.94	1.94	0
	Transportation SMIPCC cost at the end of phase	–	–	–	–	–
CDC (considering a discounted rate of 5%)		837.51	747.83	765.70	798.17	907.22

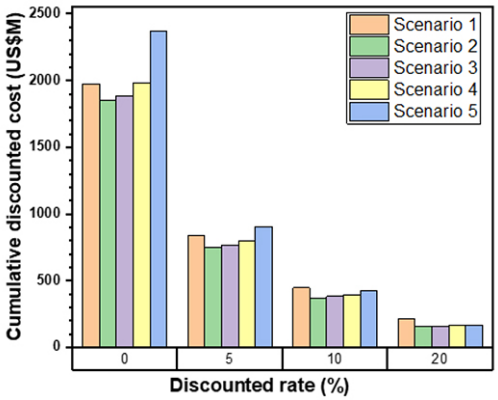

Figure 11—Cumulative discounted cost for each scenario at various discount rates

latter periods of mine life, with a high discount rate the pure TS system, with a lower capital cost, is the optimum when deciding between pure TS and pure SMIPCC systems. Conversely, at a lower discounted rate pure SMIPCC is more economically viable than the TS system.

Future work

Future research should investigate the uncertainty related to equipment operating and capital costs. This should perhaps be combined with determining the optimum ultimate pit limit and mine plan based on mathematical modelling. Further work addressing the optimal transition point between a TS system and a SMIPCC system relating to the optimum location and relocation of the semi-mobile crusher should also be considered. Even though fully mobile in-pit crusher conveyor (FMIPCC) systems require more extensive redesign of the mining operation due to the introduction of sequencing constraints, there are further economic benefits that could result from such a system which could also be addressed.

Acknowledgment

The authors would like to acknowledge the valuable comments and suggestions of the editor and anonymous reviewers, which have improved the quality of this paper. Thanks are also extended to Dr. Mehdi Rahmanpour for his initial comments in completing the paper.

References

Abbaspour, H., Drebenstedt, C., Paricheh, M., and Ritter, R. 2019. Optimum location and relocation plan of semi-mobile in-pit crushing and conveying systems in open-pit mines by transportation problem. *International Journal of Mining, Reclamation and Environment*, vol. 33, no. 5. pp. 297–317. https://doi.org/10.1080/17480930.2018.1435968

Caterpillar. 1998. Caterpillar Performance Handbook. Edition 29, Section of Construction & Mining Trucks Construction & Mining Tratrors. pp. 36–43.

Dean, M., Knights, P., Kizil, M., and Nehring, M. 2015. Selection and planning of fully mobile in-pit crusher and conveyor systems for deep open pit metalliferous applications. *Proceedings of the Third International Future Mining Conference*, University of New South Wales, Australia. Australasian Institute of Mining and Metallurgy, Melbourne. pp. 219–225.

Dos Santos, J. 1984. Sandwich belt high angle conveyors-applications in open pit mining. *Bulk Solids Handling*, vol. 4, no. 1. pp. 67–77.

Dos Santos, J.A. 2016. Sandwich belt high angle conveyors coal mine to prep plant and beyond. *Proceedings of the XVIII International Coal Preparation Congress*, Saint-Petersburg, Russia. Springer. pp. 111–117.

Dos Santos, J.A. and Stanisic, Z. 1986. In-pit crushing and high angle conveying in a Yugoslavian copper mine. *International Journal of Surface Mining, Reclamation and Environment*, vol. 1, no. 2. pp. 97–104. https://doi.org/10.1080/09208118708944108

Frizzell, E.M. and Martin, T.W.1992. In-pit crushing and conveying. *Mining Engineering Handbook*. Hartman, H.L. (ed.). Society for Mining, Metallurgy, and Exploration, Littleton, CO. pp. 1343-1351.

Hay, E., Nehring, M., Knights, P., and Kizil, M.S. 2020. Ultimate pit limit determination for semi mobile in-pit crushing and conveying system: a case study. *International Journal of Mining, Reclamation and Environment*, vol. 34, no. 7. pp. 498–518. https://doi.org/10.1080/17480930.2019.1639006

Hays, R.M. 1983. Mine planning considerations for in-pit crushing and conveying systems. P*roceedings of the SME-AIME Fall Meeting*. Brent Hiskey, J. (ed.) American Institute of Mining, Metallurgical and Petroleum Engineers, New York. pp. 3-–41.

Huss, C., Reisler, N., and Almond, R. 1983. Practical and economic aspects of in-pit crushing conveyor systems. *Proceedings of the SME-AIME Fall Meeting*. Brent Hiskey, J. (ed.). American Institute of Mining, Metallurgical and Petroleum Engineers, New York. pp. 15–31.

Kesimal, A. 1997. Different types of belt conveyors and their applications in surface mines. *Mineral Resources Engineering*, vol. 6, no. 4. pp. 195–219.

Kochanowsky, B. 1961. Portable crusher for open pit and quarry operations. *Transactions of the American Institute of Mining, Metallurgical Petroleum Engineers*, vol. 220. pp. 271–274.

Koehler, F. 2003. In-pit crushing system the future mining option. *Proceedings of the Twelfth International Symposium on Mine Planning and Equipment Selection*. Australasian Institute of Mining and Metallurgy, Melbourne. pp. 371–376.

Konak, G., Onur, A.H., and Karakus, D. 2007. Selection of the optimum in-pit crusher location for an aggregate producer. *Journal of the Southern African Institute of Mining and Metallurgy*, vol. 107, no. 3. pp.161–166.

Liu, D. and Pourrahimian, Y. 2021. A framework for open-pit mine production scheduling under semi-mobile in-pit crushing and conveying systems with the high-angle conveyor. *Mining*, vol. 1, no. 1. pp. 59–79. https://doi.org/10.3390/mining1010005

Mitchell, J. and Albertson, D. 1985. High angle conveyor offers mine haulage savings. *Proceedings of the International Materials Handling Conference, BeltCon 3*, Johannesburg. South Africa. South African Institute of Materials Handling. Vol. 3. pp. 9–11.

Nehring, M., Knights, P.F., Kizil, M.S., and Hay, E. 2018. A comparison of strategic mine planning approaches for in-pit crushing and conveying, and truck/shovel systems. *International Journal of Mining Science and Technology*, vol. 28, no. 2. pp. 205–214. https://doi.org/10.1016/j.ijmst.2017.12.026

Norgate, T. and Haque, N. 2013. The greenhouse gas impact of IPCC and ore-sorting technologies. *Minerals Engineering*, vol. 42. pp. 13–21. https://doi.org/10.1016/j.mineng.2012.11.012

Nunes, R.A., Delboni, H., Tomi, G.D., Infante, C.B., and Allan, B. 2019. A decision-making method to assess the benefits of a semi-mobile in-pit crushing and conveying alternative during the early stages of a mining project. *REM-International Engineering Journal*, vol. 72. pp. 285–291. https://doi.org/10.1590/0370-44672018720109

Osanloo, M. 2012. Future challenges in mining division, are we ready for these challenges? Do we have solid educational program?. *Proceedings of the 23rd Annual General Meeting of the Society of Mining Professors*, Poland. Wroclaw University of Technology. pp. 29–39.

Paricheh, M. and Osanloo, M. 2019a. Concurrent open-pit mine production and in-pit crushing–conveying system planning. *Engineering Optimization*, vol. 52, no. 10. pp. 1780–1795. https://doi.org/10.1080/0305215X.2019.1678150

Paricheh, M. and Osanloo, M. 2019b. How to exit conveyor from an open-pit mine: A theoretical approach. *Proceedings of the 27th International Symposium on Mine Planning and Equipment Selection - MPES 2018*, Perth, Australia. Springer. pp. 319–334.

Paricheh, M. and Osanloo, M. 2019c. A new search algorithm for finding candidate crusher locations inside open pit mines. *Proceedings of the International Symposium on Mine Planning & Equipment Selection - MPES 2018*, Perth, Australia. Springer. pp. 10–25.

Paricheh, M., Osanloo, M., and Rahmanpour, M. 2017. In-pit crusher location as a dynamic location problem. *Journal of the Southern African Institute of Mining and Metallurgy*, vol. 117, no. 6. pp. 599–607.

Paricheh, M., Osanloo, M., and Rahmanpour, M. 2018. A heuristic approach for in-pit crusher and conveyor system's time and location problem in large open-pit mining. *International Journal of Mining, Reclamation and Environment*, vol. 32, no. 1. pp. 35–55. https://doi.org/10.1080/17480930.2016.1247206

Purhamadani, E., Bagherpour, R., and Tudeshki, H. 2021. Energy consumption in open-pit mining operations relying on reduced energy consumption for haulage using in-pit crusher systems. *Journal of Cleaner Production*, vol. 291. p. 125228. https://doi.org/10.1016/j.jclepro.2020.125228

Rahmanpour, M., Osanloo, M., Adibee, N., and AkbarpourShirazi, M. 2014. An approach to locate an in pit crusher in open pit mines. *International Journal of Engineering-Transactions C: Aspects*, vol. 27, no. 9. pp. 1475–1484.

Roumpos, C., Partsinevelos, P., Agioutantis, Z., Makantasis, K., and Vlachou, A. 2014. The optimal location of the distribution point of the belt conveyor system in continuous surface mining operations. *Simulation Modelling Practice and Theory*, vol. 47. pp. 19–27.

Samavati, M., Essam, D.L., Nehring, M., and Sarker, R. 2018. Open-pit mine production planning and scheduling: A research agenda. *Data and Decision Sciences in Action*. Sarker, R., Abbass , H.A., Dunstall, S., Kilby, P., Davis,R., and Young, L. (eds). Springer. pp. 221–226.

Szalanski, S. 2010. Reducing IPCC removal costs – is IPCC the answer? *Proceedings of the International Future Mining Conference*, Sydney, NSW, 4-6 November 2015.Australasian Institute of Mining and Metallurgy, Melbourne.

Terezopoulos, N.G. 1988. Continuous haulage and in-pit crushing in surface mining. *Mining Science and Technology*, vol. 7, no. 3. pp. 253–263.

Tudeshki, H., Hardebusch, T., Rebehn, T., and RoBbach, S. 2004. cost reduction by optimization of the primary crusher position. *Bulk Solids Handling*, vol. 24, no. 1. pp. 20–24.

Tutton, D. and Streck, W. 2009. The application of mobile in-pit crushing and conveying in large, hard rock open pit mines. *Proceedings of the Mining Magazine Congress*, Niagara-on-the-Lake, Canada. Mining Magazine, London, UK.

Utley, R.W. 2011. In-pit crushing. *SME Mining Engineering Handbook*, 3rd edn. Society for Mining, Metallurgy and Exploration Inc, Englewood, CO. pp. 941-956.

Zimmermann, E. and Kruse, W. 2006. Mobile crushing and conveying in quarries - A chance for better and cheaper production! *Proceedings of the 8th International Symposium Continuous on Surface Mining, Mainz*, Aachen. RWTH Aachen University. Vol. 1. pp. 481–487. https://www.911metallurgist.com/blog/wp-content/uploads/2015/12/mobile-crushing.pdf ◆

Truck dispatching in surface mines – Application of fuzzy linear programming

A. Moradi-Afrapoli[1], S. Upadhyay[2], and H. Askari-Nasab[1]

Affiliation:
[1]Mining Optimization Laboratory (MOL), School of Mining Engineering, Department of Civil and Environmental Engineering, University of Alberta, Canada.
[2]Canadian Natural Resources Limited (CNRL), Calgary, Canada.

Correspondence to:
A. Moradi-Afrapoli

Email:
moradiaf@ualberta.ca

Dates:
Received: 6 Dec2018
Revised: 29 May 2020
Accepted:28 Jul. 2021
Published: September 2021

How to cite:
Moradi-Afrapoli, A., Upadhyay, S., and Askari-Nasab, H. 2021 Truck dispatching in surface mines – Application of fuzzy linear programming.
Journal of the Southern African Institute of Mining and Metallurgy, vol. 121, no. 9, pp. 505–512

DOI ID:
http://dx.doi.org/10.17159/2411-9717/522/2021

ORCID:
A. Afrapoli
https://orcid.org/0000-0002-2659-0112

Synopsis

Material handling in surface mines accounts for around 50% of the operational cost. Optimum truck dispatching plays a critical role in the reduction of this operational cost in truck and shovel surface mines. Researchers in this field have presented several mathematical models to solve the truck dispatching problem optimally. However, a critical survey of the literature has shown that three significant drawbacks exist in the available truck dispatching models. The published models underestimate the importance of the interaction between truck fleet, shovel fleet, and the processing plants. They also disregard goals set by strategic-level plans. Moreover, none of the available models account for the uncertainty associated with the input parameters. In this paper we present a new truck dispatching model that covers all of these drawbacks, using a fuzzy linear programming method. The performance of the developed model was evaluated through implementatin in an active surface mining operation. The results show a significant improvement in production and fleet utilization.

Keywords
Truck dispatching problem, fuzzy linear programming, surface mining, simulation, truck and shovel, material handling.

Introduction

As mining operations involve expenditures of millions or billions of dollars, cutting their costs by even two or three per cent will result in considerable savings for the stakeholders. In truck and shovel surface mining operations, material handling accounts for 50 to 60% of the total operating costs (Alarie and Gamache, 2002; Oraee and Goodarzi, 2007; Akbari, Osanloo and Shirazi, 2009; Upadhyay and Askari-Nasab, 2016; Moradi Afrapoli and Askari-Nasab, 2019). Thus, improving the performance of the material handling system and subsequently reducing its operating costs would result in significant savings. One of the several existing ways to improve the performance of material handling systems in truck and shovel surface mining operations is to make optimal decisions for truck allocation and dispatching. In this paper, we present a decision-making model that makes optimal decisions for truck dispatching in truck and shovel surface mines.

In the truck dispatching problem, decision-making models dispatch the 'best' trucks to the 'neediest' shovels. Definition of the best trucks and the neediest shovels can be found in Olson, Vohnout, and White (1993) and Temeng, Otuonye, and Frendewey (1998). Several models to solve the truck dispatching problem have been developed since the 1970s. However, the models published thus far have three limitations, which lead to non-optimal dispatching of trucks. The existing truck dispatching models usually omit the truck fleet, shovel fleet, or the processing plant from their calculations. Furthermore, the available models either ignore the production target that is set by the strategic plans or incorporate it as a soft constraint. The published models also disregard the stochastic behaviour of the input parameters.

This paper aims to introduce a new mathematical model to solve the truck dispatching problem in surface mines. Our model assigns equal weights to the impact of the truck fleet, shovel fleet, and processing plant in the truck dispatching process. Our developed model also applies fuzzy linear programming (FLP) to incorporate the imprecision of the input parameters in the solution procedure. We implemented our model in a real case study, using the study's site's in-place fleet management system, which is the backbone algorithm of Modular Mining DISPATCH® (Modular Mining Systems Inc., 2020), as the benchmark to evaluate the model performance.

Literature

Mining researchers have developed several decision-making tools for optimizing truck dispatching decisions in the last 50 years. The models thus far developed are categorized into two main classes – the single-stage and the multi-stage truck dispatching models (Alarie and Gamache; 2002; Moradi Afrapoli and Askari-Nasab, 2019).

The single-stage models make two simultaneous decisions. They simultaneously decide on the required flow rate along paths between shovels and dumps and dispatching of the trucks to shovels. The truck dispatching model developed by Hauck (1973) is categorized in the single-stage class.

The multi-stage models divide the truck dispatching problem into two sub-problems. In the first sub-problem, a mathematical model determines the rate of production for each path between shovels and dumps (truck allocation). This step is called the upper stage (Alarie and Gamache, 2002). Most of the literature related to truck allocation and dispatching problems deals with developing a decision-making model to solve the upper stage sub-problem. A detailed review of the latest published models to address the upper stage problem can be found in Moradi Afrapoli and Askari-Nasab (2019).

In the second sub-problem, a mathematical model makes decisions on the next destination of the trucks (truck dispatching). This step is called the lower stage (Alarie and Gamache, 2002). There are only a few published models in the literature that make the lower stage decisions. White and Olson (1986) and Olson, Vohnout, and White (1993) presented a truck dispatching model based on dynamic programming. Their model creates a list of available trucks and a list of active shovels. Then, based on a 1-truck-*m*-shovel approach (Alarie and Gamache, 2002) it dispatches the best truck to the right shovel.

Soumis, Ethier, and Elbrond (1989) developed a truck dispatching model that solves the lower stage sub-problem using a model based on the classical assignment problem approach. The model considers the next 10 to 15 trucks that need a new assignment.

Li (1990) presented a truck dispatching model that dispatches trucks based on a maximum inter-truck-time dispatching rule. An empty truck is sent to the shovel at which the difference between actual inter-truck time and the optimal inter-truck time is the greatest.

Temeng, Otuonye, and Frendewey (1997) presented a truck dispatching model based on the analogy of the transportation problem approach. Their proposed model can be implemented in a mine where a heterogeneous truck fleet is used for material transportation. Their model also considers the situation in which a shovel is far behind its target production and needs to be assigned more than one truck. In such a case, the model efficiently assigns more than a single truck to those shovels that are further behind their schedule.

Recently, Moradi-Afrapoli, Tabesh, and Askari-Nasab (2018, 2019) developed multiple objective truck dispatching models that can be implemented in mines where a heterogeneous truck fleet is used. Despite other available models, their developed models do not place limitations on the number of trucks to be assigned each time the decision-making model solves the problem. However, their developed models do not incorporate uncertainty.

All the dispatching models published to date are deterministic. These models do not account for the imprecision of the input parameters. However, almost all of the input parameters of a truck dispatching model are estimated values of future actions. For example, the travel of a truck from its current location to a shovel is a process that will happen after solving the dispatching problem for that particular truck. Thus, at the time of solving the problem, the models use either the expected or estimated value for the truck's travel time. This assumption pushes truck dispatching models to make decisions that are far from reality.

One way of dealing with the problems where some of the input parameters are from future events is to use the concept of fuzzy set theory. The fuzzy set theory was first applied in the field of mining engineering in the late 1980s by Nguyen (1985), Bandopadhyay and Chattopadhyay (1986), and Bandopadhyay (1987). Since then, it has been extensively applied in decision-making models for mine planning (Rahmanpour and Osanloo, 2017), equipment selection and sizing (Bascetin, Oztas, and Kanli, 2007; Aghajani Bazzazi, Osanloo, and Soltanmohammadi, 2008), plant location selection (Yavuz, 2008), and post-mining land use and reclamation (Bangian *et al.*, 2012). The application of fuzzy set theory in conventional linear programming resulted in the generation of fuzzy linear programming (FLP). The first implementations of FLP are credited to Zimmermann (1976, 1978) and Madadi and Wong (2014), and the latest application in the mining context can be found in Rahmanpour and Osanloo (2017). In this paper, we apply the concept of fuzzy set theory, using FLP, to solve our developed model for the truck dispatching problem in surface mines.

Model formulation

We first developed a deterministic mixed integer linear programming (MILP) model to solve the truck dispatching problem. The developed deterministic MILP model deals with the first limitation mentioned in the introduction by including the goals of the truck fleet, the shovel fleet, and the processing plants in the objective function. The model also removes the second limitation of the available truck dispatching models by adding an objective to meet the production target for each path. We explicitly introduce the deterministic model in this section.

The following parameters and variables were used in the development of the deterministic MILP model.

- ltt_{td} Loaded travel time from current truck t position to dump d, which is calculated as ld_{td}/lv_t where, ld_{td} is the distance from current truck t position to dump d, and lv_t is the loaded velocity of truck t
- qt_{td} The time truck t must spend in the queue at dump d waiting for permission to dump its material
- dt_{td} The time truck t spends at dump d to back up and dump its load into the dumping area
- ett_{ts} Time it takes truck t to travel empty from where its empty travel starts to shovel s, which is calculated as ed_{ts}/ev_t where ed_{ts} is the distance from current truck t position to shovel s, and ev_t is the empty velocity of truck t.
- $tinq_{tts}$ Time a truck of type tt that is already in the queue must spend in shovel s queue
- $tenr_{tts}$ Time a truck of type tt must travel from its current position to reach shovel s before truck t
- st_{tts} Spot time for a truck of type tt at shovel s
- lt_{tts} Loading time for a truck of type tt at shovel s
- tc_t Capacity of truck t (tons)
- TC_t Nominal truck capacity for truck t (tons)
- sc_s Capacity of shovel s

pc_d Capacity of dump d (tons per hour)
m_f The factor that shows what portion of the current demands can be met with the available trucks
pf_{sd} Optimal flow rate for the path from shovel s to dump d based on upper stage decisions
$pmsf_{sd}$ Portion of the required path flow rate for the current period that has been met so far

Variables:

x_{tds} Binary integer variable to assign truck t to the path connecting shovel s to dump d
AF Variable factor that adjusts trucks available to be assigned with the demands of dumping locations

The deterministic MILP model is presented in Equations [1] to [8]. The objective function of the model consists of two parts. The objective coefficient of the first part is calculated using Equation. [1]:

$$C_{tds} = \left| ltt_{td} + qt_{td} + dt_{td} + ett_{ts} - \sum_{tt=1}^{TT} \left(tinq_{tts} + tenr_{tts}\right) \times \left(st_{tts} + lt_{tts}\right) \right| \quad [1]$$

$$\forall t \in \{1,...,T\} \,\&\, \forall tt \in \{1,...,TT\} \;\&\; \forall s \in \{1,...,S\} \;\&\; \forall d \in \{1,...,D\}$$

where C_{tds} is the time difference between the time truck t will reach to shovel s after dumping its load at dump d and the next time shovel s will be available.

In the first part of the objective function, the MILP model minimizes the summation of C_{tds} (Equation [1]) over all the possible truck dispatching decisions.

In the second part of the objective function, our developed MILP model optimizes the production target of the available paths. The MILP model minimizes the deviation from the production target of the paths by maximizing the adjustment factor (AF). To eliminate the effect of the second part of the objective function on the decisions of the first part, we multiply it with a very big number (VBN). The AF appears two more times in the model. The first time it is presented is in Equation [5], where it adjusts the inequality constraint for delivering enough material to the processing plants. The second appearance of the AF in the model is in Equation [6]. In Equation [6], AF is limited to values less than or equal to unity or the match factor (mf). The definition of mf is essential for the model. As presented in Equation. [8], mf is defined as the cumulative capacity of the trucks requesting the next destination, at the time of running the mathematical model, divided by the cumulative production target of the active paths.

$$\min Z = \sum_{t=1}^{T}\sum_{d=1}^{D}\sum_{s=1}^{S} C_{tds} x_{tds} + VBN(1-AF) \quad [2]$$

$$\forall t \in \{1,...,T\}, \forall d \in \{1,...,D\}, and\ \forall s \in \{1,...,S\}$$

$$\sum_{d=1}^{D}\sum_{s=1}^{S} tc_t x_{tds} \le TC_t \quad \forall t \in \{1,...,T\} \quad [3]$$

$$\sum_{t=1}^{T}\sum_{d=1}^{D} tc_t x_{tds} \le sc_s \quad \forall s \in \{1,...,S\} \quad [4]$$

$$\sum_{t=1}^{T}\sum_{s=1}^{S} tc_t x_{tds} \ge AF \times pc_d \quad \forall d \in \{1,...,D\} \quad [5]$$

$$AF \begin{cases} \le mf & \text{if } mf > 1 \\ \le 1 & \text{otherwise} \end{cases} \quad [6]$$

$$x_{tds} \in \{0,1\} \quad \forall t \in \{1,...,T\}, \forall s \in \{1,...,S\}, \text{ and } \forall d \in \{1,...,D\} \quad [7]$$

$$mf = \frac{\sum_{t=1}^{T} tc_t x_{tds}}{\sum_{s=1}^{S}\sum_{d=1}^{D} (pf_{sd} - pmsf_{sd})} \quad \forall t \in \{1,...,T\}, \forall d \in \{1,...,D\}, and\ \forall s \in \{1,...,S\} \quad [8]$$

The decisions are made by optimizing the objective function under the operational constraints [3] to [8]. Constraint [3] makes sure that the truck t cannot accept loads greater than its nominal capacity. Constraint [4] ensures that the summation of truck capacities assigned to a shovel does not exceed the nominal digging rate of that particular shovel. Constraint [5] limits the model to sending at least AF times the plant capacity to each plant. Constraint [6] puts an upper limit cap on AF. Finally, Equation [7] guarantees that the decision variables can take only binary integer values.

After developing the deterministic model, we identified the fuzzy parameters involved in the proposed model. Then, based on the identified fuzzy parameters, we translated the deterministic MILP model to an FLP model. The fuzzy version of our deterministic MILP model can be presented as follows.

$$\min \tilde{Z} = \sum_{t=1}^{T}\sum_{d=1}^{D}\sum_{s=1}^{S} \tilde{C}_{tds} x_{tds} + VBN(1-AF) \quad [9]$$

Subject to

$$\sum_{d=1}^{D}\sum_{s=1}^{S} \tilde{tc}_t x_{tds} \le \tilde{T}\tilde{C}_t \;\forall t \in \{1,...,T\} \quad [10]$$

$$\sum_{t=1}^{T}\sum_{d=1}^{D} \tilde{tc}_t x_{tds} \le \tilde{sc}_s \quad \forall s \in \{1,...,S\} \quad [11]$$

$$\sum_{t=1}^{T}\sum_{s=1}^{S} \tilde{tc}_t x_{tds} \ge AF \times \tilde{pc}_d \quad \forall d \in \{1,...,D\} \quad [12]$$

and Equations [6] to [8]

where

$$\tilde{C}_{tds} = \left| \tilde{ltt}_{td} + \tilde{qt}_{td} + \tilde{dt}_{td} + \tilde{ett}_{ts} - \sum_{tt=1}^{TT} \left(tinq_{tts} + tenr_{tts}\right) \times \left(\tilde{st}_{tts} + \tilde{lt}_{tts}\right) \right| \quad [13]$$

It is worth noting that $\tilde{x}$ represents the fuzzy version of parameter x in the deterministic MILP model.

Defuzzification of the model

The uncertainties in the input parameters of the FLP model cause two significant problems: the problem of extracting optimum objective function value-containing fuzzy parameters, and the problem of the relationship between fuzzy sides of the constraints. Solving these two problems is tied to the process of ranking fuzzy numbers (Madadi and Wong, 2014). Several approaches have been introduced in the literature for the application of fuzzy set theory to rank fuzzy numbers. A detailed explanation of these approaches can be found in Lai and Hwang (1992) and van Leekwijck and Kerre (1999).

In this research, we implement the method developed by Jiménez *et al.* (2007) to rank the fuzzy constraints and fuzzy objective functions. The technique uses the concept of optimality to deal with the fuzzy objective functions and the idea of feasibility to deal with the fuzzy constraints. One essential advantage of ranking fuzzy numbers by implementing this method is that it preserves the linearity of the LP model, which helps to present a computationally efficient model to solve. The

technique developed by Jiménez *et al.* (2007) is also capable of preventing the number of constraints or objective functions from increasing (Ghasemy Yaghin, Torabi, and Fatemi Ghomi, 2012). Thus, it can be implemented for solving large-scale FLP models (Madadi and Wong, 2014).

The method developed by Jiménez *et al.* (2007) is based on two mathematically strong concepts of expected value and expected interval of fuzzy numbers (Pishvaee and Torabi, 2010) that were initially presented by Yager (1981) and Dubois and Prade (1987) and was developed later by Heilpern (1992) and Jiménez *et al.* (2007).

To start with the defuzzification process, we first define some essential terms. A fuzzy number is defined as a fuzzy set on the real line R that has a membership function presented in Equation [14].

$$u=\mu_{\tilde{a}}=\begin{cases}0 & \forall x\in(-\infty,a_1]\\ f_a(x) & \forall x\in[a_1,a_2],\text{increasing}\\ 1 & \forall x\in[a_2,a_3]\\ g_a(x) & \forall x\in[a_3,a_4],\text{decreasing}\\ 0 & \forall x\in[a_4,+\infty)\end{cases};\tilde{a}=(a_1,a_2,a_3,a_4) \quad [14]$$

A cut through the fuzzy number produces a non-fuzzy set and is defined as given in Equation [15].

$$a_\alpha=\{x\in R\,;\,\mu_{\tilde{a}}(x)\geq\alpha\,;\,0\leq\alpha\leq 1\}\quad or$$
$$a_\alpha=[f_a^{-1}(u)\,,\;g_a^{-1}(u)] \quad [15]$$

The membership function for cases where f_a and g_a are linear functions is trapezoidal, and in cases where $a_2 = a_3$ and the fa and g_a are linear functions, triangular. In this paper, all the parameters are assumed to follow the triangular membership function. The expected interval and the expected value of a triangular fuzzy number, which were first introduced by Heilpern (1992), can be calculated using Equation [16] and Equation [17], respectively.

$$EI(\tilde{a})=[E_1^a,E_2^a]=\left[\int_0^1 f_a^{-1}(u)\,du\,,\int_0^1 g_a^{-1}(u)\,du\right]=\left[\frac{a_1+a_2}{2},\frac{a_2+a_3}{2}\right] \quad [16]$$

$$EV(\tilde{a})=\left[\frac{E_1^a+E_2^a}{2}\right]=\frac{a_1+2a_2+a_3}{4} \quad [17]$$

According to the ranking method developed by Jiménez *et al.* (2007), a is greater than or equal to b in the degree defined by Equation [18] (Pishvaee and Torabi, 2010).

$$\mu_M(\tilde{a},\tilde{b})=\begin{cases}0 & if\ E_2^a-E_1^b<0\\ \dfrac{E_2^a-E_1^b}{E_2^a-E_1^b-(E_1^a-E_2^b)} & if\ 0\in[E_1^a-E_2^b,\,E_2^a-E_1^b]\\ 1 & if\ E_1^a-E_2^b>0\end{cases} \quad [18]$$

If $\mu m\,(\tilde{a},\tilde{b})\geq\alpha$ then it is said that at least in the degree of α, $\tilde{a}$ is greater than or equal to $\tilde{b}$. Based on Arenas Parra *et al.* (2005), $\tilde{a}$ and $\tilde{b}$ are equal in degree of α if:

$$\frac{\alpha}{2}\leq\mu_M(\tilde{a},\tilde{b})\leq 1-\frac{\alpha}{2} \quad [19]$$

The FLP models with trapezoidal or triangular fuzzy parameters (Equation [20]) can be converted to their equivalent crisp models (Equation [21]) by implementing the definitions explained above and the Jiménez *et al.* (2007) method for treating fuzzy objective function and the Arenas Parra *et al.* (2005) method for treating fuzzy constraints.

s.t.

$$\begin{aligned}&\tilde{a}_i x\leq\tilde{b}_i, && i=1,\ldots,t\\ &\tilde{a}_i x=\tilde{b}_i, && i=t+1,\ldots,l\\ &\tilde{a}_i x\geq\tilde{b}_i, && i=l+1,\ldots,m\\ &x\geq 0\end{aligned} \quad [20]$$

min $EV\gamma(Z) = EV\gamma\,(\alpha)\;x$

s.t.

$$\begin{aligned}&[(1-\alpha)E_1^{a_i}+\alpha E_2^{a_i}]x\leq\alpha E_1^{b_i}+(1-\alpha)E_2^{b_i}, && i=1,\ldots,t\\ &[(1-\alpha)E_2^{a_i}+\alpha E_1^{a_i}]x\geq\alpha E_2^{b_i}+(1-\alpha)E_1^{b_i}, && i=t+1,\ldots,l\\ &[(1-\frac{\alpha}{2})E_2^{a_i}+\frac{\alpha}{2}E_1^{a_i}]x\geq\frac{\alpha}{2}E_2^{b_i}+(1-\frac{\alpha}{2})E_1^{b_i}, && i=l+1,\ldots,m\\ &[\frac{\alpha}{2}E_2^{a_i}+(1-\frac{\alpha}{2})E_1^{a_i}]x\leq(1-\frac{\alpha}{2})E_2^{b_i}+\frac{\alpha}{2}E_1^{b_i}, && i=l+1,\ldots,m\end{aligned} \quad [21]$$

With γ degree of optimism, the objective function ($EV\gamma(Z) = EV\gamma\,(\alpha)\;x$ where Z = (Z_1, Z_2, Z_3, Z_4), can be defined as:

$$EV_\gamma(\tilde{Z})=\gamma E_2^Z+(1-\gamma)E_1^Z=\gamma\frac{Z_3+Z_4}{2}+(1-\gamma)\frac{Z_1+Z_2}{2} \quad [22]$$

Using the defuzzification method explained in Equations [14] to [22], the equivalent crisp model for the fuzzy truck dispatching model presented in this paper can be formulated as follows:

$$Z^p=\sum_{t=1}^{T}\sum_{d=1}^{D}\sum_{s=1}^{S}\left|\left(ltt_{td}^p+qt_{td}^p+dt_{td}^p+ett_{ts}^p\right)-\sum_{tt=1}^{TT}(tinq_{tts}+tenr_{tts})\times\left(st_{tts}^p+lt_{tts}^p\right)\right| \quad [23]$$

$$Z^m=\sum_{t=1}^{T}\sum_{d=1}^{D}\sum_{s=1}^{S}\left|\left(ltt_{td}^m+qt_{td}^m+dt_{td}^m+ett_{ts}^m\right)-\sum_{tt=1}^{TT}(tinq_{tts}+tenr_{tts})\times\left(st_{tts}^m+lt_{tts}^m\right)\right| \quad [24]$$

$$Z^o=\sum_{t=1}^{T}\sum_{d=1}^{D}\sum_{s=1}^{S}\left|\left(ltt_{td}^o+qt_{td}^o+dt_{td}^o+ett_{ts}^o\right)-\sum_{tt=1}^{TT}(tinq_{tts}+tenr_{tts})\times\left(st_{tts}^o+lt_{tts}^o\right)\right| \quad [25]$$

$$\min\ EV_\gamma(\tilde{Z})+VBN(1-AF)=\gamma\frac{Z^m+Z^o}{2}+(1-\gamma)\frac{Z^p+Z^m}{2}+VBN(1-AF) \quad [26]$$

Subject to

$$\sum_{d=1}^{D}\sum_{s=1}^{S}\left[(1-\alpha)\frac{tc_t^p+tc_t^m}{2}+\alpha\frac{tc_t^m+tc_t^o}{2}\right]x_{tds}\leq\alpha\frac{TC_t^p+TC_t^m}{2}+(1-\alpha)\frac{TC_t^m+TC_t^o}{2}\quad\forall t\in\{1,\ldots,T\} \quad [27]$$

$$\sum_{t=1}^{T}\sum_{d=1}^{D}\left[(1-\alpha)\frac{tc_t^p+tc_t^m}{2}+\alpha\frac{tc_t^m+tc_t^o}{2}\right]x_{tds}\leq\alpha\frac{sc_s^p+sc_s^m}{2}+(1-\alpha)\frac{sc_s^m+sc_s^o}{2}\quad\forall s\in\{1,\ldots,S\} \quad [28]$$

$$\sum_{t=1}^{T}\sum_{s=1}^{S}\left[(1-\alpha)\frac{tc_t^m+tc_t^o}{2}+\alpha\frac{tc_t^p+tc_t^m}{2}\right]x_{tds}\geq AF\times\left(\alpha\frac{pc_d^m+pc_d^o}{2}+(1-\alpha)\frac{pc_d^p+pc_d^m}{2}\right)\quad\forall d\in\{1,\ldots,D\} \quad [29]$$

$$AF \begin{cases} \leq mf & \text{if } mf > 1 \\ \leq 1 & \text{otherwise} \end{cases} \quad [30]$$

$$x_{tds} \in \{0,1\} \ \forall t \in \{1,...,T\}, \ and \ \forall d \in \{1,...,D\} \quad [31]$$

$$mf = \frac{\sum_{t=1}^{T} lc_t x_{tds}}{\sum_{s=1}^{S}\sum_{d=1}^{D}(pf_{sd} - pmsf_{sd})} \quad [32]$$
$$\forall t \in \{1,...,T\}, \forall d \in \{1,...,D\}, and \ \forall s \in \{1,...,S\}$$

where γ is the degree of optimism of the decision-maker and α is the degree of the minimum acceptable feasibility of the decision vector (Madadi and Wong, 2014).

Application in a case study

We applied the FLP model in a mining case study to evaluate its performance. The case study is an opencast iron ore mine located in central Iran. The mine has two processing plants fed by a truck and shovel material handling system. Based on the short-term production schedule of the mine, the production fleet must be capable of meeting an hourly feed rate of 2300 t for each of the active processing plants with a stripping ratio of 1.3.

The material handling fleet consists of two types of shovels (Hitachi Hit 2500 and Hit 5500), and one type of truck (Cat 785C). The mine has five active faces. Two small shovels (Hit 2500) work on the ore mining faces and serve the processing plants. Two large shovels (Hit 5500) and one small shovel work on the waste mining faces. The mined material is transported to the destination areas (plants or waste dumps) using 28 trucks. The operation uses an optimization model developed by White and Olson (1986) and Olson, Vohnout, and White (1993) to solve its truck dispatching problem. We used that model as the benchmark in this study.

Input from historical data

We incorporated uncertainties associated with all the parameters in the simulation model of the case study and the truck dispatching model. To do so, we first retrieved one year of operational data from the fleet database. Then, after preprocessing and cleaning bad data, we fitted several distributions to the data. We then selected the best-fitted distribution on each parameter using the results of the chi-square test and Kolmogorov–Smirnov test (Rossetti, 2015). The parameters and the best distributions fitted on them are presented in Table I.

In Table I, bc_s is shovel s bucket capacity, and lct_s is the loading cycle time for shovel s. The distributions provided in Table I are used in the simulation model of the case study. Whenever a value for a parameter is required, the random sampler of the simulation software, Rockwell Arena (Rockwell Automation Technologies Inc., 2020) in our case, randomly samples from the parameter's associated distribution to incorporate uncertainty into the simulation modelling. Any time a signal is received by the truck dispatching model, a triangular function with a minimum of the first quantile, mean of the second quantile, and maximum of the third quantile is exported from the parameters presented in Table I to be used in the FLP model. For the parameters such as the nominal capacity of trucks, hourly capacity of shovels, and hourly capacity of plants, a ±10% value from the manufacturer's catalogues was selected to be used as the minimum and maximum values in the triangular fuzzy function of the parameters. For instance, for the Cat 785C, with a nominal capacity of 140 t, the triangular function has a minimum of 126 t and a maximum of 154 t. The ±10% of nominal capacity is sourced from the manufacturer's catalogues as the capacity to be used for the best practice and the lowest operational and maintenance costs. Each time the FLP model is called for making a decision, it uses γ (the degree of optimism of the decision-maker) and α (the degree of the minimum acceptable feasibility of the decision vector) to sample from the triangular distributions of the fuzzy parameters and apply those parameters in its calculations.

The model set-up and evaluation

Material handling in surface mines is an expensive operation. Because of that, testing of developed technologies in a real mining operation is not economically viable. Therefore, researchers test new technologies on the simulated version of a mining operation before implementing them in the actual operations. We followed the same route in this paper. We used the simulation model of the case study developed by Moradi Afrapoli *et al.* (2018) to evaluate the performance of the FLP truck dispatching model. The simulation of the case study was

Table I

Stochastic input parameters retrieved from historical fleet data with their best-fitted distributions tested by chi-square and KS tests (Moradi Afrapoli, Tabesh, and Askari-Nasab, 2019)

No.	Parameter	Equipment	Best fitted distribwution
1	qt_{td} (s)	Truck	1 + lognormal (23.1, 66.6)
2	dt_{td} (s)	Truck	Normal (60, 27)
3	ev_{ts} (km/h)	Truck and shovel	Normal (30.6, 12.2)
4	lv_{td} (km/h)	Truck and shovel	1 + gamma (2.89, 5.99)
5	st_{tts} (s)	Shovel and truck Hitachi EX5500: 1 + lognormal (66.6, 100.0)	Hitachi EX2500: 1 + lognormal (34.6, 32.9)
6	lt_{tts} (s)	Shovel and truck Hitachi EX5500: 1 + gamma (25.3, 3.55)	Hitachi EX2500: Normal (175, 70.9)
7	bc_s (m³)	Shovel Normal (21, 2)	Normal (14,1)
8	lct_s (s)	Shovel Normal (16, 1)	Normal (17, 0.5)

run for ten days of operation, each day consisting of one 12-hour shift. We used the first shift of the simulated operation to warm up the simulation model and to reach steady-state operation. Then, we evaluated the performance of our developed model by comparing the results of its application in the next nine shifts with the results from the mine's in-place truck dispatching model.

Based on the short-term schedule, in 120 hours of operation, 1.2696 Mt of ore plus waste should be removed from the pit. The simulation of the operation meets the criteria with its in-place truck dispatching model and our FLP truck dispatching model. Apart from the total material removed, other key performance indicators (KPIs) were measured in the case study. Table II lists the measured KPIs.

As the processing plant is one of the most expensive parts of a mining operation, keeping its performance at the highest level is essential. One responsibility of the material handling system is to feed the processing plant to its full capacity. The case study involves two processing plants. The truck and shovel fleet of the operation works towards delivering 27.60 kt of ore to each plant per shift to meet the full capacity requirement. In other words, the material handling system delivers 2300 t of ore to each processing plant in each hour of the operation. Figure 1 shows how each processing plant was fed during the simulation.

Implementation of our developed model instead of the in-place model improved the hourly ore delivery to plant 1 (Figure 1a and plant 2 (Figure 1b) by 21% and 15%, respectively. The leading cause of this improvement is the incorporation of AF as the second component of our objective function (Equation [2]). This component of the objective function minimizes the deviation from the plant capacity. In addition to the tonnage of material delivered to the processing plants, another essential factor to be met is the quality (grade) of the material. The processing plants accept ore with magnetic weight recovery (MWT) grade of between 60% and 80%. Preference for plant 1 is an average MWT grade of 65%, and for plant 2 an average of 75%. Figure 2 represents the distribution of MWT grade in material delivered to each plant on a shift-by-shift basis.

As depicted by Figure 2, both of the truck dispatching models delivered material to the plants within the acceptable MWT grade range. However, by replacing the in-place truck dispatching

Table II

KPIs for evaluating the performance of the developed FLP truck dispatching model

No.	Area of concern	KPI to evaluate
1	Processing plants	Hourly feed rate
2	Processing plants	Hourly head grade
3	Shovels	Utilization
4	Trucks	Queue time

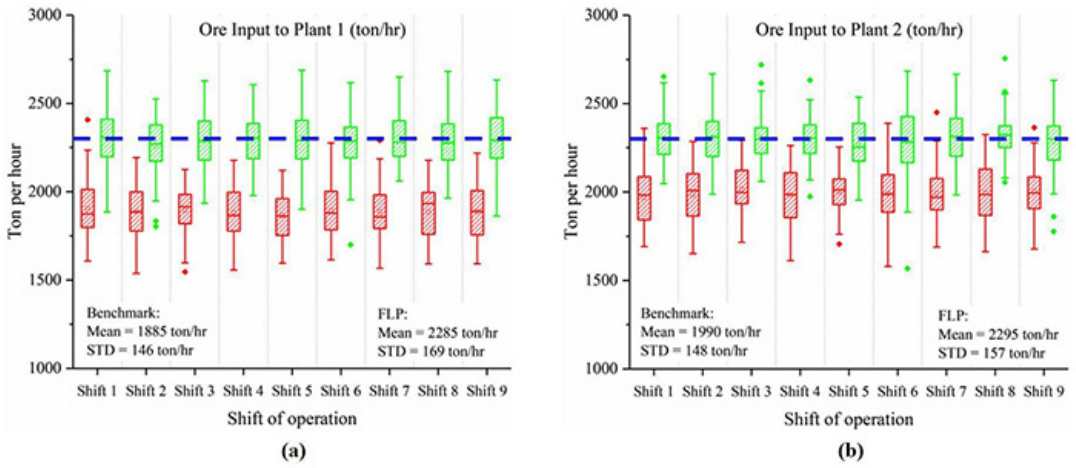

Figure 1—Tonnage of ore delivered to processing plants per hour (required capacity – blue dashed line, benchmark – red boxes, FLP – green boxes, dots – outliers)

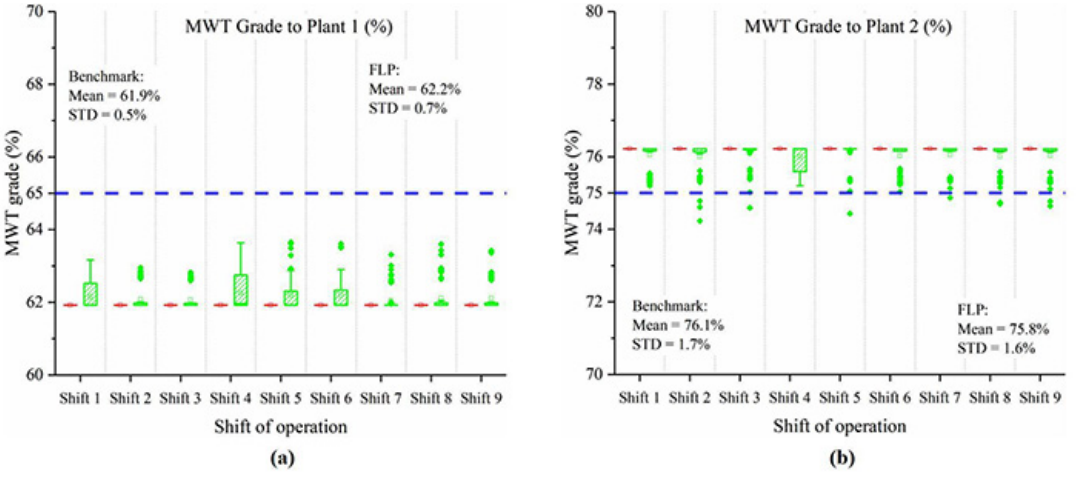

Figure 2—Grade of ore delivered to processing plants per hour (required capacity – blue dashed line, benchmark – red boxes, FLP – green boxes, dots – outliers

model with the FLP model, the tendency of the MWT grade towards the desired average MWT grade (65% for plant 1 and 75% for plant 2) increased.

In the case study, five shovels are working in the fleet to fulfill the short-term production schedule requirement. Shovel 1 and shovel 2 are at the ore mining faces, and the remainder of the shovels at the waste mining faces. Table III represents utilization for each active shovel and the entire shovel fleet in the simulation study of the mine.

Table III shows that although both truck dispatching models utilized the shovel fleet almost the same, the benchmark model used the waste shovels more than the ore shovels. The benchmark truck dispatching model sends trucks to the closest shovels without prioritizing any particular shovel. In the case study, waste shovels are mining overburden and sitting closer to dumping location than the ore shovels. Thus waste shovels are utilized more than ore shovels. However, according to the same table, the FLP truck dispatching model employed the ore shovels more than the waste shovels. Instead of the unnecessary waste movement required by the production schedule, the FLP model prioritized the ore shovels to meet the requirement of the processing plants.

A fleet of 28 Cat 785C trucks transports material from the mining faces to the destinations (either crushers or waste disposal area). The cumulative time that each truck spent in the queue is presented in Figure 3. The fleet in the benchmark truck dispatching model wasted an average of 1486±71 minutes per truck in the queue during the simulation. Replacing the benchmark dispatching model with the FLP truck dispatching model improved truck fleet efficiency. The FLP model utilized the truck fleet such that each truck spent a cumulative average of 1253±50 minutes in different queues (a 15% improvement) during the simulation.

This time saving is due to the incorporation of the length of the queue in the decision-making procedure. The in-place truck dispatching model (and most of the published truck dispatching models) ignores the expected queue time for the trucks. However, our developed model incorporates the expected queue time, which helps in making more precise decisions with less wait time in queues for trucks.

Table III

Shovel utilization (%) – comparison between the benchmark model and the FLP model

Shovel	Benchmark		Fuzzy		Diff.
	Mean	StD	Mean	StD	
Shovel 1	82.7	1.1	95.8	1.9	13.1
Shovel 2	78.9	1.2	95.2	2	16.3
Shovel 3	93.6	1.4	80.6	1.3	–13.0
Shovel 4	92.5	1.4	82	1.6	–10.5
Shovel 5	99.8	5.9	94.4	1.8	–5.4
Entire fleet	89.5	2.2	89.6	1.72	0.1

Conclusions

This paper introduced a new mixed-integer linear programming model to solve the truck dispatching problem in surface mines. The proposed model makes dispatching decisions by simultaneously minimizing deviation from the production target set by the strategic plan, cumulative idle time of the shovel fleet, and cumulative wait time of the truck fleet. The model applies a fuzzy linear programming approach to incorporate the associated uncertainties in the decision-making procedure. We used the developed truck dispatching model in a real mining case study with a benchmark from the backbone algorithm of Modular Mining DISPATCH® (Modular Mining Systems Inc., 2020). The results showed that our FLP model improved the ore production and truck wait time in the queues by more than 15%. The model also prioritized ore shovels over waste shovels in order to feed the plants to their maximum capacity. This improvement in production and equipment efficiency will result in lower costs and higher profits for the operation. The authors anticipate that implementing the developed FLP model in a case with a fleet of mixed truck types will result in more realistic truck dispatching decisions.

References

Aghajani Bazzazi, A., Osanloo, M., and Soltanmohammadi, H. 2008. Loading-haulage equipment selection in open pit mines based on fuzzy-TOPSIS method. Gospodarka Surowcami Mineralnymi Mineral Resources Management. *Journal of the Polish Academy of Sciences*, vol. 24, no. 4, part 3. pp. 87–102.

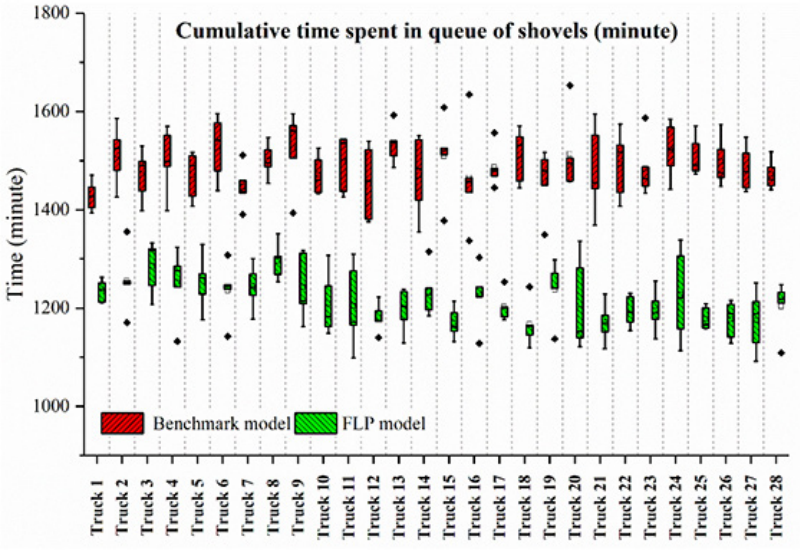

Figure 3—Cumulative time spent in queues at different locations by each truck (benchmark – red boxes, FLP – green boxes, dots – outliers)

Akbari, A.D., Osanloo, M., and Shirazi, M.A. 2009. Minable reserve estimation while determining ultimate pit limits (UPL) under price uncertainty by real option approach (ROA). *Archives of Mining Sciences*, vol. 54, no. 2. pp. 321–339.

Alarie, S. and Gamache, M. 2002. Overview of solution strategies used in truck dispatching systems for open pit mines. *International Journal of Surface Mining, Reclamation and Environment*, vol. 16, no. 1. pp. 59–76. doi: 10.1076/ijsm.16.1.59.3408

Arenas Parra, M., Bilbao Terol, A., Pérez Gladish, B., and Rodríguez Uría, M.V. 2005. Solving a multiobjective possibilistic problem through compromise programming. *European Journal of Operational Research*, vol. 164, no. 3 (Special Issue), pp. 748–759. doi: 10.1016/j.ejor.2003.11.028

Bandopadhyay, S. 1987. Partial ranking of primary stripping equipment in surface mine planning. *International Journal of Surface Mining, Reclamation and Environment*, vol. 1, no. 1. pp. 55–59. doi: 10.1080/09208118708944102

Bandopadhyay, S. and Chattopadhyay, A. 1986 Selection of post-mining uses of land via fuzzy algorithm. *Proceedings of the 19th International Symposium on the Application of Computers in Mine Planning*. Ramani, R.V (ed.). Society of Mining Engineers of AIME. pp. 321–332.

Bangian, A. H., Ataei, M., Sayadi, A., and Gholinejad, A. 2012. Optimizing post-mining land use for pit area in open-pit mining using fuzzy decision making method. *International Journal of Environmental Science and Technology*, vol. 9, no. 4. pp. 613–628. doi: 10.1007/s13762-012-0047-5

Bascetin, A., Oztas, O., and Kanli, A. 2007. A computer software using fuzzy logic for equipment selection in mining engineering. *Journal of the Southern African Institute of Mining and Metallurgy*, vol. 106, no. 1. pp. 63–70. https://journals.co.za/content/saimm/107/2/AJA0038223X_3299 [accessed: 1 March 2018].

Dubois, D. and Prade, H. 1987. The mean value of a fuzzy number. *Fuzzy Sets and Systems*, vol. 24, no. 3. pp. 279–300. doi: 10.1016/0165-0114(87)90028-5

Ghasemy Yaghin, R., Torabi, S.A.A., and Fatemi Ghomi, S.M.T.M.T. 2012. Integrated markdown pricing and aggregate production planning in a two echelon supply chain: A hybrid fuzzy multiple objective approach. *Applied Mathematical Modelling*, vol. 36, no. 12. pp. 6011–6030. doi: 10.1016/j.apm.2012.01.029

Hauck, R.F. 1973. A real-time dispatching algorithm for maximizing open-pit mine production under processing and blending requirements. *Proceedings of the Seminar on Scheduling in Mining, Smelting and Metallurgy*: Canadian Institute of Mining, Metallurgy and Petroleum, Montreal. pp. 1–10.

Heilpern, S. 1992. The expected value of a fuzzy number. *Fuzzy Sets and Systems* vol. 47, no. 1. pp. 81–86. doi: 10.1016/0165-0114(92)90062-9

Jiménez, M., Parra, M.A., Bilbao-Terol, A., and Rodríguez, M.V. 2007. Linear programming with fuzzy parameters: An interactive method resolution. *European Journal of Operational Research*, vol. 177, no. 3. pp. 1599–1609. doi: 10.1016/j.ejor.2005.10.002

Lai, Y.-J and Hwang, C.-L. 1992. A new approach to some possibilistic linear programming problems. *Fuzzy Sets and Systems*, vol. 49, no. 2. pp. 121–33. doi: 10.1016/0165-0114(92)90318-X

Li, Z. 1990. A methodology for the optimum control of shovel and truck operations in open-pit mining. *Mining Science and Technology*, vol. 10, no. 3. pp. 337–340. doi: 10.1016/0167-9031(90)90543-2

Madadi, N. and Wong, K.Y. 2014 A multiobjective fuzzy aggregate production planning model considering real capacity and quality of products. *Mathematical Problems in Engineering*, 2014. doi: 10.1155/2014/313829

Modular Mining Systems Inc. 2020. Dispatch. http://www.modularmining.com/product/dispatch/

Moradi Afrapoli, A. and Askari-Nasab, H. 2019. Mining fleet management systems: a review of models and algorithms. *International Journal of Mining, Reclamation and Environment*, vol. 33, no. 1. pp. 42–60. doi: 10.1080/17480930.2017.1336607

Moradi Afrapoli, A., Tabesh, M., and Askari-Nasab, H. 2018. A stochastic hybrid simulation-optimization approach towards haul fleet sizing in surface mines. *Mining Technology: Transactions of the Institute of Mining and Metallurgy*. doi: 10.1080/25726668.2018.1473314

Moradi Afrapoli, A., Tabesh, M., and Askari-Nasab, H. 2019. A multiple objective transportation problem approach to dynamic truck dispatching in surface mines. *European Journal of Operational Research*, vol. 276, no. 1. pp. 331–342. doi: 10.1016/j.ejor.2019.01.008

Nguyen, V.U. 1985. Some fuzzy set applications in mining geomechanics. *International Journal of Rock Mechanics and Mining Sciences & Geomechanics Abstracts*, vol. 22, no. 6. pp. 369–379. doi: 10.1016/0148-9062(85)90002-6

Olson, J.P., Vohnout, S.I., and White, J. 1993. On improving truck/shovel productivity in open pit mines. *CIM Bulletin*, vol. 86, no. 973. pp. 43–49.

Oraee, K. and Goodarzi, A. 2007. General approach to distribute waste rocks between dump sides in open cast mines. *Proceedings of the Sixteenth International Symposium on Mine Planning and Equipment Selection*. Bangkok, Thailand. Reading Matrix Inc., Irvine, CA. pp. 701-712.

Pishvaee, M.S. and Torabi, S.A. 2010. A possibilistic programming approach for closed-loop supply chain network design under uncertainty. *Fuzzy Sets and Systems*, vol. 161, no. 20. pp. 2668–2683. doi: 10.1016/j.fss.2010.04.010

Rahmanpour, M. and Osanloo, M. 2017. Application of fuzzy linear programming for short-term planning and quality control in mine complexes. *Journal of the Southern African Institute of Mining and Metallurgy*, vol. 117, no. 7. pp. 685–694.

Rockwell Automation Technologies Inc. 2020. Arena Simulation Software. Austin, TX. https://www.arenasimulation.com

Rossetti, M.D. 2015. Simulation Modeling and Arena. 2nd edn. Wiley, Hoboken, NJ. https://books.google.com.tr/books?id=j2xuCAAAQBAJ

Soumis, F., Ethier, J., and Elbrond, J. 1989. Truck dispatching in an open pit mine. *International Journal of Surface Mining, Reclamation and Environment*, vol. 3, no. 2. pp. 115–119. doi: 10.1080/09208118908944263

Temeng, V. a., Otuonye, F.O., and Frendewey, J.O. 1997. Real-time truck dispatching using a transportation algorithm. *International Journal of Surface Mining, Reclamation and Environment*, vol. 11, no. 4. pp. 203–207. doi: 10.1080/09208119708944093

Temeng, V.A., Otuonye, F.O., and Frendewey, J.O. 1998. A non preemptive goal programming approach to truck dispatching in open pit mines. *Mineral Resources Engineering*, vol. 7, no. 2. pp. 59–67. doi: doi:10.1142/S0950609898000092

Upadhyay, S.P.P. and Askari-Nasab, H. 2016. Truck-shovel allocation optimisation: A goal programming approach. *Mining Technology*, vol. 125, no. 2. pp. 1–11. doi: http://doi.org/10.1179/1743286315Y.0000000024

White, J.W. and Olson, J.P. 1986. Computer-based dispatching in mines with concurrent operating objectives. *Mining Engineering*, vol. 38, no. 11. pp. 1045–1054.

Van Leekwijck, W. and Kerre, E.E. 1999. Defuzzification: criteria and classification. *Fuzzy Sets and Systems*, vol. 108, no. 2. pp. 159–178. doi: 10.1016/S0165-0114(97)00337-0

Yager, R.R. 1981. A procedure for ordering fuzzy subsets of the unit interval, *Information Sciences*, vol. 24, no. 2. pp. 143–161. doi: 10.1016/0020-0255(81)90017-7

Yavuz, M. 2008. Selection of plant location in the natural stone industry using the fuzzy multiple attribute decision making method. *Journal of the Southern African Institute of Mining and Metallurgy*, vol. 108, no. 10. pp. 641–649. http://www.scielo.org.za/scielo.php?script=sci_arttext&pid=S2225-62532008000900008 [accessed: 1 March 2018].

Zimmermann, H.-J. 1978. Fuzzy programming and linear programming with several objective functions, *Fuzzy Sets and Systems*, vol. 1, no. 1. pp. 45–55. doi: 10.1016/0165-0114(78)90031-3

Zimmermann, H. 1976. Description and optimization of fuzzy systems. *International Journal of General Systems*, vol. 2, no. 4. pp. 209–215. doi: 10.1080/03081077608547470 ◆

Analysis of rope load sharing on multi-rope friction winders

M.E. Greenway[1,2], S.R. Grobler[2], and S. Bilessuris[2]

Affiliation:
[1]University of Western Australia, Australia.
[2]Worley Services Pty Ltd, Perth, Australia.

Correspondence to:
M.E. Greenway

Email:
malcolm.greenway@worley.com

Dates:
Received: 15 Jun. 2020
Revised: 1 Aug. 2021
Accepted: 27 Aug. 2021
Published: September 2021

How to cite:
Greenway, M.E.,. Grobler, S.R., and Bilessuris,S. 2021 Analysis of rope load sharing on multi-rope friction winders. Journal of the Southern African Institute of Mining and Metallurgy, vol. 121, no. 9, pp. 513–522

DOI ID:
http://dx.doi.org/10.17159/2411-9717/1254/2021

Synopsis

Ensuring that all the head ropes on a multi-rope friction winder share the load equally has been a design and maintenance issue since they were first developed. Accurate machining of the rope grooves is necessary to meet this objective. Early analysis of the change of rope loads for ropes in grooves that are mismatched in depth treated the grooves as rigid. Groove depth tolerances deduced from this analysis are stringent and difficult to achieve in practice. Test work indicated that the inherent flexibility of groove lining materials alleviates the load-sharing problem. However, no analysis of rope load changes due to mismatched flexible grooves has been published. In this paper we develop new equations for the rope load variation for flexible grooves. By allowing flexibility to reduce to zero, the corresponding rigid rope groove equations are obtained. New criteria for tolerable groove depth variations are developed from this analysis, which depend on the flexibility of the groove lining material.

Keywords
friction winder, rope load sharing, mismatched rope grooves, flexible groove liners.

Introduction

Friction winders are often called Koepe winders after Frederick Koepe, their inventor, who first developed a single-rope friction hoist in Germany in 1878. The first multi-rope friction winders were developed and commissioned in Germany in 1947 by GHH. Ever since, these winders have proved popular and cost-effective winding installations in the mining industry world-wide. Friction winders can be positioned directly in the headframe – when they are referred to as 'tower mounted' – or adjacent to the headframe – when they are referred to as 'ground mounted'. Tower-mounted winders sometimes have deflecting sheaves to reduce the spacing between the ascending and descending ropes to suit the conveyance locations in the shaft. These configurations are illustrated in Figure 1.

The issue of load sharing between the head ropes has been a legitimate concern since the first developments and is both a design and a maintenance issue for all friction winders to the current day. Useful technical papers (Hitchin, 1958; Eithun, Landau, and Mondal, 1960; Bar, 1976; Dean, 1970) published in the literature in the period 1950 – 1976 have since formed the basis of rope load control, monitoring, and maintenance on friction winders. The realization that perfect load sharing was unachievable resulted in the industry norm for the control of head rope loads, aiming at controlling these loads to within ±10% of the mean rope load.

Assuming rigid grooves, Hitchin (1958) discussed the effect of grooves of unequal depth on the rope load changes for a two-rope winder, illustrating the changes graphically. No equations from his analysis were provided. He drew attention to tower-mounted winders being more sensitive to groove mismatch than ground-mounted winders. Eithun, Landau, and Mondel (1960) also considered rigid grooves, providing equations of the right functional form although containing mathematical discrepancies. They used an example of a four-rope friction winder. Bar (1976), quoting Mettler (1956), gave an equation for the maximum rope load caused by mismatched groove depths for an n-rope winder. No analysis behind this equation was given. All these authors, besides stressing the need for matching rope groove circumferences to maintain tolerable rope load sharing, mention that left unchecked, gross rope slip will occur in the groove of smallest circumference, leading to accelerated groove wear. Dean (1970) linked the structural failure of friction winder ropes to poor control of groove depths and gross rope slip.

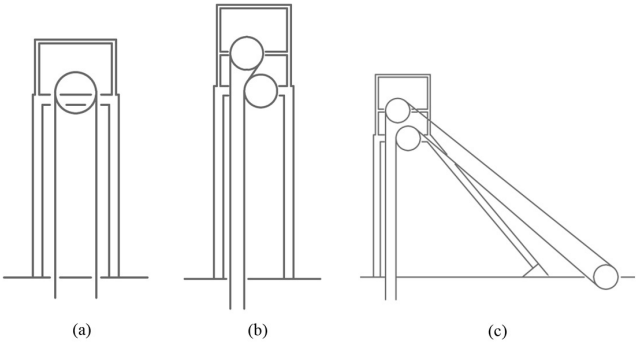

Figure 1—Configurations of friction winders. (a) Tower mounted without deflection sheaves, (b) tower mounted with deflection sheaves, (c) ground mounted

The papers by Bar (1976) and Hitchin (1958) both mention the alleviation of rope load deviations from the mean when flexible groove liner material is used. Neither gives an analysis of the form of load variation during the wind. Bar refers to experiments conducted and quotes peak rope load reductions to 50% for rubber and 33% for plastic materials when the flexibility of the groove lining material is considered.

In this paper we develop new equations for the rope load variation for flexible grooves. By allowing flexibility to reduce to zero, the corresponding rigid rope groove equations are obtained. New criteria for tolerable groove depth variations are developed from this analysis, which depend on the flexibility of the groove lining material.

The load-sharing problem is quite a subtle one, so the paper takes a measured, gradual approach, leaving the mathematical developments, which may be distracting to some readers, to the Appendix. Firstly, the importance of achieving good load sharing is outlined, and all the causes of unequal load sharing are mentioned together with strategies and operating practices to alleviate them. The most troublesome cause – that of groove depth discrepancies – is taken forward and becomes the focus of the paper.

Prior to introducing the new parameter of the problem – that of the groove's flexibility – a qualitative explanation is given of how the rigid grooves on a two-rope Koepe winder with different depths generate unequal loads in the head ropes when the winder operates, in both the conveyance ascending and descending modes. The load changes are illustrated by replicating a graph of Hitchin (1958).

Friction winders with four and six ropes are much more common than two-rope winders. It is necessary to generalize the two-rope analysis to an n-rope winder. This is done in the Appendix by first assessing the situation where only one groove (taken as groove 1) is disturbed so as to be shallower than the remaining grooves, which all share the same depth. Then by using a superposition principle, this restriction is relaxed so that each groove can have a unique depth. The resulting equations can be used to predict the loads in the individual ropes of an n-rope friction winder with given defined groove depth differences. The rigid groove equations are quoted in the text and illustrated by replicating a graph of Eithun, Landau, and Mondal (1960) for the case of a four-rope winder.

The same equations are rearranged to provide the criteria for groove accuracy that will maintain the variation of rope loads within tolerance (±10% of mean rope load). This equation is applied to an example winder to illustrate how stringent the accuracy criteria become.

Finally, a new parameter to represent the groove flexibility is introduced and numerical values for the example winder are developed from a 2D finite element analysis of the groove material. The rope load variations that apply to a Koepe winder with flexible grooves for ascending and descending conveyance travel are given in the text. This is illustrated by repeating the Hitchin example, but this time with a flexible groove material to illustrate the benefit. A new rope groove depth accuracy criterion is developed to account for the groove flexibility, together with a graph to illustrate the improvement offered by groove flexibility.

The importance of load sharing among the head ropes of a multi-rope friction winder

Equal sharing of the suspended load among the ropes on a multi-rope friction winder is desirable for several reasons.

- Regulators allow the statutory rope factors of safety to be calculated based on equal load sharing. Any discrepancy in load sharing means that some ropes will take higher loads than the mean rope load and others will take lower loads. Effectively, the ropes with the higher load may be breaching the factor of safety regulation.
- Head rope fatigue damage is a function of the axial load range experienced in the ropes during winding, and to a lesser extent due to the ropes bending around the drum and sheaves. Both these aspects are exacerbated in ropes that take higher loads than the mean rope load. This results in shorter rope life.
- If the loads in the ropes vary severely it is possible for the ropes to slip in the grooves in the winder drum, which leads to accelerated wear of the rope groove friction lining material and may result in structural upset of the rope.
- If the loads in the ropes with the lower loads reduce to the extent that they become slack, there is the possibility that the ropes will distort or kink and become permanently damaged, requiring their immediate discard (reduced life).

Factors that influence unequal load sharing among the head ropes

Differences in the head rope loads of multi-rope friction winders arise fundamentally from:

1. Differences in free lengths of the head ropes at the attachment to the conveyances
2. Differences in the rope-length advance rate of the ropes as they pass over the driving friction drum. This is affected by:
   a. Variations in the rope tread circumferences of the driving friction drum
   b. Differences in the strain of the individual ropes (due to load differences)
   c. Differences in the diameters of the various ropes
   d. Differential deflection of the rope grooves of the winder drum under the different imposed rope loading
3. Differences in the modulus of elasticity of the ropes
4. Differences in the amount of 'permanent stretch' of the ropes.

The best practice strategy to mitigate the issues arising from differences in the rope properties (points 2c, 3, and 4 above), is to purchase and install ropes from the same production run. Furthermore, when one rope requires discarding, all the head ropes are discarded and replaced simultaneously. This is common practice.

The appropriate strategy to mitigate factor 2d above is to ensure the drum radial stiffness is the same for each rope groove.

Head rope attachments are normally adjustable so that rope lengths can be equalized/adjusted on initial installation (to mitigate factor 1), and in service (to mitigate factor 4).

Other than equalizing the free lengths of the head ropes, the most significant influence mentioned above is the differences in rope groove circumference (factor 2a above) (or equivalently the effective groove depth). This is the focus of this paper.

Qualitative discussion of load variation in a two-rope friction winder with mismatched groove depths

Consider a friction drum that is assumed 'rigid' (*i.e.* it doesn't deflect under the rope loads) and the friction tread material is similarly rigid (doesn't compress under the rope loads). The drum has two grooves of mean groove radius R_m but with a difference from the mean of ΔR - one groove radius being $R_m + \Delta R$ (groove 1) and the other being $R_m - \Delta R$ (groove 2). Refer to Figure 2 and the associated nomenclature.

Initially, consider the conveyance positioned at shaft bottom where the two ropes of equal length and with identical physical properties are anchored to the conveyance. The rope loads at the conveyance will be equal. At the top end of the ropes where they begin to wrap around the friction drum, the rope loads will be higher than at the capels as the weight of the rope itself also needs to be supported. Nevertheless, since the ropes have identical properties (including mass per metre) the loads there will be equal. The elastic stretch in each rope will therefore be the same. The total length of rope suspended from the drum to the conveyance is therefore made up of the unstretched or free length plus the elastic stretch. Under constant speed conditions, the loads in the ropes at the drum remain the same for the ideal configuration because friction winders employ 'balance ropes' that compensate for the weight of the hoist ropes that pass over the drum. In this paper, the effects of additional load changes due to normal accelerating and decelerating loads are neglected.

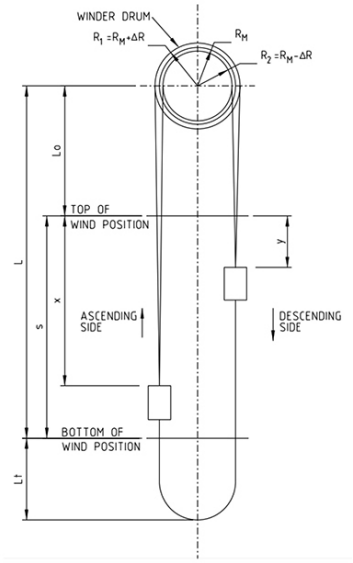

Nomenclature

- x measures the ascending conveyance position with the top of the wind position being the reference location
- y measures the descending conveyance position with the top of the wind position being the reference location
- L_0 is the length of the head ropes from the top of the wind position to the tangent point on the winding drum
- s is the winding depth
- $L = L_0 + s$

Nomenclature continued –

- R_m is the mean radius of all rope grooves on the drum
- R_1 is the radius of the *unloaded* larger rope groove - $R_1 = R_m + \Delta R$
- R_2 is the radius of the *unloaded* smaller rope groove - $R_2 = R_m - \Delta R$
- ΔR is the difference of the larger grope groove radius from the mean radius
- R_1' is the radius of the loaded larger rope groove - $R_1' = R_1 - f_g F_1$
- R_2' is the radius of the loaded smaller rope groove - $R_2' = R_2 - f_g F_2$
- f_g is the radial flexibility of the rope groove liner
- ϵ_1 is the elastic strain in rope 1
- ϵ_2 is the elastic strain in rope 2
- e_1 is the change of elastic stretch in rope 1 due to mismatch of groove radii
- e_2 is the change of elastic stretch in rope 2 due to mismatch of groove radii
- Δe is the difference in the change of elastic stretch - $\Delta e = e_1 - e_2$
- $\Delta \epsilon$ is the difference in the change of elastic strain - $\Delta \epsilon = \epsilon_1 - \epsilon_2$
- φ is the clockwise rotation of the winding drum
- E is the effective elastic modulus of the rope
- A is the cross sectional steel area of the rope
- l is a general length of rope
- F is the load (tension) in a rope
- F_1 is the load in rope 1
- F_2 is the load in rope 2
- F_m is the mean load of ropes 1 & 2
- $F_{1_{max}}$ is the maximum load in rope 1
- $F_{2_{min}}$ is the minimum load in rope 2

Figure 2—Reference dimensions for a friction winder and associated nomenclature

Now consider the lengths of rope 1 and rope 2 as the winder hoists the conveyance up from shaft bottom. For the first turn of the friction drum, groove 1 will pass a greater length of rope to the descending side of the drum than groove 2. On the ascending side of the drum, this will cause the elastic stretch in rope 1 to increase and that in rope 2 to decrease, with the result that the strain (elastic stretch per unit length) in rope 1 will increase and that in rope 2 decrease. For the next turn of the drum, the difference in the rope lengths passed over the drum will be the same but because these ropes now have a different amount of strain, the difference in the effective 'unstrained' lengths of rope passed across the drum reduces from the previous drum turn. And so on for subsequent turns. This poses the question whether groove 2 may eventually pass more unstrained length of rope than groove 1 per turn of the drum. The analysis in the Appendix shows that after reaching about the 1/3rd shaft depth position this difference in unstrained lengths passed becomes negative – in other words the shallower groove passes more 'unstrained' length of rope than the deeper groove, with the result that the difference in stretch now progressively reduces for every further turn of the drum. However, the difference in stretch does not reduce to zero.

The difference in load (tension) between the ropes is proportional to the elastic strain, which is the difference in elastic stretch per unit length of the rope – the rope length varying throughout the wind. The stretch difference increases from zero at the start of the ascending wind, increasing the strain and the load in rope 1 and reducing it in rope 2. These changes in strain are small initially due to the long length of rope, but they become more rapid towards the end of wind when the remaining length of rope approaches its minimum length. Despite the stretch reducing towards the top of the wind, the analysis shows the strain keeps increasing due to the shortening length of the ropes. When the winder reaches the top of wind position the discrepancy in rope load will be greatest. The load in rope 1 will have increased above the mean load to reach a maximum value at the end of wind, and the load in rope 2 will have reduced below the mean to reach a minimum.

Considering the ropes on the descending conveyance, the initial rope loads in ropes 1 and 2 will be the terminating values for the ascending conveyance (assuming that there is no load added or removed from the conveyances and that no slip of the ropes over the drum has occurred). The rope coming across the drum from the ascending side initially has a zero stretch difference, but more rope will be fed into rope 1 than rope 2 due to the difference in groove radii. The difference in strained lengths of rope passed over the drum from the ascending side is zero initially, but progressively reflects the strain differences in the ascending ropes. Compared to the initially short ropes, the effective length of the descending ropes increases rapidly as the conveyance descends. This has the effect of quickly reducing the differences in strain (and hence load) as the ropes grow in length. Again, in the latter part of the wind, the shorter rope groove

(groove 2) passes more unstrained rope than groove 1, which has the effect of reducing the difference in rope stretch and hence in rope load. At the end of the wind the ropes have equal load.

The pattern of rope load *versus* conveyance location in the shaft is thus quite different between the ascending side and the descending side. Using Equation [A5] from the Appendix, this is illustrated in Figure 3, which agrees with the analysis of Hitchin (1958).

In the plot, the load in one of the ropes reduces to almost zero (see Figure 3). The analysis of rope loads is valid only if all loads remain positive (*i.e.* in tension). It is possible, by increasing the groove depth discrepancies, for the rope loads to decrease to zero. This emphasises the need to manage rope loads in practice. Another issue is that the T_1/T_2 tension ratio across the drum may change sufficiently to result in gross rope slip on the drum. While the analysis can be used to predict incipient slip, if slip occurs the analysis will be invalid.

Equations for rope load variation of an *n*-rope friction winder with mismatched groove depths

The loads in the individual ropes of an n-rope friction winder with given defined groove depth differences are developed in the Appendix. For rigid grooves, these equations are:

Ascending side:

$$F_i = F_m + EA\,\frac{n}{(n-1)}\,\frac{\Delta R_i}{R_m}\,\ln\left(\frac{L_0+s}{L_0+x}\right) \qquad [A23]$$

Descending side:

$$F_i = F_m + \frac{n}{(n-1)}EA\,\frac{\Delta R_i}{R_m}\left\{\left(\frac{L_0}{L_0+y}\right)\ln\left(\frac{L_0+s-y}{L_0}\right)+\left(\frac{s-y}{L_0+y}\right)\ln\left(\frac{L_0+s-y}{L_0+s}\right)\right\} \qquad [A24]$$

In these equations, the notation is as given in Figure 2, but in addition, F_i is the load in the 'ith' rope, which has a groove depth disparity of ΔR_i. The maximum and minimum loads in the respective ascending ropes are given by

$$F_{i_{max}} = F_m + \frac{n}{(n-1)}EA\,\frac{\Delta R_i}{R_m}\,\ln\left(\frac{L_0+s}{L_0}\right) \qquad [A25]$$

with the maxima resulting from positive ΔR_i and minima from the negative ΔR_i To keep the maximum rope load due to a rope groove radius discrepancy of ΔR_i as low as possible, L_0, R_m, and n should be made as large as possible where the design allows.

Equation [A25] agrees with the equation quoted in Bar (1976) except that the $\frac{n}{(n-1)}$ term is inverted in Bar. Equations [A23] and [A24] are used with the parameters from the four-rope example discussed by Eithun, Landau, and Mondal (1960)

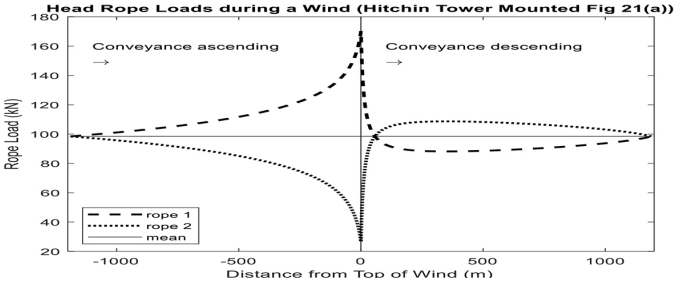

Figure 3—Plot of rope load variation for a tower-mounted winder at the drum, corresponding to Hitchin's (1958) example

to prepare a plot of the rope load variation at the drum (see Figure 4) – the groove depths for ropes 3 and 4 were equal in this example. The plot given in Eithun, Landau, and Mondal is replicated.

Groove depth tolerance criteria

Equation [A25] allows a determination of the maximum allowable rope groove discrepancy. It can be rearranged as follows:

$$\Delta R_i = \left(\frac{F_{i_{max}}}{F_m} - 1\right)\frac{(n-1)}{n}\,\frac{R_m F_m}{EA}\,\frac{1}{\ln\left(\frac{L_0+s}{L_0}\right)} \qquad [1]$$

To restrict the maximum rope load variation to ±10% of the mean rope load, this criterion becomes:

$$\Delta R_i \le 0.1\,\frac{(n-1)}{n}\,\frac{R_m F_m}{EA}\,\frac{1}{\ln\left(\frac{L_0+s}{L_0}\right)} \qquad [2]$$

For illustrative purposes, this equation is applied to an example four-rope tower-mounted cage and counterweight friction winder with the following parameters:

- Cage empty mass M_0 = 13 000 kg
- Cage payload M_p = 10 000 kg
- Winding distance s = 420 m
- L_0 = 12 m
- Mean rope groove radius R_m = 1.3 m
- Head rope diameter d = 30 mm
- Mass per unit length of the head rope ρ_h = 4.0 kg/m
- Rope modulus of elasticity E = 110 GPa
- Rope *steel* area

$$A = 0.5\,d^2 = 0.5 \times (30 \times 10^{-3})^2 = 450 \times 10^{-6}\ m^2$$

[use of 0.5 $\left(\text{not } \frac{\pi}{4}\right)$ accounts for "fill factor"]

For the fully loaded cage, Equation [2] yields $\Delta R_i \le 0.040$ mm. It is immediately apparent that this is a very small deviation and it is almost impractical to machine to this tolerance. If this example winder were ground-mounted with say L_0 = 92 m, then Equation [2] would give $\Delta R_i \le 0.084$ mm.

Analysis of flexible groove linings and mismatched groove depths

The influence of the flexibility of the groove lining material is analysed in the Appendix. To achieve this, a new parameter needs to be introduced. This is the extent to which the groove radius is reduced with an increase in the tension in the rope wrapping around that groove liner. If the change of rope tension,

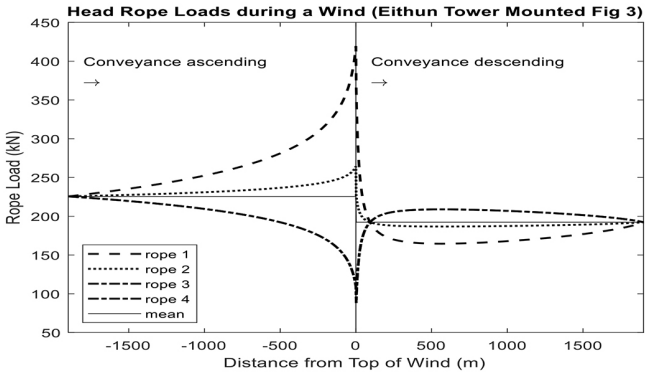

Figure 4—Plot of rope load variation for a tower-mounted winder at the drum, corresponding to the Eithun, Landau, and Mondal (1960) example

ΔT, causes an additional elastic reduction of the groove radius by Δr, then the radial flexibility of the groove lining material, denoted f_g, is given by $f_g = \Delta r / \Delta T$.

The resulting form of the rope load variations during a wind, developed in the Appendix for an n-rope friction winder with flexible groove liners, are given by:

On the ascending side:

$$F_i = F_m + \frac{n}{(n-1)} EA \frac{\Delta R_i}{R_m}\left(\frac{R_m}{f_g AE}\right) \left[1-\left(\frac{(L_0+x)}{(L_0+s)}\right)^{\left(\frac{f_g AE}{R_m}\right)}\right] \quad [A20]$$

On the descending side:

$$F_i = F_m + \frac{n}{(n-1)} EA \frac{\Delta R_i}{R_m}\left(\frac{R_m}{f_g AE}\right) \left\{\left(\frac{L_0}{L_0+s}\right)^{\left(\frac{f_g AE}{R_m}\right)}\left(\frac{L_0}{L_0+y}\right)\left[\left(\frac{L_0+s-y}{L_0}\right)^{\left(\frac{f_g AE}{R_m}\right)}-1\right]\right. \quad [A21]$$
$$\left. + \left(\frac{s-y}{L_0+y}\right)\left[\left(\frac{L_0+s-y}{L_0+s}\right)^{\left(\frac{f_g AE}{R_m}\right)}-1\right]\right\}$$

The maximum and minimum loads in the individual ropes are given by

$$F_{i_{max}} = F_m + \frac{n}{(n-1)} EA \frac{\Delta R_i}{R_m} \left(\frac{R_m}{f_g AE}\right)\left[1-\left(\frac{L_0}{L_0+s}\right)^{\left(\frac{f_g AE}{R_m}\right)}\right] \quad [A22]$$

with the maxima resulting from positive ΔR_i and minima from the negative ΔR_i.

Examining the form of Equation [A22], the term inside the large brackets is a ratio of length parameters similar to the rigid groove case, but for the flexible groove a power term is evident with the power being $\left(\frac{f_g AE}{R_m}\right)$. This can be interpreted as the ratio of the flexibility of the liner material to the flexibility of a piece of hoist rope equal in length to the groove radius.

Assessment of groove liner flexibility

To assess numerically the benefit of flexible groove liners requires a typical value of f_g to be determined. Reverting to the example winder mentioned above, it has a groove liner shown in Figure 5. The figure depicts an elevation of the drum showing the four grooves. A detailed cross-section through one of the grooves on the drum is shown to illustrate how the material is retained in the groove. An isometric view of a segment of liner material is shown, as well as a dimensioned cross-section. The lining is a commercially available material (Becorit K25). This has a modulus of elasticity of 165 MPa and a Poisson's ratio of 0.4.

The rope exerts a pressure on the semicircular boundary of the rope groove. For the equilibrium of the rope wrapping around the drum under tension T, the equivalent line load per unit length of liner, P, exerted by the rope on the groove liner is $P = 2\ T/D$ where D is the drum diameter (*i.e.* the PCD of the rope on the drum). The pressure distribution on the rope groove in the liner is assumed to be a radial pressure varying sinusoidally such that the pressure is maximum at the bottom of the groove. With the angle θ measured from a horizontal axis at the centre of the rope, the pressure is given by $p(\theta) = p_0 \sin\theta$, where p_0 is the maximum pressure attained. Horizontal and vertical components of this pressure distribution may be integrated to calculate the net horizontal and vertical forces. The net horizontal force is zero as expected. The net vertical force per unit length of liner is $\pi\ d\ \frac{p_0}{4}$ where d is the groove diameter. For equilibrium, this must equal the applied line load. Hence p_0, is related to the rope tension by $p_0 = \frac{8\ T}{\pi\left(\frac{D}{d}\right)}$. The specific pressure value used in the analysis is $p_0 = 2.43$ MPa corresponding to a 60 kN/m line load and a head rope tension of 73.4 kN (due to the fully loaded cage).

To determine the deflection of the centre of the rope groove under the rope loading, a 2D finite element analysis has been undertaken using Nastran. The elements are plane strain and the material is hyper-elastic using a Mooney-Rivlin material model. The hyper-elastic modelling solution technique was used as the low modulus value of the groove lining material may lead to large strains. The boundaries of the liner in contact with the steel supports of the drum are treated as fixed except for the bevelled bottom corners, where there is a clearance to the supporting steel. These boundaries are free to deflect.

The deflections for the Becorit liner are shown in an exaggerated plot in Figure 6a. The deflection of the lowest point in the centre of the groove is 0.216 mm. This gives a groove flexibility under rope load of $f_g = \frac{0.216}{73.4} = 0.00294$ mm per kN of rope load.

For a liner modelled in rubber with a modulus of elasticity of 12 MPa and a Poisson's ratio of 0.5, the corresponding deflections are shown in Figure 6b. The deflection of the groove centre is now 0.402 mm. In this case $f_g = \frac{0.402}{73.4} = 0.00548$ mm per kN of rope load.

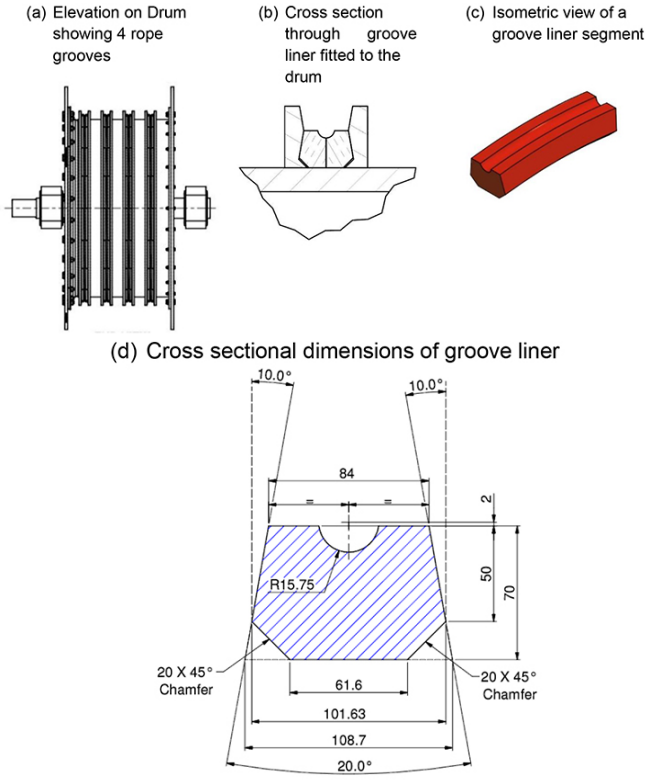

Figure 5—Details of the rope groove liner on the example winder

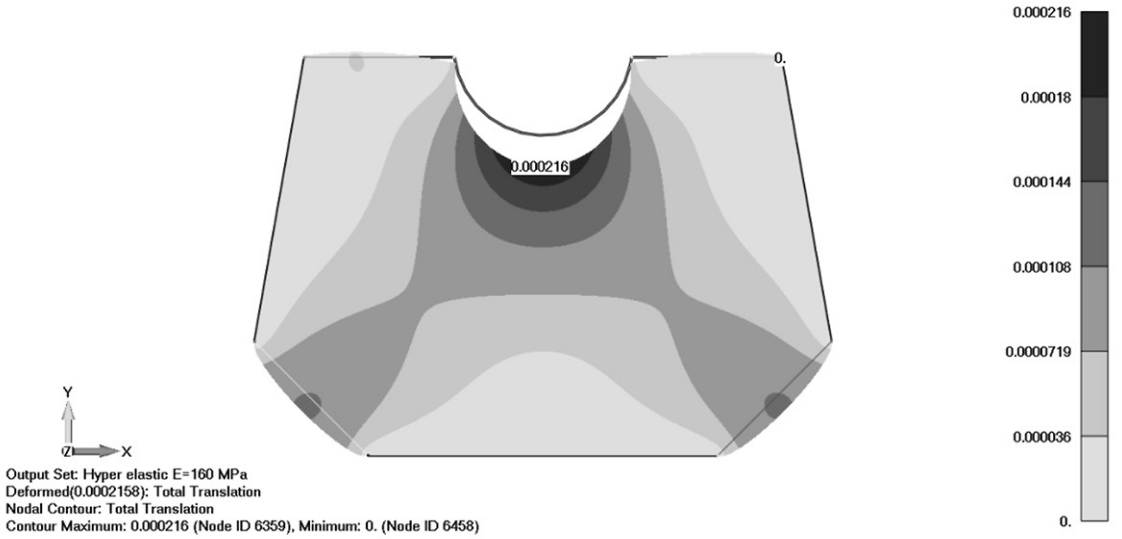

Figure 6a—Plot of the groove liner deflections (exaggerated), Becorit liner

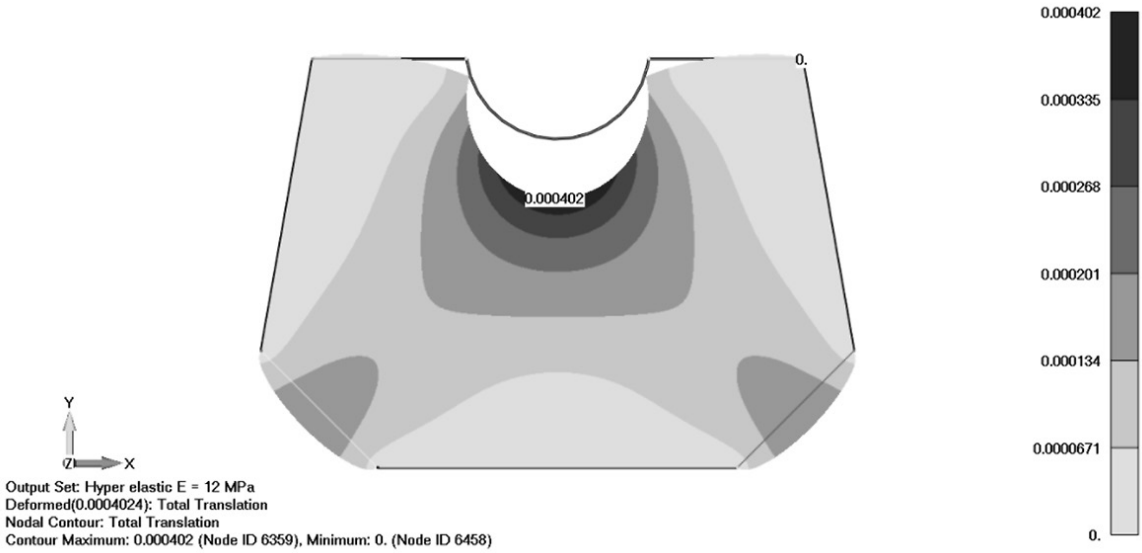

Figure 6b— Plot of the groove liner deflections (exaggerated), rubber liner

Discussion of rope load variation with flexible groove liners and revised groove depth tolerance

Using the value of f_g determined here with the parameters of Hitchin's tower-mounted winder case allows that to be re-assessed with flexible grooves. A plot of the rope load variations with flexible grooves in Becorit material is shown in Figure 7. This plot should be compared with Figure 3 for the rigid groove case. The maximum rope load reduces to 161.6 kN (5% lower) with the flexible grooves. With the liner in rubber, the rope load reduces by 8.8%.

From Equation [A22] the criterion on the allowable rope groove depths for flexible grooves to maintain the rope loads within ±10% of the mean rope load is

$$\Delta R_i \leq 0.1 \frac{(n-1)}{n} f_g F_m \frac{1}{\left[1-\left(\frac{L_0}{L_0+s}\right)^{\left(\frac{f_g AE}{R_m}\right)}\right]} \quad [3]$$

Using the parameters applicable to the example friction winder gives $\Delta R_i \leq 0.052$ mm, which is 23% larger than the value considering the grooves as rigid. This gives some improvement in the tolerable groove discrepancy, making accurate machining easier.

The general improvement in groove depth tolerance with flexible rope groove liners can be demonstrated by ratioing the criteria of Equations [3] and [2]. A graph of $\frac{\Delta R_{flex}}{\Delta R_{rigid}}$ *versus* the

$$\frac{\Delta R_{flex}}{\Delta R_{rigid}} = \frac{f_g AE}{R_m} \frac{\ln\left(\frac{L_0+s}{L_0}\right)}{\left[1-\left(\frac{L_0}{L_0+s}\right)^{\left(\frac{f_g AE}{R_m}\right)}\right]} \quad [4]$$

parameter $\frac{f_g AE}{R_m}$ is shown in Figure 8 for various values of $\frac{(L_0+s)}{L_0}$

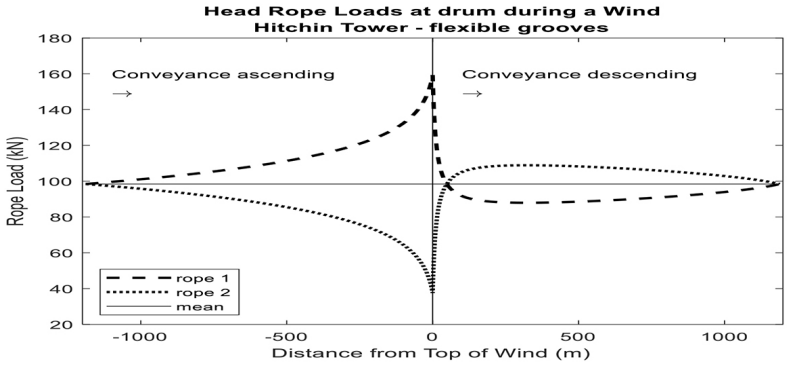

Figure 7—Plots of rope load variation at the drum for a tower-mounted winder with flexible grooves, corresponding to Hitchin's examples (compare with Figure 3)

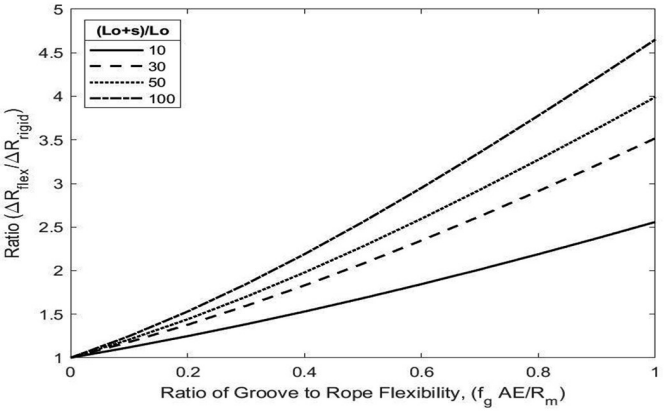

Figure 8—Increase of flexible groove tolerance *versus* rigid groove tolerance

Conclusion

Fundamental relationships for the variation of rope load in the head ropes of multi-rope friction winders have been determined. Both rigid grooves and grooves with flexible liners were considered. From these relationships, criteria that define the allowable tolerance on groove depth mismatch have been developed to maintain the rope load variations within 10% of the mean rope load. Through these criteria the extent to which existing flexible groove materials enhance the load sharing between the ropes has been demonstrated.

The design parameters that affect the severity of load variation with mismatched grooves have been discussed. In summary:

- Existing flexible lining materials can reduce rope load variations for a given groove depth mismatch by about 5%
- Winders with more head ropes provide better load sharing than those with fewer head ropes
- Ground-mounted winders have smaller rope load variations than tower-mounted winders for the same groove depth mismatch.

The basic relationships developed enable questions about the performance of rope load sharing in multi-rope friction winders to be answered. They may be used in various ways:

- To improve winding system performance to enhance rope life
- To improve the design of rope groove flexible liners
- To forensically assess liner wear, and rope and conveyance behaviour problems that may develop if maintenance practice lapses

Acknowledgment

The authors wish to thank Worley and the University of Western Australia for permission to publish this paper.

References

Bar, S. 1976. Control of rope forces in multi-rope winding installations. *The South African Mechanical Engineer*, February. pp 1-12.

Dean, H. 1970. Hoist-rope stress analysis and preventative maintenance for multi-rope friction hoists. *CIM Transactions*, vol. LXXIII. pp. 277–289.

Eithun, E., Landau, F., and Mondal, J. 1960. Load equalisation on multi-rope winders, *The South African Mechanical Engineer*, vol. 10. pp 111–138.

Hitchen, H. 1958. British Wire Ropes Publication 188: Multi-rope friction winders, Paper read to the Sheffield University Mining Society, 25 February. pp 1–35.

Mettler, E. 1956. Uber den Seilkraftausgleich bei Vierseil-forderrungen. Ausschnitt aus Entwicklungsarbeiten der Gutehoffnungshutte Sterkrade AG, Werk Sterkrade. R. Bergbau, H. 21.

Appendix

Analysis of head rope load variations due to rope groove mismatch – flexible rope grooves

The analysis is first applied to a two-rope friction winder with one high and one low rope groove. It is then generalized to an n-rope friction winder with one high groove and all the others equal. It is further generalized by allowing every groove a unique groove depth. The nomenclature used has been given in Figure 2. The development of the groove flexibility parameter f_g is discussed in the main text.

Development of rope load variation for a two-rope friction winder with flexible rope groove liners

Ascending conveyance

Consider the winder drum in the general position with the left-hand conveyance being hoisted up x distant from the top of the wind. Consider the difference in the lengths of ropes 1 and 2 passed over the drum during an increment of drum rotation by $d\varphi$.

Difference in the unstrained lengths = Difference in the increment of the loaded drum groove circumference minus the difference in the strained lengths

But the strained lengths of ropes 1 and 2 after the increment remain equal (both rope ends being attached at one end to the conveyance and at the other end to the drum). The difference in lengths 'reports' as a difference in the rope stretch between the two head ropes.

Therefore, the following equation can be written:

$$de_1 - de_2 = (R'_1 d\varphi - R'_2 d\varphi) - [\epsilon_1 R'_1 d\varphi - \epsilon_2 R'_2 d\varphi]$$

$$de_1 - de_2 = (R_m + \Delta R - f_g F_1)\, d\varphi - (R_m - \Delta R - f_g F_2) d\varphi - [\epsilon_1 (R_m + \Delta R - f_g F_1) d\varphi - \epsilon_2 (R_m - \Delta R - f_g F_2) d\varphi]$$

$$de_1 - de_2 = 2\Delta R d\varphi - f_g AE(\epsilon_1 - \epsilon_2)\, d\varphi - [\epsilon_1 (R_m + \Delta R) - \epsilon_2 (R_m - \Delta R) - f_g AE(\epsilon_1^{\,2} - \epsilon_2^{\,2})] d\varphi$$

$$de_1 - de_2 = 2\Delta R d\varphi - \Delta\epsilon (R_m + f_g AE) d\varphi - (\Delta R - f_g AE(\epsilon_1 - \epsilon_2))[\epsilon_1 + \epsilon_2] d\varphi$$

Now note that $d\varphi = -\frac{dx}{R_m}$ as x reduces as φ increases, hence the negative sign.

Neglecting products of small quantities such as $\frac{\Delta R}{R_m} \times \epsilon_1$ *etc.* and noting that $\Delta\epsilon = \frac{\Delta e}{(L_0 + x)}$, the above equation becomes

$$\frac{d(\Delta e)}{dx} - \frac{\Delta e \left(1 + \frac{f_g AE}{R_m}\right)}{(L_0 + x)} = -2\frac{\Delta R}{R_m} \qquad [A1]$$

Solve this first-order ordinary differential equation by the 'Integrating Factor' method, noting that at the starting point of the upward wind, the difference in rope stretch (and hence the rope loads) is zero. *i.e.* when $x = s$, $\Delta e = 0$. Hence

$$\Delta e = 2\frac{\Delta R}{R_m}\left(\frac{R_m}{f_g AE}\right)(L_0 + x)\left[1 - \left(\frac{(L_0 + x)}{(L_0 + s)}\right)^{\left(\frac{f_g AE}{R_m}\right)}\right] \qquad [A2]$$

Note that when $x = 0$, at the end of the upward wind,

$$\Delta e = 2\frac{\Delta R}{R_m}\left(\frac{R_m}{f_g AE}\right) L_0\left[1 - \left(\frac{L_0}{L_0 + s}\right)^{\left(\frac{f_g AE}{R_m}\right)}\right] \qquad [A2']$$

Now as this is a two-rope friction winder, $\Delta e = e_1 - e_2$, and because the combined rope load always equals the weight of the ropes and conveyance attached, $e_1 + e_2 = 0$. Hence, $e_1 = \frac{\Delta e}{2}$ and $e_2 = \frac{\Delta e}{2}$. Rope stretch e and rope load F are related by the rope stiffness, which is given by $\frac{E\,A}{l}$ where E is the modulus of rope elasticity, A is the cross-sectional steel area of the rope, and l is its length $F = \frac{E\,A}{l} e$. Hence the loads in rope 1 and rope 2 can be written (with the plus sign for F_1 and the negative sign for F_2)

$$F_1, F_2 = F_m \pm EA\frac{\Delta R}{R_m}\left(\frac{R_m}{f_g AE}\right)\left[1 - \left(\frac{(L_0 + x)}{(L_0 + s)}\right)^{\left(\frac{f_g AE}{R_m}\right)}\right] \qquad [A3]$$

The maximum force in rope 1 and the minimum force in rope 2 are given by

$$F_{1_{max}}, F_{2_{min}} = F_m \pm EA\frac{\Delta R}{R_m}\left(\frac{R_m}{f_g AE}\right)\left[1 - \left(\frac{L_0}{L_0 + s}\right)^{\left(\frac{f_g AE}{R_m}\right)}\right] \qquad [A4]$$

with the selection of the appropriate sign.

The relationship for rigid grooves is obtained from Equation [A3] by allowing the flexibility to tend to zero and using the limit $\lim_{h\to 0}\left(\frac{a^h - 1}{h}\right) = \ln a$. Hence

$$F_1, F_2 = F_m \pm EA\frac{\Delta R}{R_m}\ln\left(\frac{L_0 + s}{L_0 + x}\right) \qquad [A5]$$

with

$$F_{1_{max}}, F_{2_{min}} = F_m \pm EA\frac{\Delta R}{R_m}\ln\left(\frac{L_0 + s}{L_0}\right) \qquad [A6]$$

Descending conveyance

Now consider the descending side for the conveyance on the right-hand side in Figure 2. The starting loads in the head ropes 1 and 2 will be the ending loads of the previous upward wind and will be given by the relationships in Equation [A6] for F_1 and the corresponding equation for F_2. Also, if y is measured down the ropes from the same reference position, y and φ will increase together. The ropes that are fed from the ascending conveyance into the initially short lengths of rope on the descending conveyance will start with same difference in their elastic stretch as at the termination of the ascending wind. This will change progressively, as has been calculated for the upcoming conveyance. The basic equation for the difference in the lengths of ropes 1 and 2 passed over the drum during an increment of drum rotation by φ remains the same.

Difference in the unstrained lengths = Difference in the increment of the loaded drum groove circumference minus the difference in the strained lengths

$$-(de_1 - de_2) = 2\Delta R d\varphi - \Delta\epsilon(R_m + f_g AE) d\varphi - (\Delta R - f_g AE(\epsilon_1 - \epsilon_2))[\epsilon_1 + \epsilon_2] d\varphi$$

except recognizing now that an increase in length passed through by rope 1 has the effect of reducing the existing difference in elastic stretch, and hence the sign on the left-hand side of the equation above is negative. Also, $d\varphi = \frac{dy}{R_m}$, so using $\Delta\epsilon = \frac{\Delta e}{(L_0 + x)}$ and the solution for $\Delta e(x)$, which has been determined in Equation [A2], the incremental change in the difference of rope elastic stretch becomes

$$-d(\Delta e) = 2\frac{\Delta R}{R_m} dy - \Delta\epsilon\left(1 + \frac{f_g AE}{R_m}\right) dy - \left(\frac{\Delta R}{R_m} - \frac{f_g AE}{R_m}(\epsilon_1 - \epsilon_2)\right)[\epsilon_1 + \epsilon_2] dy$$

Neglecting products of small quantities such as $\frac{\Delta R}{R_m} \times \epsilon_1$, *etc.* and noting that $\Delta\epsilon = \frac{\Delta e}{(L_0 + x)}$ the above equation becomes

$$-\frac{d(\Delta e)}{dy} = 2\frac{\Delta R}{R_m} - 2\frac{\Delta R}{R_m}\frac{R_m}{f_g AE}\left[1 - \left(\frac{(L_0 + x)}{(L_0 + s)}\right)^{\left(\frac{f_g AE}{R_m}\right)}\right]$$

x and y are related through $s = x + y$. After substituting for x, the above equation may be integrated (using the condition for Δe when $y = 0$ given by Equation [A2']:

$$\frac{\Delta e}{2\Delta R} = \frac{(L_0 + s)}{f_g AE}\left[\left(\frac{L_0 + s - y}{L_0 + s}\right)^{\left(\frac{f_g AE}{R_m}\right)+1} - \left(\frac{L_0}{L_0 + s}\right)^{\left(\frac{f_g AE}{R_m}\right)+1}\right] - \frac{(s - y)}{f_g AE} \qquad [A7]$$

This gives $\Delta e = 0$ when $y = s$, which is the expected equality of rope loads at the bottom end of the wind.

Proceeding as before, the rope load in rope 1 and rope 2 can now be written as

$$F_1, F_2 = F_m \pm \frac{\Delta R}{f_g}\left\{\left(\frac{L_0}{L_0+y}\right)\left(\frac{L_0}{L_0+s}\right)^{\left(\frac{f_gAE}{R_m}\right)}\left[\left(\frac{L_0+s-y}{L_0}\right)^{\left(\frac{f_gAE}{R_m}\right)+1}-1\right]-\frac{(s-y)}{(L_0+y)}\right\}$$

This equation can be rearranged as follows:

$$F_1, F_2 = F_m \pm \frac{EA\Delta R}{R_m}\left(\frac{R_m}{f_gAE}\right)\left\{\left(\frac{L_0}{L_0+s}\right)^{\left(\frac{f_gAE}{R_m}\right)}\left(\frac{L_0}{L_0+y}\right)\left[\left(\frac{L_0+s-y}{L_0}\right)^{\left(\frac{f_gAE}{R_m}\right)}-1\right]+\left(\frac{s-y}{L_0+y}\right)\left[\left(\frac{L_0+s-y}{L_0+s}\right)^{\left(\frac{f_gAE}{R_m}\right)}-1\right]\right\} \quad [A8]$$

The maximum and minimum rope loads are as in Equation [A4].

As before, allowing the flexibility parameter to tend to zero produces the relationship for rigid grooves.

$$F_1, F_2 = F_m \pm EA\frac{\Delta R}{R_m}\left\{\frac{L_0}{(L_0+y)}\ln\left(\frac{L_0+s-y}{L_0}\right)+\frac{(s-y)}{(L_0+y)}\ln\left(\frac{L_0+s-y}{L_0+s}\right)\right\} \quad [A9]$$

Generalization of rope load variation for an n-rope friction winder with flexible rope groove liners

Now consider a multi-rope friction winder with n ropes. Initially it is assumed that rope 1 groove is larger than all the others, which have the same radius. The following nomenclature is added to the previous list.

Nomenclature

- n the number of head ropes used on the friction winder
- R_0 the radius of all the grooves which are not disturbed
- e_0 is the change of elastic stretch in a rope (o) in an undisturbed rope groove
- ε_0 is the elastic strain in a rope (o) running in an undisturbed rope groove
- $\Delta e'$ is the difference in the change of elastic stretch. $\Delta e' = e_1 - e_0$
- $\Delta\varepsilon'$ is the difference in the change of elastic strain. $\Delta\varepsilon' = \varepsilon_1 - \varepsilon_0$
- F_0 is the load in any rope running in an undisturbed groove
- F_m is the mean load of all the ropes
- $F_{0_{min}}$ is the minimum load in the ropes running in an undisturbed groove

The radius of rope groove 1 exceeds the mean radius by an amount ΔR so that $R_1 = R_m + \Delta R$

The other groove radii have a radius R_0, which is given by $R_0 = R_m - \frac{\Delta R}{(n-1)}$

Consideration will be given now to the difference in rope stretch that develops between rope 1 and any one of the other ropes.

$$\Delta e' = e_1 - e_o$$

Ascending conveyance – one oversize groove

Consider again the incremental movement of the winder drum and the ascending conveyance.

$$de_1 - de_o = (R_1'd\varphi - R_o'd\varphi) - [\epsilon_1 R_1'd\varphi - \epsilon_0 R_0'd\varphi]$$

$$de_1 - de_o = \left(R_m + \Delta R - f_gF_1\right)d\varphi - \left(R_m - \frac{\Delta R}{(n-1)} - f_gF_0\right)d\varphi - \left[\epsilon_1(R_m + \Delta R - f_gF_1)d\varphi - \epsilon_0\left(R_m - \frac{\Delta R}{(n-1)} - f_gF_0\right)d\varphi\right]$$

$$de_1 - de_o = \frac{n}{(n-1)}\Delta R d\varphi - (\epsilon_1 - \epsilon_0)\left(R_m + f_gAE\right)d\varphi - \left(\epsilon_1 - \frac{\epsilon_0}{(n-1)}\right)\Delta R d\varphi + f_gAE(\epsilon_1+\epsilon_0)(\epsilon_1-\epsilon_0)$$

Now note that $d\varphi = -\frac{dx}{R_m}$; as x reduces as φ increases, hence the negative sign. Neglecting products of small quantities such as $\frac{\Delta R}{R_m}\times\epsilon_1$, *etc.*, the difference in stretch can be written

$$d(\Delta e') = -\frac{n}{(n-1)}\frac{\Delta R}{R_m}dx + \Delta\epsilon' dx + \frac{\Delta R}{R_m}\left[\epsilon_1 + \frac{\epsilon_0}{(n-1)}\right]dx$$

and noting that $\Delta\epsilon' = \frac{\Delta e'}{(L_0+x)}$ the above equation becomes

$$\frac{d(\Delta e')}{dx} - \frac{\Delta e'\left(1+\frac{f_gAE}{R_m}\right)}{(L_0+x)} = -\frac{n}{(n-1)}\frac{\Delta R}{R_m} \quad [A10]$$

and this first-order equation can be solved as before, yielding

$$\Delta e' = \frac{n}{(n-1)}\frac{\Delta R}{R_m}\left(\frac{R_m}{f_gAE}\right)(L_0+x)\left[1-\left(\frac{(L_0+x)}{(L_0+s)}\right)^{\left(\frac{f_gAE}{R_m}\right)}\right] \quad [A11]$$

To obtain the relationship for rope stretch and rope loads, the requirement (from equilibrium of forces) is that $e_1 + (n-1)e_0 = 0$, hence $e_0 = -\frac{e_1}{(n-1)}$ and so $\Delta e' = e_1 - e_o = \frac{n}{(n-1)}e_1 = -(n-1)\,e_0 - e_o = -n\,e_o$. Hence

$$e_1 = \frac{\Delta R}{R_m}\left(\frac{R_m}{f_gAE}\right)(L_0+x)\left[1-\left(\frac{(L_0+x)}{(L_0+s)}\right)^{\left(\frac{f_gAE}{R_m}\right)}\right] \quad [A12]$$

$$e_o = -\frac{1}{(n-1)}\frac{\Delta R}{R_m}\left(\frac{R_m}{f_gAE}\right)(L_0+x)\left[1-\left(\frac{(L_0+x)}{(L_0+s)}\right)^{\left(\frac{f_gAE}{R_m}\right)}\right] \quad [A13]$$

Proceeding as before from these differences in rope stretch, the load in rope 1 can be written

$$F_1 = F_m + EA\frac{\Delta R}{R_m}\left(\frac{R_m}{f_gAE}\right)\left[1-\left(\frac{L_0+x}{L_0+s}\right)^{\left(\frac{f_gAE}{R_m}\right)}\right] \quad [A14]$$

and the maximum force in rope 1 is given by

$$F_{1_{max}} = F_m + EA\frac{\Delta R}{R_m}\left(\frac{R_m}{f_gAE}\right)\left[1-\left(\frac{L_0}{L_0+s}\right)^{\left(\frac{f_gAE}{R_m}\right)}\right] \quad [A15]$$

Similarly, the load in all the other ropes (rope o) can be written

$$F_o = F_m - \frac{1}{(n-1)}EA\frac{\Delta R}{R_m}\left(\frac{R_m}{f_gAE}\right)\left[1-\left(\frac{L_0+x}{L_0+s}\right)^{\left(\frac{f_gAE}{R_m}\right)}\right] \quad [A16]$$

and the minimum load in the other ropes can be written

$$F_{o_{min}} = F_m - \frac{1}{(n-1)}EA\frac{\Delta R}{R_m}\left(\frac{R_m}{f_gAE}\right)\left[1-\left(\frac{L_0}{L_0+s}\right)^{\left(\frac{f_gAE}{R_m}\right)}\right] \quad [A17]$$

Descending conveyance – one oversize groove

For the descending side, the analysis proceeds in a similar manner to that done previously, yielding

$$F_1 = F_m + EA\frac{\Delta R}{R_m}\left(\frac{R_m}{f_g AE}\right)\left\{\left(\frac{L_0}{L_0+s}\right)^{\left(\frac{f_g AE}{R_m}\right)}\left(\frac{L_0}{L_0+y}\right)\left[\left(\frac{L_0+s-y}{L_0}\right)^{\left(\frac{f_g AE}{R_m}\right)}-1\right]+\left(\frac{s-y}{L_0+y}\right)\left[\left(\frac{L_0+s-y}{L_0+s}\right)^{\left(\frac{f_g AE}{R_m}\right)}-1\right]\right\} \quad [A18]$$

$$F_o = F_m - \frac{1}{(n-1)}EA\frac{\Delta R}{R_m}\left(\frac{R_m}{f_g AE}\right)\left\{\left(\frac{L_0}{L_0+s}\right)^{\left(\frac{f_g AE}{R_m}\right)}\left(\frac{L_0}{L_0+y}\right)\left[\left(\frac{L_0+s-y}{L_0}\right)^{\left(\frac{f_g AE}{R_m}\right)}-1\right]+\left(\frac{s-y}{L_0+y}\right)\left[\left(\frac{L_0+s-y}{L_0+s}\right)^{\left(\frac{f_g AE}{R_m}\right)}-1\right]\right\} \quad [A19]$$

The maximum and minimum rope loads occur on the ascending side and are given by Equations [A15] and [A17].

Application to n-rope friction winder with discrepancies on all grooves

The above relationships for an *n*-rope friction winder can be used to plot the rope load variations for both the ascending side and the descending side. They apply to a drum which has all grooves equal except for groove 1, which is over-size.

Initially, the above equations do not appear to be helpful to the general situation where each groove may have its own unique size. However, it can be recognized that the rope load variations are self-similar and scale linearly with the value of ΔR. Hence, contrary to first impressions, it is indeed possible to use the above relationships to determine the rope load variation for the rope in each groove of an *n*-rope friction winder. For the general situation, the groove depth variations from the mean radius R_m will be denoted ΔR_1, ΔR_2, ... ΔR_i, ... ,ΔR_n. The actual groove radius of groove *i* is written

$$R_i = R_m + \Delta R_i$$

and the condition that the mean radius is R_m requires

$$\sum_{i=1}^{n}\Delta R_i = 0$$

As the sum of the deviations from the mean is zero, some of the ΔR_i will be positive, and others will be negative. To obtain the unique loads in each rope which arise from the deviation of every groove from the mean, the loads from the equations above for each deviation acting alone are added up. The load arising in rope *i* from the deviation of groove rope *i* is offset by the loads arising in rope *i* from the other grooves, *j*, for $j = 1, n$ *with* $j \neq i$ as follows:

For the ascending side:

$$F_i = F_m + \frac{EA}{R_m}\left(\frac{R_m}{f_g AE}\right)\left\{\Delta R_i - \frac{1}{(n-1)}\sum_{j=1,j\neq i}^{n}\Delta R_j\right\}\left[1-\left(\frac{(L_0+x)}{(L_0+s)}\right)^{\left(\frac{f_g AE}{R_m}\right)}\right]$$

and for the descending side:

$$F_i = F_m + \frac{EA}{R_m}\left(\frac{R_m}{f_g AE}\right)\left\{\Delta R_i - \frac{1}{(n-1)}\sum_{j=1,j\neq i}^{n}\Delta R_j\right\}\left\{\left(\frac{L_0}{L_0+s}\right)^{\left(\frac{f_g AE}{R_m}\right)}\left(\frac{L_0}{L_0+y}\right)\left[\left(\frac{L_0+s-y}{L_0}\right)^{\left(\frac{f_g AE}{R_m}\right)}-1\right]+\left(\frac{s-y}{L_0+y}\right)\left[\left(\frac{L_0+s-y}{L_0+s}\right)^{\left(\frac{f_g AE}{R_m}\right)}-1\right]\right\}$$

Now it can be noticed that the term in brackets involving the groove errors can be expressed alternatively as

$$\left\{\Delta R_i - \frac{1}{(n-1)}\sum_{j=1,j\neq i}^{n}\Delta R_j\right\} = \left\{\Delta R_i + \frac{1}{(n-1)}\Delta R_i - \frac{1}{(n-1)}\sum_{j=1}^{n}\Delta R_j\right\} = \frac{n}{(n-1)}\Delta R_i$$

This allows some simplification of the loads as follows:

Ascending side:

$$F_i = F_m + \frac{n}{(n-1)}EA\frac{\Delta R_i}{R_m}\left(\frac{R_m}{f_g AE}\right)\left[1-\left(\frac{(L_0+x)}{(L_0+s)}\right)^{\left(\frac{f_g AE}{R_m}\right)}\right] \quad [A20]$$

Descending side:

$$F_i = F_m + \frac{n}{(n-1)}EA\frac{\Delta R_i}{R_m}\left(\frac{R_m}{f_g AE}\right)\left\{\left(\frac{L_0}{L_0+s}\right)^{\left(\frac{f_g AE}{R_m}\right)}\left(\frac{L_0}{L_0+y}\right)\left[\left(\frac{L_0+s-y}{L_0}\right)^{\left(\frac{f_g AE}{R_m}\right)}-1\right]+\left(\frac{s-y}{L_0+y}\right)\left[\left(\frac{L_0+s-y}{L_0+s}\right)^{\left(\frac{f_g AE}{R_m}\right)}-1\right]\right\} \quad [A21]$$

The maximum and minimum loads in the respective ropes are given by

$$F_{i_{max}} = F_m + \frac{n}{(n-1)}EA\frac{\Delta R_i}{R_m}\left(\frac{R_m}{f_g AE}\right)\left[1-\left(\frac{L_0}{L_0+s}\right)^{\left(\frac{f_g AE}{R_m}\right)}\right] \quad [A22]$$

with the maxima resulting from positive ΔR_i and minima from the negative ΔR_i.

As before, allowing the flexibility parameter to tend to zero produces the relationship for rigid grooves.

On the ascending side:

$$F_i = F_m + EA\frac{n}{(n-1)}\frac{\Delta R_i}{R_m}\ln\left(\frac{L_0+s}{L_0+x}\right) \quad [A23]$$

On the descending side:

$$F_i = F_m + EA\frac{n}{(n-1)}\frac{\Delta R_i}{R_m}\left\{\left(\frac{L_0}{L_0+y}\right)\ln\left(\frac{L_0+s-y}{L_0}\right)+\left(\frac{s-y}{L_0+y}\right)\ln\left(\frac{L_0+s-y}{L_0+s}\right)\right\} \quad [A24]$$

The maximum and minimum loads in the respective ropes are given by

$$F_{i_{max}} = F_m + EA\frac{n}{(n-1)}\frac{\Delta R_i}{R_m}\ln\left(\frac{L_0+s}{L_0}\right) \quad [A25]$$

with the maxima resulting from positive ΔR_i and minima from the negative ΔR_i. ◆

NATIONAL & INTERNATIONAL ACTIVITIES

2021

18–19 October 2021 — **Southern African Rare Earths International Online Conference 2021**
Contact: Camielah Jardine
Tel: +27 11 834-1273/7, Fax: +27 11 838-5923/833-8156
E-mail: camielah@saimm.co.za, Website: http://www.saimm.co.za

25–29 October 2021 — **SAMCODES Online Conference 2021**
'*Good Practice and Lessons Learnt*'
Contact: Gugu Charlie
Tel: +27 11 834-1273/7, Fax: +27 11 838-5923/833-8156
E-mail: gugu@saimm.co.za, Website: http://www.saimm.co.za

11 November 2021 — **17TH Annual Online Student Colloquium 2021**
Contact: Gugu Charlie
Tel: +27 11 834-1273/7, Fax: +27 11 838-5923/833-8156
E-mail: gugu@saimm.co.za, Website: http://www.saimm.co.za

15, 17, 19, 22, 24, 26 November 2021 — **Global Tailings Standards and Opportunities Online Conference 2021**
'*For the Mine of the Future*'
Contact: Gugu Charlie
Tel: +27 11 834-1273/7, Fax: +27 11 838-5923/833-8156
E-mail: gugu@saimm.co.za, Website: http://www.saimm.co.za

2022

23–24 February 2022 — **Drill and Blast Hybrid Workshop 2022**
Contact: Camielah Jardine
Tel: +27 11 834-1273/7, Fax: +27 11 838-5923/833-8156
E-mail: camielah@saimm.co.za, Website: http://www.saimm.co.za

February 27–March 3, 2022 — **TMS Furnace Tapping 2022**
Anaheim Convention Center & Anaheim Marriott , Anaheim, California, USA
https://www.tms.org/AnnualMeeting/TMS2022/Programming/Furnace_Tapping_2022/AnnualMeeting/TMS2022/Programming/furnaceTapping.aspx?hkey=718f6af7-1852-445c-be82-596102913416

16–19 May 2022 — **8th Sulphur and Sulphuric Acid Conference 2022**
The Vineyard Hotel, Newlands, Cape Town, South Africa
Contact: Camielah Jardine
Tel: +27 11 834-1273/7, Fax: +27 11 838-5923/833-8156
E-mail: camielah@saimm.co.za, Website: http://www.saimm.co.za

20–27 May 2022 — **ALTA 2022 Hybrid Conference 2022**
Perth, Australia, Tel: +61 8 9389 1488
E-mail: alta@encanta.com.au, Website: www.encanta.com.au

14–16 June 2022 — **Water | Managing for the Future**
Vancouver, BC, Canada, https://www.mineconferences.com

14–16 June 2022 — **Copper Cobalt Africa** *In Association with* **The 10th Southern African Base Metals Conference**
Avani Victoria Falls Resort, Livingstone, Zambia
Contact: Camielah Jardine
Tel: +27 11 834-1273/7, Fax: +27 11 838-5923/833-8156
E-mail: camielah@saimm.co.za, Website: http://www.saimm.co.za

9–13 July 2022 — **Sustainable Development in the Minerals Industry (SDIMI) 2022 10th International Hybrid Conference**
Swakopmund Hotel and Entertainment Centre, Swakopmund, Namibia
Contact: Gugu Charlie
Tel: +27 11 834-1273/7, Fax: +27 11 838-5923/833-8156
E-mail: gugu@saimm.co.za, Website: http://www.saimm.co.za

21–25 August 2022 — **XXXI International Mineral Processing Congress 2022**
Melbourne, Australia + Online, www.impc2022.com

24–25 August 2022 — **Battery Materials Conference 2022**
Misty Hills Conference Venue, Muldersdrift, Johannesburg, South Africa
Contact: Camielah Jardine
Tel: +27 11 834-1273/7, Fax: +27 11 838-5923/833-8156
E-mail: camielah@saimm.co.za, Website: http://www.saimm.co.za

8–14 September 2022 — **32nd SOMP Annual Meeting and Conference 2022**
Windhoek Country Club & Resort, Windhoed, Namibia
Contact: Camielah Jardine
Tel: +27 11 834-1273/7, Fax: +27 11 838-5923/833-8156
E-mail: camielah@saimm.co.za, Website: http://www.saimm.co.za

28–30 September 2022 — **PGM The 8th International Conference 2022**
Sun City, Rustenburg, South Africa
Contact: Camielah Jardine
Tel: +27 11 834-1273/7, Fax: +27 11 838-5923/833-8156
E-mail: camielah@saimm.co.za, Website: http://www.saimm.co.za

28–29 September 2022 — **Thermodynamic from Nanoscale to Operational Scale (THANOS) International Hybrid Conference 2022**
on Enhanced use of Thermodynamic Data in Pyrometallurgy Teaching and Research
Mintek, Randburg, South Africa
Contact: Camielah Jardine
Tel: +27 11 834-1273/7, Fax: +27 11 838-5923/833-8156
E-mail: camielah@saimm.co.za, Website: http://www.saimm.co.za

Company affiliates

The following organizations have been admitted to the Institute as Company Affiliates

3M South Africa (Pty) Limited
AECOM SA (Pty) Ltd
AEL Mining Services Limited
African Pegmatite (Pty) Ltd
Air Liquide (PTY) Ltd
Alexander Proudfoot Africa (Pty) Ltd
AMEC Foster Wheeler
AMIRA International Africa (Pty) Ltd
ANDRITZ Delkor (Pty) Ltd
Anlgo Operations Proprietary Limited
Anglogold Ashanti Ltd
Arcus Gibb (Pty) Ltd
ASPASA
Aurecon South Africa (Pty) Ltd
Aveng Engineering
Aveng Mining Shafts and Underground
Axiom Chemlab Supplies (Pty) Ltd
Axis House (Pty) Ltd
Bafokeng Rasimone Platinum Mine
Barloworld Equipment -Mining
BASF Holdings SA (Pty) Ltd
BCL Limited
Becker Mining (Pty) Ltd
BedRock Mining Support (Pty) Ltd
BHP Billiton Energy Coal SA Ltd
Blue Cube Systems (Pty) Ltd
Bluhm Burton Engineering (Pty) Ltd
Bond Equipment (Pty) Ltd
Bouygues Travaux Publics
Castle Lead Works
CDM Group
CGG Services SA
Coalmin Process Technologies CC
Concor Opencast Mining
Concor Technicrete
Council for Geoscience Library
CRONIMET Mining Processing SA (Pty) Ltd
CSIR Natural Resources and the Environment (NRE)
Data Mine SA
Digby Wells and Associates
DRA Mineral Projects (Pty) Ltd
DTP Mining - Bouygues Construction
Duraset
Elbroc Mining Products (Pty) Ltd
eThekwini Municipality
Ex Mente Technologies (Pty) Ltd
Expectra 2004 (Pty) Ltd
Exxaro Coal (Pty) Ltd
Exxaro Resources Limited
Filtaquip (Pty) Ltd
FLSmidth Minerals (Pty) Ltd
Fluor Daniel SA (Pty) Ltd
Franki Africa (Pty) Ltd-JHB
Fraser Alexander (Pty) Ltd
G H H Mining Machines (Pty) Ltd
Geobrugg Southern Africa (Pty) Ltd
Glencore
Gravitas Minerals (Pty) Ltd
Hall Core Drilling (Pty) Ltd
Hatch (Pty) Ltd
Herrenknecht AG
HPE Hydro Power Equipment (Pty) Ltd
Immersive Technologies
IMS Engineering (Pty) Ltd
Ingwenya Mineral Processing (Pty) Ltd
Ivanhoe Mines SA
Joy Global Inc.(Africa)
Kudumane Manganese Resources
Leica Geosystems (Pty) Ltd
Longyear South Africa (Pty) Ltd
Lull Storm Trading (Pty) Ltd
Maccaferri SA (Pty) Ltd
Magnetech (Pty) Ltd
MAGOTTEAUX (Pty) Ltd
Malvern Panalytical (Pty) Ltd
Maptek (Pty) Ltd
Maxam Dantex (Pty) Ltd
MBE Minerals SA Pty Ltd
MCC Contracts (Pty) Ltd
MD Mineral Technologies SA (Pty) Ltd
MDM Technical Africa (Pty) Ltd
Metalock Engineering RSA (Pty)Ltd
Metorex Limited
Metso Minerals (South Africa) Pty Ltd
Micromine Africa (Pty) Ltd
MineARC South Africa (Pty) Ltd
Minerals Council of South Africa
Minerals Operations Executive (Pty) Ltd
MineRP Holding (Pty) Ltd
Mining Projections Concepts
Mintek
MIP Process Technologies (Pty) Limited
MLB Investment CC
Modular Mining Systems Africa (Pty) Ltd
MSA Group (Pty) Ltd
Multotec (Pty) Ltd
Murray and Roberts Cementation
Nalco Africa (Pty) Ltd
Namakwa Sands(Pty) Ltd
Ncamiso Trading (Pty) Ltd
New Concept Mining (Pty) Limited
Northam Platinum Ltd - Zondereinde
Opermin Operational Excellence
OPTRON (Pty) Ltd
Paterson & Cooke Consulting Engineers (Pty) Ltd
Perkinelmer
Polysius A Division Of Thyssenkrupp Industrial Sol
Precious Metals Refiners
Rams Mining Technologies
Rand Refinery Limited
Redpath Mining (South Africa) (Pty) Ltd
Rocbolt Technologies
Rosond (Pty) Ltd
Royal Bafokeng Platinum
Roytec Global (Pty) Ltd
RungePincockMinarco Limited
Rustenburg Platinum Mines Limited
Salene Mining (Pty) Ltd
Sandvik Mining and Construction Delmas (Pty) Ltd
Sandvik Mining and Construction RSA(Pty) Ltd
SANIRE
Schauenburg (Pty) Ltd
Sebilo Resources (Pty) Ltd
SENET (Pty) Ltd
Senmin International (Pty) Ltd
SISA Inspection (Pty) Ltd
Smec South Africa
Sound Mining Solution (Pty) Ltd
SRK Consulting SA (Pty) Ltd
Time Mining and Processing (Pty) Ltd
Timrite (Pty) Ltd
Tomra (Pty) Ltd
Traka Africa (Pty) Ltd
Ukwazi Mining Solutions (Pty) Ltd
Umgeni Water
Webber Wentzel
Weir Minerals Africa
Welding Alloys South Africa
Worley

BM
BASE METALS
2022

COPPER COBALT AFRICA

IN ASSOCIATION WITH THE 10TH SOUTHERN AFRICAN BASE METALS CONFERENCE

14–16 JUNE 2022
AVANI VICTORIA FALLS RESORT,
LIVINGSTONE, ZAMBIA

SAIMM is proud to host the Third Copper Cobalt Africa Conference.

To be held in Livingstone, Zambia, this anticipated and prestigious event provides a unique forum for discussion, sharing of experience and knowledge, and networking for all those interested in the processing of copper and cobalt in an African context, in one of the world's most spectacular settings - the Victoria Falls.

The African Copper Belt has experienced a period of significant difficulties since the last conference, held in 2018. Owing to a global slowdown in commodity demand, many operations have scaled down production or been placed on care and maintenance. For those continuing in business, this has resulted in considerable focus on process and operating cost optimisation, productivity improvements, product quality enhancements, skills development and capacity building, and consolidation of best practice within the industry. Ongoing projects are required to be well-defined and -motivated, and subject to greater technical and financial scrutiny, to ensure that they are able to rapidly ramp up and deliver immediate value.

In contrast, the burgeoning global lithium-ion battery market has opened up several new opportunities in the region for the production of high-purity base-metal salts for cathode material applications as well as consideration of recycling efforts for end-of-life products. This conference provides a platform for discussion of new and more agile ways of operating and remaining relevant and innovative in a world that has changed considerably since the global COVID-19 pandemic.

Technical topics span the value chain from geometallurgy, project development, operations and processing, to high-purity value-added products, recycling, and sustainability issues. Industry operators will be able to share technical experience and practices, meet vendors, and learn about new technologies and processes that can add value to their operations. World-class plenary speakers will offer a unique opportunity to hear first-hand opinions on the status and overview of the industry.

A Continuing Professional Development short course, focusing on technology developments in the copper and cobalt industries, will be presented by leading engineers and accredited by the Engineering Council of South Africa.

For international participants, this conference offers an ideal opportunity to gain in-depth knowledge of and exposure to the African copper and cobalt industries, and to better understand the various facets of minerals processing and extraction in this part of the world.

Hosted by the Metallurgy Technical Programme Committee of the Southern African Institute of Mining and Metallurgy (SAIMM), this conference aims to:

- Promote dialogue between operators, vendors and service providers on common metallurgical challenges facing the industry;
- Enhance understanding of new and existing technologies that can lead to safe and optimal resource utilization;
- Encourage participation and build capacity amongst young and emerging professionals from the Copper Belt region.

The Organizing Committee looks forward to your participation.

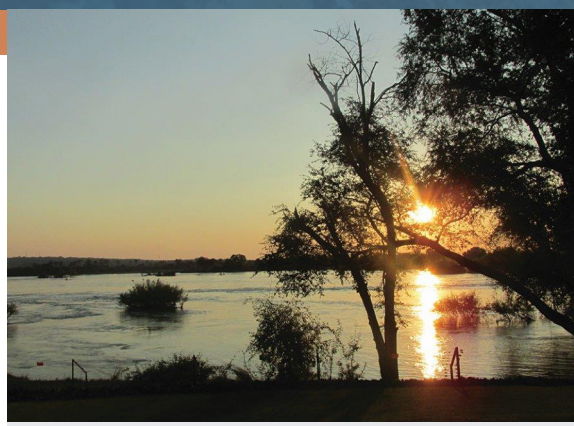

CONFERENCE TOPICS

- Mineralogy
- Geometallurgy
- Minerals processing
- Pyrometallurgy and roasting
- Hydrometallurgy
- Operational practices and improvements
- Project development and execution
- Novel technologies
- Recycling and urban mining
- Waste treatment and minimization
- Environmental issues

FOR FURTHER INFORMATION, CONTACT:

Camielah Jardine,
Head of Conferencing

E-mail: camielah@saimm.co.za
Tel: +27 11 834-1273/7
Web: www.saimm.co.za

SAIMM
THE SOUTHERN AFRICAN INSTITUTE OF MINING AND METALLURGY

BATTERY MATERIALS CONFERENCE 2022

24-25 AUGUST 2022

MISTY HILLS CONFERENCE CENTRE,
MULDERSDRIFT, JOHANNESBURG

The intensified search over the past decade for alternatives to fossil-fuels as stores of energy has led to an exponential growth in the demand for batteries and research into battery technologies. The largest application by far has been in transportation, followed by electrical distribution grids.

Of the raw materials required for battery manufacture, metals such as cobalt, manganese and vanadium are highly concentrated in southern Africa. The supply of lithium, on the other hand, is concentrated in Australia, Chile and Argentine.

These activities have created both opportunities and challenges. Opportunities such as new value chains for the associated raw materials, with several production companies with battery-material metals in their plant feedstocks undertaking research towards producing battery-grade products. And challenges such as the means for recycling these batteries once they reach the end of their (first) life.

The aim of this conference is to provide the opportunity for thought leaders in the global battery value chain to exchange ideas on recent developments in the fields of:

- Materials and high-purity intermediates for battery components
- Flow-battery electrolytes
- Processes for the recycling of batteries
- Market outlook and legislative implications
- Related case studies.

FOR FURTHER INFORMATION, CONTACT:

Camielah Jardine,
Head of Conferencing

E-mail: camielah@saimm.co.za
Tel: +27 11 834-1273/7
Web: www.saimm.co.za

SAIMM
THE SOUTHERN AFRICAN INSTITUTE OF MINING AND METALLURGY